Switching the Gas Transport of Metal–Organic Framework Thin Film Membranes with External Stimuli

DER NATURWISSENSCHAFTLICHEN FAKULTÄT DER

GOTTFRIED WILHELM LEIBNIZ UNIVERSITÄT HANNOVER

Zur Erlangung des Grades

Doktor der Naturwissenschaften (Dr. rer. nat.)

genehmigte Dissertation

von

Alexander Knebel, M. Sc.

2018

Referent: Prof. Dr. Jürgen Caro

Korreferent: Prof. Dr. Armin Feldhoff

Weiterer Korreferent: Prof. Dr. Jorge Gascon Sabate

Tag der Promotion: 18.07.2018

"The first step is to establish that something is possible; then probability will occur"

— Elon Musk

This thesis represents data and results generated during my doctoral studies in the research group of Prof. Dr. Jürgen Caro at the Leibniz University Hanover, Institute for Physical Chemistry and Electrochemistry, Germany. During the time of my employment from October 2015 to present (2018) I authored several articles with my contribution varying from first-authorship to shared first-authorship and co-authorship, which are all present in this thesis, either representing the main part or otherwise to be found in the publication list at the appendix. Additionally, two (three) patents, regarding the most prominent work, were filed within this time with me being the main contributor – light switchable and electrically switchable gas transport in Metal-Organic Frameworks, respectively. The electrical switching was first filed as EU patent, afterwards expanded on recommendation of the Erfinderzentrum Hannover to a world patent. The switching by light was patented together with our colleagues from the Karlsruhe Institute of Technology (KIT) for the EU.

My labour within the first eight months was supported directly by the Institute for Physical Chemistry and Electrochemistry. In-between, Prof. Dr. Jürgen Caro and I drafted a DFG proposal for the priority program (SPP) 1928 "COORNETS – Coordination Networks: Building Blocks for Functional Systems", which was granted by August 2016 and further became the project I was working on. I found a few excellent and deeply respectable co-workers, reviewers, co-authors and colleagues within the project partners, especially Prof. Dr. Dirk Volkmer (University Augsburg, Germany), Prof. Dr. Christof Wöll, Dr. Lars Heinke, Prof. Dr. Stefan Bräse (KIT) and Prof. Dr. Roland A. Fischer (Technical University Munich) and of course the PhD candidates and postdocs working in their research groups.

I found excellent colleagues also outside the SPP 1928, for instance Prof. Dr. Armin Feldhoff, Prof. Dr. Heitjans, Dr. Kai Volkmann and Dr. Benjamin Geppert from our Institute in Hanover. Additionally, I very much appreciated the opportunity to go to King Abdullah University in Saudi Arabia for a research stay in the group of Prof. Dr. Jorge Gascon.

In the following paragraphs, I will go deeper into my contributions to the publications used in this thesis: The first paper to appear in this thesis is a review paper with me as first-author, published in CHEMICAL ENGINEERING & TECHNOLOGY, giving an overview about the switching abilities in MOFs and shows the placement of the publications featured in this thesis in the actual state-of-the-art literature. Together with Dr. Chen Zhou, Prof. Dr. Aisheng

Huang and Dr. Jian Zhang, we were preparing the draft of the manuscript together with Prof. Dr. Jürgen Caro. Additionally, Prof. Dr. Leonid Kustov and I helped Prof. Dr. Jürgen Caro through revising.

The next article (with cover feature) in this thesis, published in CHEMISTRY – A EUROPEAN JOURNAL, deals with thin layer technology, which was transferred to the use-case of membranes with me being first and corresponding author. Under my supervision, Paul Wulfert-Holzmann (who is shared-first author) was working closely together with me on the *"Hierarchical Nanostructures of Metal-Organic Frameworks Applied in Gas Separation ZIF-8-on-ZIF-67 Membranes"* during his master thesis. Also under my supervision, Janet Pavel's contribution was mainly the synthesis protocol for nanosized ZIF particles from her bachelor thesis. Besides that, my contribution was the idea, concept and the writing of the manuscript (and making of the cover picture). The technical realization and automating of the layer-by-layer apparatus lied in my responsibility, where I was supported by Ina Strauß. I contributed also in characterization via SEM and EDXM, the validation of gas permeation data and XRD. Furthermore, I would like to thank Dr. Sebastian Friebe for his helpful support in mixed-matrix membranes permeation measurements and Frank Steinbach for the TEM analysis. Alexander Mundstock helped with revising the manuscript.

In the next chapter I show three research articles about gas transport investigations in light-switchable MOFs, prepared as thin-layered membranes. The paper *"Tunable molecular separation by nanoporous membranes"* was published in NATURE COMMUNICATIONS with me being shared first and corresponding author. This was a pioneering work for light-switchable MOFs applied in gas separation. I contributed the concept of a specially designed reactor that enabled in situ switching of gas permeation, gas permeation data as well as SEM and EDXS analysis. Additionally, I was strongly involved in the writing process of the paper and contributed text passages and figures. The same applies for the second article in this chapter *"Switching Thin Films of Azobenzene-Containing Metal-Organic Frameworks with Visible Light"* published in CHEMISTRY – A EUROPEAN JOURNAL. Without the organic chemistry from the KIT, Prof. Dr. Stefan Bräse, Dr. Sylvain Grosjean and the group of Prof. Dr. Christof Wöll, Dr. Lars Heinke (Dr. Zhengbang Wang, Danny Wagner, Kai Müller) and the other co-workers from Berlin, Dr. David Bléger and Fangli Zhao, these two publications would not have been possible. The third publication in this chapter has its origin entirely at the Leibniz University Hanover with me as first and corresponding author. *"Azobenzene Guest Molecules*

as Light-Switchable CO₂ Valves in an Ultrathin UiO-67 Membrane" was a cooperation project - initiated and drafted by me - of the group of Prof. Dr. Jürgen Caro and Prof. Dr. Peter Behrens and his student Alexander Mohmeyer, published in ACS CHEMISTRY OF MATERIALS. They provided me with fast and accurate adsorption measurements and also helpful revision of the manuscript. Under my supervision and close cooperation the synthesis work to this study was performed by Lion Sundermann. I conducted the gas permeation data, XRD, SEM and EDXS measurements. I was also responsible for the spectroscopic analysis by IR and UV/Vis spectroscopy and appreciated help from Dr. Sebastian Friebe and Ina Strauß with the interpretation of these. Furthermore, I wrote the manuscript.

The next chapter and its research article *"Defibrillation of Soft Porous Metal-Organic Frameworks with Electric Fields"* is the highlight of this thesis and was published in the very famous and prominent journal SCIENCE. It is the first experimental work on the influence of electric fields on MOFs. I very much appreciated assistance from Dr. Kai Volgmann and Prof. Dr. Paul Heitjans in the dielectric spectroscopy and from Dr. Daniil Kolokolov and Prof. Dr. Alexander Stepanov for H^2 NMR, Dr. Benjamin Geppert for XRD evaluation, Dr. Jens Twiefel for polarization experiments, but especially from Prof. Dr. Dirk Volkmer for the DFT calculations of the MOF material upon poling with an electric field. I was responsible for the idea, concept and drafting the manuscript and generation of most of the experimental data: Preparation of ZIF-8 membranes, reactor design and technical realization, gas permeation, XRD, SEM, and EDXS. The paper was highlighted by the SCIENCE magazine through a contribution by Prof. Dr. Jorge Gascon.

My doctoral advisor Prof. Dr. Jürgen Caro has assisted very carefully and in all cases with drafting and revising of the manuscripts and patents and was always involved in generating and evaluating the presented concepts.

ABSTRACT

Within the scope of the thesis lies the synthesis of new metal-organic framework (MOF) membranes with the focus on state-of-the-art separation values. Therefore, we prepared thin layer MOF membranes, either as supported continuous membrane or as polymer-filler composite mixed-matrix membrane (MMM). High-end technologies such as the liquid-phase epitaxy are used to produce MOF layers by layer-by-layer growth. We used self-assembly to synthesise ultrathin MOF-on-MOF heterostructures with extremely controllable thickness. It is also possible to synthesise heterostructured nanoparticles. Free standing MMMs were prepared with these particles using doctor blading and tested in gas permeation. But also conventional solvothermal synthesis protocols were developed to yield ultrathin MOF layers.

The layer-by-layer technique allows the preparation of tailor-made MOF membranes with light-switchable moieties by self-assembly. These structures are pillared-layer type structures and enable switchable functionalization. Thus, azobenzene (AZB) or fluoro-AZB light-switches were mounted as side-chains to the backbone of the linker molecule. Gas transport through these surface-mounted MOF (SURMOF) membranes can be remotely controlled with UV (ultraviolet) or visible light-induced cis-trans isomerism. By using fluoro-AZB moieties, the switching wavelength is completely shifted into the visible part of the spectrum. The mechanism for switchable gas-separation could be explained by the different dipolar moments. When the AZB is in trans configuration, the dipolar moment of the N=N bridge is 0 D, while it is 3 D for cis. We also show that AZB guest molecules in an ultrathin UiO-67 layer are light-switchable. The mechanism is different: separation is based on size-exclusion at the pore-windows, which can be reversibly opened and closed by the cis-trans isomerism.

Further, we show electrical switching of the zeolitic imidazolate framework 8 (ZIF-8), which is the first experimental study towards the influence of electric fields on the porous structure of MOFs. A ZIF-8 membrane was mounted between 2 net-electrodes, forming a MOF-membrane-capacitor. At electrical field strength of 500 V/mm the MOF undergoes a phase-transformation into a polarized space group, in which the linker molecules' rotational motions are blocked. Further, the pore-opening diameter is slightly changed, which decreases selectivity for smaller molecules, but is just the right size to increase selectivity for propene/propane mixtures. Thus, we improve molecular sieving with the ZIF-8 framework.

Keywords: Metal-Organic Frameworks, Thin Layers, Gas Separation, Light-Switchable Membranes, Electric Field Switching

KURZFASSUNG

In der Doktorarbeit wurden Metall-Organische Gerüstverbindungen (MOFs) als Membran mit dem Fokus auf optimale Trenneigenschaften synthetisiert. Dazu wurden MOF-Dünnschichtmembranen auf Trägern synthetisiert oder MOF-Polymer-Composite als Mixed Matrix Membranen (MMMs) hergestellt. High-End-Technologien wie die Flüssigphasenepitaxie erlauben MOF-Membranen Schicht für Schicht aufzubauen. Diese Self-Assembly-Technik wird verwendet, um ultradünne MOF-Schichten hochkontrolliert und heteroepitaktisch abzuscheiden. Damit ist es auch möglich, heteroepitaktische Partikel zu synthetisieren. Mit den Partikeln wurden beispielsweise freistehende MMMs hergestellt und für die Gastrennung verwendet. Aber auch die konventionelle Solvothermalsynthese konnte optimiert werden, um ultradünne MOF-Schichten zu synthetisieren.

Diese Schicht-für-Schicht-Technik ermöglicht die Herstellung von maßgeschneiderten MOF-Membranen mit lichtschaltbaren Seitengruppen. Diese MOFs sind Schicht-Säulen-Strukturen und ermöglichen die Lichtschaltung. Azobenzol (AZB) oder Fluoro-AZB-Seitengruppen wurden in die Säulen der MOFs eingebaut und der Gastransport durch Membranen mit diesen oberflächenverankerten MOFs (SURMOFs) kann mit UV (ultraviolettem) oder sichtbarem Licht ferngesteuert werden. Wird Fluoro-AZB verwendet, so liegen die Schaltwellenlängen komplett im sichtbaren Bereich des Spektrums. Der Mechanismus für die schaltbare Gastrennung konnte durch die Adsorption erklärt werden. Das Dipolmoment der N=N-Brücke des AZBs beträgt 0 D in der trans-, jedoch 3 D in der cis-Konformation. Des Weiteren konnte gezeigt werden, dass AZB auch als Gast in den Poren einer UiO-67 Schicht eine Schaltbarkeit des Gastransports über einen anderen Mechanismus ermöglicht: Diese Separation basiert auf Größenausschluss am Porenfenster des UiO-67, welche durch cis-trans-Isomerie auf und zu geschaltet werden kann.

Als letztes wird eine Pionierstudie zum Einfluss von elektrischen Feldern auf MOFs gezeigt, welche auch die erste experimentelle Arbeit dazu ist. Eine ZIF-8-Membran wurde zwischen zwei Netzelektroden montiert. Bei einer elektrischen Feldstärke von 500 V/mm entstehen polarisierte Polymorphe, in denen die Gerüstflexibilität vermindert ist. Außerdem ändert sich der Porendurchmesser minimal, sodass die Größenselektivität für kleinere Moleküle schlechter wird, sich aber die Propen/Propan-Trennung verbessert.

Keywords: Metall-Organische Gerüstverbindungen, Dünnschicht, Gastrennung, Lichtschaltbare Membranen, Schaltung durch elektrisches Feld

x

AZB	Azobenzene
CCDC	Cambridge Crystallographic Data Center
CP	Coordination Polymer
DFT	Density Functional Theory
EDXM	Energy Dispersive X-Ray Mapping
EDXS	Energy Dispersive X-Ray Spectroscopy
H_2BDC	Terephthalic acid
H_2BPDC	Biphenyl-4,4'-dicarboxylic acid
HKUST	Hong Kong University of Science and Technology
Hmim	2-Methylimidazole
IRMOF	Isoreticular Metal-Organic Framework
Me	Metal ion
MIL	Materiauxs de l'Institute Lavoisier
MMM	Mixed-Matrix Membrane
MOF	Metal-Organic Framework
PCP	Porous Coordination Polymer
SBU	Secondary Building Unit
SEM	Scanning Electron Microscopy
SOD	Sodalite
SURMOF	Surface Anchored Metal-Organic Framework
TCNQ	Tetracyanoquinodimethane
TEM	Transmission Electron Microscopy
UiO	Universitete i Oslo
UV	Ultraviolet
vis	Visible
XRD	X-Ray Diffraction
ZIF	Zeolitic Imidazolate Framework

CONTENTS

XIII

1. Theoretical Background

1.1. Motivation and Perspectives for Gas Separation Membranes

Membranes as solution for the separation and refinery of gases have emerged within the last decades as a key technology for green energy. Membranes are outstanding candidates for CO_2 capture in pre- and post-combustion processes, as well as the oxy-fuel combustion with the aim to reduce greenhouse gas emission and stop global warming.[1] Additionally, a big and important part of membrane technology focuses on the separation of basic gases like helium, hydrogen, nitrogen, methane, ethylene and propylene from their natural gas mixtures.[2]

Hydrogen is one of the most important energy carriers of the future: it has a very high energy density and burns with oxygen to water, which makes it harmless for our climate system.[3] With today's technology standards, H_2 and O_2 can be burned under controlled conditions, either in gas turbines or in fuel cells through proton conductive membranes and, thus, can be used to generate energy.[4] It is a long way to replace common fuel engines and it is unclear if fuel cells or accumulators will power electrical engines in future cars, however, H_2 will definitely be the fuel for electricity generation. Even if a reliable H_2-economy or electrical economy in regard to auto mobility is still missing in modern society (even though it is strongly developing at the moment) H_2 will definitely be the key energy carrier of future generations and replace the fossil fuel economy, as we know it today.[5,6]

In this context, the generation of H_2, which is still relying on fossil fuels, is often swept under the carpet. By producing H_2, a large quantity of CO_2 is simultaneously produced. This is where membranes are a promising technology for carbon capture application in order to reduce greenhouse gas emission. On the one hand the membrane serves for the carbon capture, separating CO_2; on the other hand it is refining the H_2 towards high purification levels. Exemplarily, in a pre-combustion power plant H_2 is produced in high amounts by gasification and steam reforming of fuel (methane and higher carbohydrates), followed by a water-gas shift reaction (c. f. Figure 1). The outcome of the reactions is H_2, but also CO_2 in a 1:1 mixture.[7] The latter one has to be removed while H_2 is burned in a gas turbine (or fuel cell). This is where separation is the focus and where membranes are of high importance.

There is not only pre-combustion, but also a more actual problem, the direct burning of fossil fuels for energy generation. CO_2 as the "climate-killer" should be removed from industrial waste gas. Here, people are looking for a membrane system that separates CO_2 from

N_2 in a post-combustion process (c. f. Figure 1), meaning after the burning of fossil fuels, for example in a thermal power plant operating with natural gas or coal.[8] There were also concepts of removing CO_2 directly from ambient air to stop climate change.[9]

A third type of combustion should be mentioned, the oxy-combustion or also called oxy-fuel process, where an oxygen-enriched atmosphere is used to burn industrial waste gases again, breaking it down to CO_2 and N_2. Here, pure O_2 is needed, which makes oxy-combustion one of the most energy intensive processes of the three (c. f. Figure 1), but leads to a cleaner combustion process.[8,10] A perspective to produce the desired pure O_2 are dense, ceramic membranes, often perovskites. Through oxygen defect vacancies at 900 °C and above a high flux of oxygen ions can be provided, and thereby the separation of pure oxygen from gas mixtures is possible.[11] However, the focus of this thesis lies in porous membranes for gas separation and ceramic membranes should not be explained in depth further.
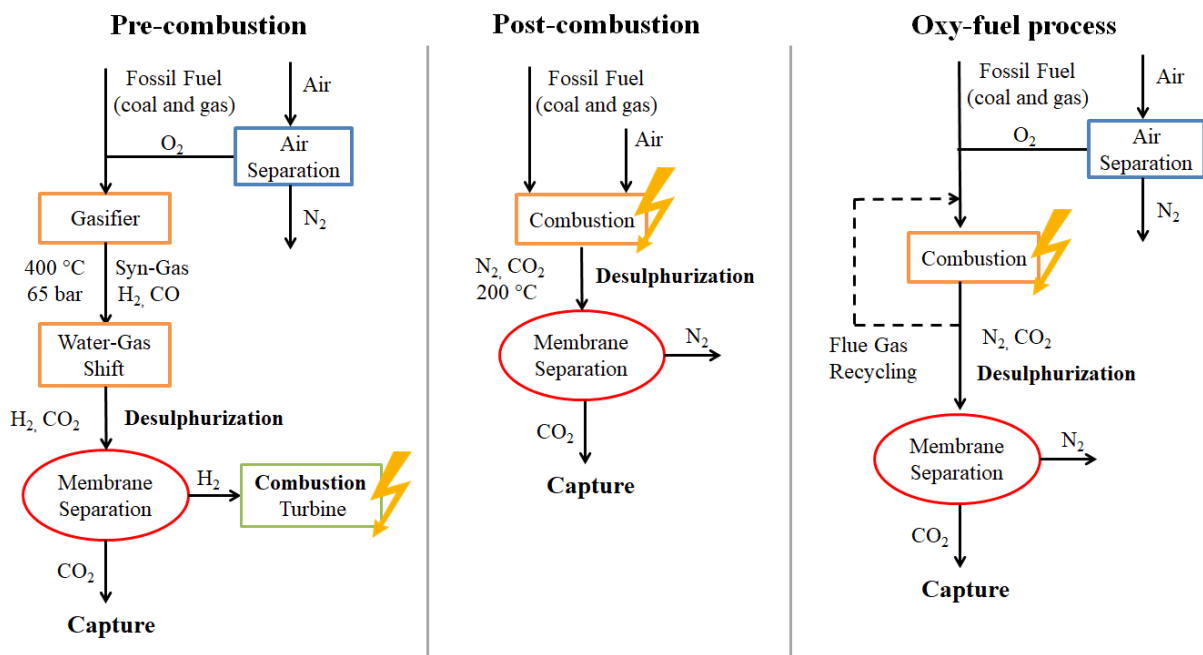
Figure 1 *The three types of combustion with additional CO_2 capture: pre-combustion, post-combustion and the oxy-fuel process.[1,7,8,10] Schematic, technical flow chart representations.*

Nevertheless, the CO_2 captured in all of these processes must be stored without contact to the atmosphere – of course – to stop the greenhouse effects and global warming, making it a challenging task. There are several ideas to solve the storage issue, for example the disposal into the oceans, storage in geological formations or in man-made caverns in the underground.[7] The storage in the ocean, however, is only a time-based strategy and transfers the problem to

the next generations. The storage in caverns, natural or man-made, is probably the method of choice when it comes to carbon sequestration.[12]

Changing the topic and looking back at the introduction sentences, the purification of basic gases was mentioned. For instance, in natural gas, a lot of interesting gases are found, mainly CH_4 and higher carbohydrates, but it is the main source for He, too. Thus, some developments are also aiming in the direction of He separation from natural gas, for example with porous graphene membranes, because He is a highly important and limited resource (especially for research).[13,14]

CH_4 is more and more important when facing the shortage of fossil energy carriers and it is no wonder that CH_4 separation tasks are highly focused.[15] The main reason behind the CH_4 separation is, of course, the use of it as energy source in gas power plants. But methane is also useful for the process for the sustainable conversion to basic chemicals, for example methanol[16] or H_2[3]. Separating CH_4 from N_2 is important for digesting biological waste to bio-ethanol, where high amounts of CH_4 and N_2 are side products.[17]

Further thinking of basic things almost everyone on this planet is using will quickly direct the thoughts toward plastic. A lot of basic stuff, such as bottles, boxes, cases, computer parts, and many more are often made of polyethylene or polypropylene, generating a high demand on the gases ethylene and propylene in high purity for polymerization. Separation of these basic chemicals is highly energy intensive, whereas membranes could be a key technology (Figure 2) and could save up to 70 % of energy in regard to the state-of-the-art separation processes.[18,19]

In most cases, gas mixtures like propane and propylene are purified using cryogenic distillation as state-of-the-art technology, which is highly energy intensive, nevertheless a highly evolved technology.[20]
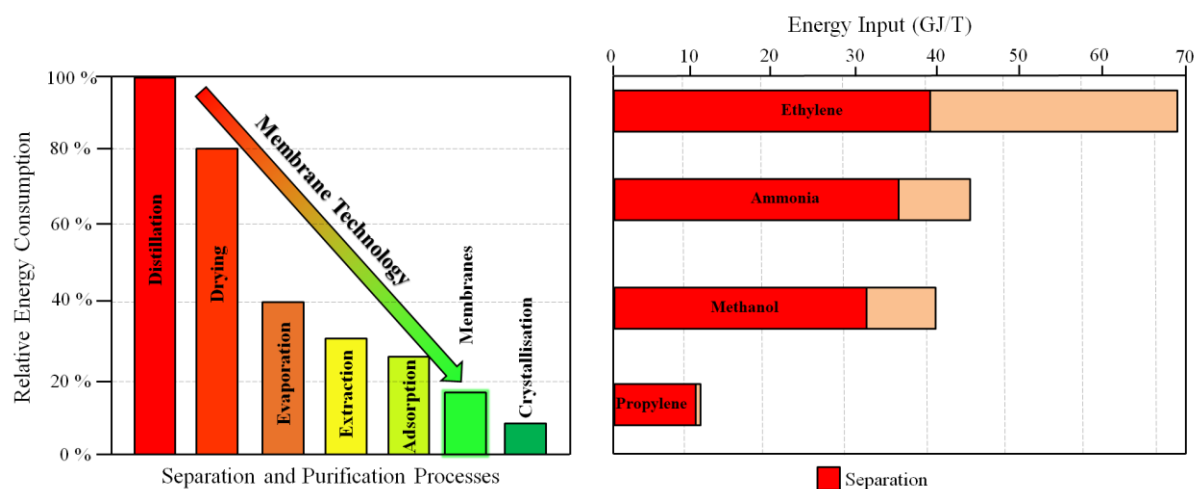
Figure 2 *Energy consumption of different technologies for separation and purification purpose and the role of membrane technology (left graph). Necessary energy input to generate 1 T of ethylene, ammonia, methanol and propylene and the corresponding amount of energy that has to be used on the separation process (right graph).*[18,19]

Yet, another emerging concept with more and more practical utilization is the pressure swing adsorption, which, no doubt, has a better relative energy balance compared to distillation (c.f. Figure 2), nevertheless is not a continuous process and hard to design for practical use.[21] Membranes have the advantage to work in a continuous process with even lower relative energy consumption than technical adsorption processes.

But still, not only the membrane material parameters limit the outcome of the separation process, also the operation conditions of the process.[22] As an example, a variation in the feed gas composition, meaning the initial mixture that is separated with the membrane, brings variations to the retentate, the depleted feed gas. Additionally and probably more important, this brings a variation to the permeate, the mixture after the separation. This problem could be overcome using stimuli responsive membranes, regulating the permeate composition by external stimuli to yield always the same. This would improve purification and separation. Thinking further, a multi-purpose membrane consisting of one material, switchable for all different separation tasks, would make membrane fabrication and processing extremely easy. Promising candidates for these stimuli responsive membrane materials are Metal-Organic Frameworks (MOFs), which will be discussed further in the following chapters. But first of all, we need to understand the physical principles of diffusion in microporous materials and the types of membranes that exist in the MOF context.

1.2. Gas Diffusion in Porous Inorganic and Polymeric Media

1.2.1. Mass Transport through Porous Inorganic Materials

In this thesis (a) pure, crystalline and porous Metal-Organic Framework (MOF) membranes, (b) pure polymer membranes and (c) polymer-filler mixed-matrix membranes (MMMs) were investigated. This means that beside the porous materials it is also useful to consider solubility based polymeric membranes separation, even though the interconnection is the MOF. This will be addressed in a later chapter of this thesis. The focus of the following chapter will lie on the porous, inorganic material, in which three fundamental mass transport mechanisms are of interest.

Within large pores, first of all, the bulk diffusion must be considered, meaning the diffusion of one gas into another gas, which is given by FICK's law in Equation 1. This applies for distances, where molecule-molecule collisions are predominant.[23] The flow of gas i in the z-direction $J_{i,z}$ is effectively the mass transport rate in the medium per area, which is proportional to the negative concentration gradient, normal to the surface it diffuses through.

$$J_{i,z} = -D \left(\frac{\delta c}{\delta z} \right) \qquad \text{(Eq. 1)}$$

Here, z is the length along the diffusion pathway, c the concentration of gas, and D the FICK Diffusion coefficient in $cm^2 \cdot s^{-1}$.[24]

But the gas diffusion through porous materials is also dependent on the size of the pores, and for each category of different pore diameters we find dominant mechanisms. For diffusion through mesopores, which lie in the size-range of 2-50 nm, the predominant diffusion mechanism is KNUDSEN diffusion, which is also always accompanied by bulk diffusion.[23,25] This type of diffusion can be described by the kinetic gas theory, since the mean-free path of the gas molecules or atoms is in the range of - or smaller than - the distance of the pore-walls to each other. The pore or capillary is considered to be in a steady-state under constant temperature, pressure and only a single gas flowing through it. Equation 2 gives the KNUDSEN diffusion coefficient $D_{K,i}$ using a model of a long, cylindrical pore with a diameter d_p of 2-50 nm.

$$D_{K,i} = \frac{d_p}{3} \sqrt{\frac{8RT}{\pi M_i}} \qquad \text{(Eq. 2)}$$

Here, R is the ideal gas constant, T is the temperature, and M_i is the molar mass of the species. If the system is in the Knudsen regime, the gas molecules are assumed to move in straight lines between the pore walls and are not interacting with each other, pictured in Figure 3. When a molecule collides with the wall, it gets reflected and continues to travel.[26]
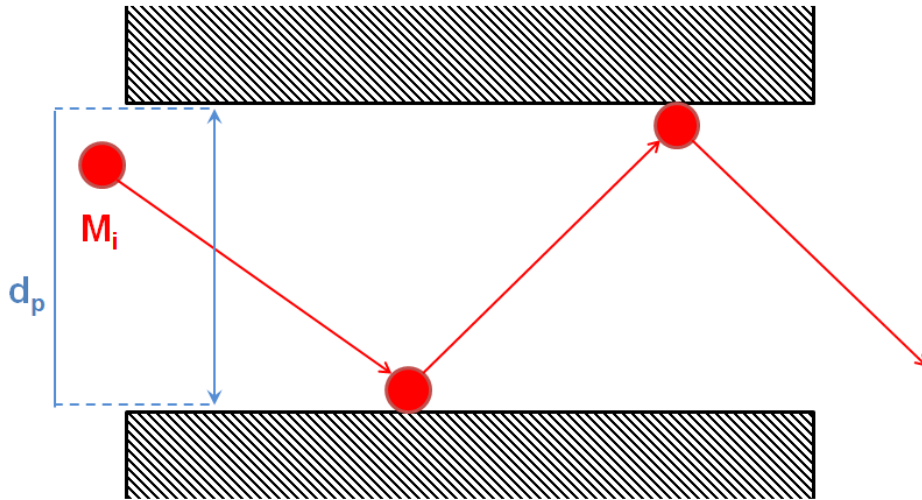
Figure 3 *KNUDSEN diffusion of a gas in a cylindrical long pore or capillary channel and the parameters for this type of diffusion. The red ball is the gas molecule or atom.*

This mechanism is of importance when looking at a membrane grown on top of a ceramic support disc. The used supports in this work have a pore diameter of below 50 nm and exhibit kinetic gas separation just by themselves due to the KNUDSEN diffusion.[27] This can be used as a measure of successful layer formation of the crystalline membranes: is the layer not completely intergrown and shows a lot of defects, the separation will not be better than the KNUDSEN diffusion.

Beside the kinetic gas separation by KNUDSEN diffusion, for smaller pores below 2 nm adsorptive diffusion and molecular sieving are the mechanisms of interest. The first is mainly based on capillary condensation, while the latter is a size-selective process. Adsorptive diffusion is based on gas that adsorbs at the pore walls and moves further by bulk and surface diffusion. Here, the gas first is adsorbed on a surface side near to a pore, afterwards it diffuses into the pore, through the pore channel and gets desorbed on the other side of the pore.[28] The separation of binary mixtures by adsorption in very confined pore-space is relying on the competitive gas-solid interaction. Generally, it can be assumed that a gas that is stronger adsorbed at the pore wall travels slower through the pore, than a gas that is not or only weakly adsorbed, as shown in Figure 4. Thus, the retention time of the gases give a correlation to the

separation: The weakly adsorbed species travels quicker, and less of the strongly adsorbed species can travel through the membrane at the same time.[29,30]
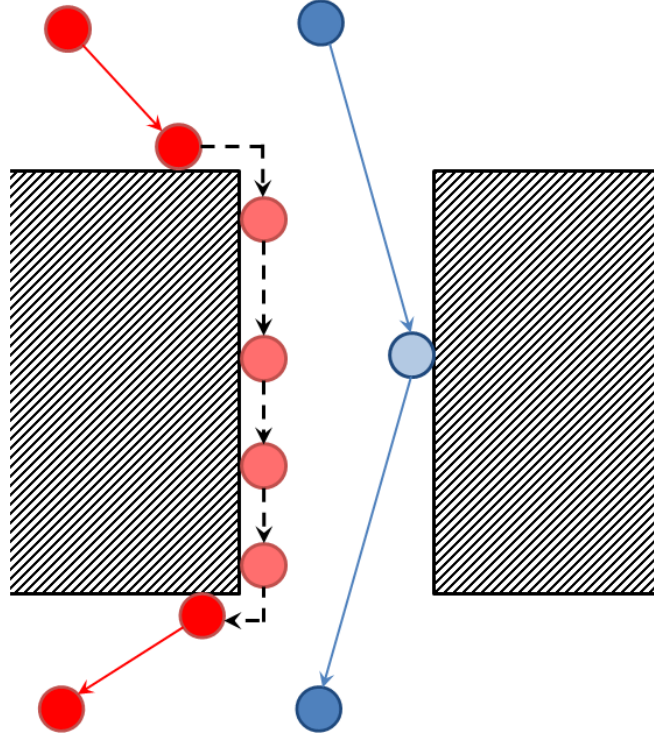
Figure 4 *Adsorption based separation: the strong adsorbing species (red) travels through the pore via surface diffusion, while the less adsorbing species (blue) is going through the pore almost unhindered. This can be an example for H_2/CO_2 separation, where H_2 is the blue sphere, while the red ball is CO_2.*

The third mechanism is the molecular sieving mechanism. Molecular sieving is the size-selection of gases through confined pore geometries, as shown in Figure 5. In a porous material, the pores can be so narrow, that only gases with the right kinetic diameter can pass through the pore, and all other molecules are reflected at the surface.[26,31] The kinetic diameter is defined as the smallest sphere a molecule can occupy. In such a medium with highly confined pore space, for a spherical gas (e.g. Argon), the diffusion coefficient can be expressed as shown in Equation 3:

$$D = \rho_g d_p \sqrt{\frac{8RT}{\pi M}} \cdot e^{-\frac{\Delta E}{RT}} \qquad \text{with} \quad \rho_g = \frac{1}{3}\frac{S_n}{S_p} \qquad \text{(Eq. 3)}$$

Here ρ_g is the geometrical probability that the gas jumps into the direction of the pore, with S_n being the area of the pore opening that leads to another pore (pore-neck cross-section)

and S_p the cross section area of the pore. The e-function is giving the energetic probability of a jump into the pore.[32]
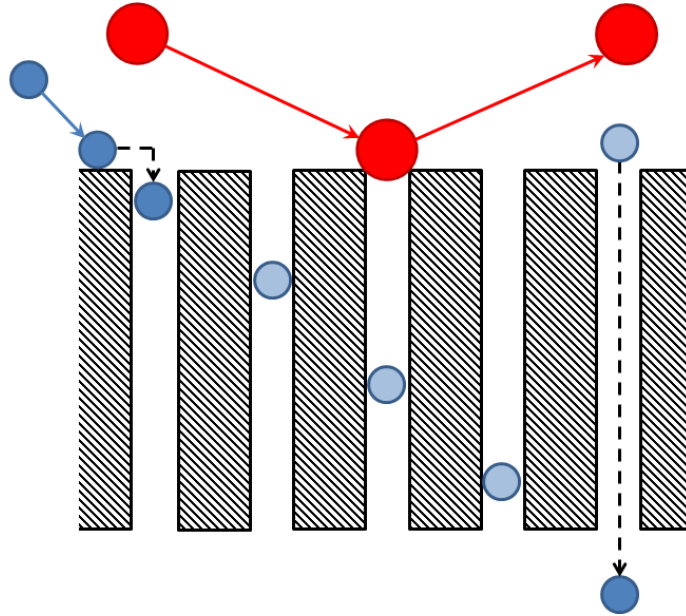
Figure 5 *Schematic visualization of the molecular sieving mechanism. Gases with a kinetic diameter too big to fit into the pore are rejected (red balls) while the small molecules can go through the pore by surface diffusion (blue balls).*

When looking at the linear pore in this molecular sieve in Figure 5 there is a probability that CO_2, which is a linear molecule, but cannot be correctly described by a sphere, can diffuse through the pore by its geometry. This is called the shape selectivity of a molecular sieve, and would make equation 3 a lot more complicated. In this case, the activation energy that is determined by the pore's geometry and the geometrical probability for the molecule to enter the pore has to be considered.[32]

1.2.2. Physics of Membrane Permeation and Separation

The knowledge about diffusion through porous materials and polymers is helpful when describing the separation process through membranes. First of all, it is necessary to define the driving force for gas permeation through a membrane as a chemical potential gradient. Therefore, the MAXWELL-STEFAN approach is a widely accepted description and should be used for the mathematical specification of gas transport through a membrane. The chemical potential gradient $\nabla \mu_i$, so the force that is applied to species i, for a binary gas mixture can be expressed as in Equation 4:

$$-\nabla\mu_i = RTx_j \left(\frac{u_i - u_j}{D_{i,j}^m}\right) \text{ with } \quad \nabla\mu_i = \frac{\delta\mu}{\delta z} \qquad \text{(Eq. 4)}$$

Here, x_j is a fractional loading of the component (dimensionless), u is the velocity of the species in regard to the surface and the $D_{i,j}^m$ is the MAXWELL-STEFAN diffusion coefficient.[33] The fractional loading $x_{i,j}$ can be described by a LANGMUIR adsorption model, as applied in Equation 5:

$$x_j = \frac{q_j}{q^{sat}} = \frac{K_j p_j}{1 + K_j p_j} \quad \text{with} \quad K_j = \frac{k_{ads}}{k_{des}} \qquad \text{(Eq. 5)}$$

Here, q_j is the loading of component j in terms of molecules per unit cell, whereas q^{sat} is the saturation loading. Thus, it can be expressed with the LANGMUIR adsorption isotherm, where p_j is the partial pressure of the component, while K_j is the equilibrium constant for the same component, which is again made up of the quotient of the rate constant of adsorption k_{ads}, divided by the rate constant of desorption k_{des}.[33,34] The $D_{i,j}^m$ is the mixed component MAXWELL-STEFAN diffusion coefficient. For a single component D_i^s can be formulated as in Equation 6:

$$D_i = D_i^s \left(\frac{\delta\ln(p_i)}{\delta\ln(c_i)}\right) \qquad \text{(Eq. 6)}$$

From that we can determine the flow of gas by applying FICK's law (Eq. 1) in Equation 7:

$$J_z = -D_i^s \left(\frac{\delta\ln(p_i)}{\delta\ln(c_i)}\right)\left(\frac{\delta c_i}{\delta z}\right) \qquad \text{(Eq. 7)}$$

The general technical terminology for membrane separation is as follows: An analyte gas or gas mixture is fed to a membrane in an upstream, and then permeates through the membrane with the direction of chemical potential gradient to the other side, as shown in Figure 6.
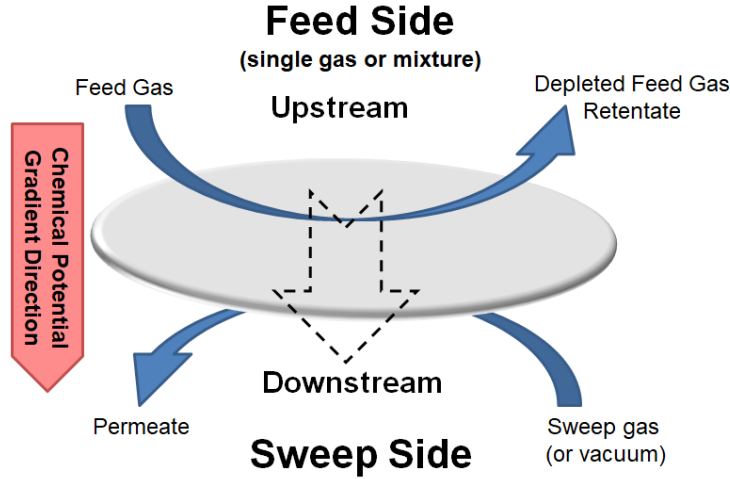
Figure 6 *Schematic illustration of the gas permeation process.*

On the downstream or sweep side, either another gas is flown along the membrane (sweep gas) or vacuum is applied.[35] Gas that is flown over the membrane is called feed gas, while the depleted feed gas is named retentate. Gas that permeates through the membrane is, obviously, named permeate.

However, in technical terms, describing gas permeation properties of membranes and evaluating their qualities, three parameters are used. The flux through a membrane F is the amount of the gas species n_i per time t and permeable area A (Equation 8).

$$F = \frac{n_i}{t \cdot A} \tag{Eq. 8}$$

In Equation 9 the permeance Γ is shown, which is the pressure normalized flux, actually the quotient of the flux and the pressure difference Δp between upsteam and downstream.

$$\Gamma = \frac{F}{\Delta p} \tag{Eq. 9}$$

The permeability P is further the thickness normalized permeance (Equation 10), multiplying the permeance with the thickness d of the membrane.

$$P = \Gamma \cdot d \tag{Eq. 10}$$

The selectivity or separation factor $\alpha_{i,j}$ in membrane permeation can be calculated by dividing the molar fractions of the components i and j from a binary mixture (real separation

factor) or the values from single gas measurements (ideal selectivity) from the retentate with the molar fractions of the components from the permeate. As the membrane permeation is operated with an excess supply of gas on the feed side, it can be assumed, that the retentate composition is the feed gas composition. Equation 11 shows the calculation of the selectivity:

$$\alpha_{i,j} = \frac{n_{i,p} / n_{j,p}}{n_{i,r} / n_{j,r}} \qquad \text{(Eq. 11)}$$

The indices p and r stand for permeate and retentate, respectively. For a better understanding, the chemical potential gradient that is the driving force (as described above) can be a (partial) pressure or a concentration gradient over the membrane.[35]

1.2.3. Solubility Based Mass Transport through Polymeric Media

In dense polymeric membranes, that are the industrial most relevant types of membranes, the gas transport is solubility based. Here, the polymer material can either be rubbery or glassy.[36] In a combination with fillers, forming MMMs, many people see the future of cheap but very good performing membranes systems.[37,38]

Transport properties of polymers are dependent on different factors such as: free volume, mobility of the polymer chains and therefore the degree of crosslinking within the polymer, the degree of unsaturation, degree of crystallinity and glass transition temperature.[39] All intrinsic properties of the polymer that leave a lot of space for polymer scientists.

For dense polymeric membranes, the solution-diffusion model is applicable here, despite the fact that it was designed for liquid separations. The differences in permeability can be explained by the interaction possibilities such as electrostatic interaction, hydrogen bonds and Van der Waals bonds – so more or less on the same interplay than in the porous system, which relies on adsorption (with the slope of the adsorption isotherm S, a thermodynamic paramter) and diffusion D (a kinetic parameter).[40] Thus, the permeability P is depending on these both factors and can be written as in Equation 12:

$$P = D \cdot S \qquad \text{(Eq. 12)}$$

As we are talking about a solution-diffusion, the solubility of gases can be described as the condensability, which is increasing with higher temperatures.[41] It is just a matter of the shape and kinetic diameter of the penetrating species that, for example, CO_2 is going slower through a polymeric matrix than H_2.[42]

1.3. Types and Preparation of MOF-Based Gas Separation Membranes

1.3.1. Overview and Preparation of Supported MOF Membranes

When talking of MOF-based membranes for gas separation we distinguished between 2 types of systems. In the first place, there are crystalline MOF membrane layers, synthesised on ceramic supports by solvothermal synthesis under high pressure and high temperature[43]; then there are MMMs. The synthesis protocols of supported MOF membranes can vary a lot, using different solvents, temperatures or even temperature ramps, different autoclave filling levels, different starting chemicals and additives, which enormously influence the resulting crystalline layer. To grow thin layers, supports can be soaked with a solution containing one or more components and after that be added to the reaction solution, also called counter-diffusion method, which gives control over the membrane layer through diffusion.[43–45] When changing the solvent it is possible to influence growth on different lattice planes that can lead to different outward facing pore channels and gas transport properties.[44] There are a lot of ways to produce membranes by solvothermal synthesis, but only a few yielding ultrathin layers with state-of-the-art properties.[46–48] However, there are many techniques like electrospinning[49], dip-coating[50], spin-coating[51], gel-vapour deposition[47], spraycoating[52] that allow thin layer growth. One of the most promising techniques is the liquid-phase epitaxy or also called layer-by-layer deposition.[53,54] Most of the time, this technique was used to grow defined thin-layers on flat surfaces to be used for electronic applications, drug delivery system probing and fundamental science on highly defect-free surfaces.[55–58] However, these technique also allows the fabrication of crystalline membranes[59] and also tailor made MOF smart-membranes[60,61]. We could show that with this technique synthesis of layers with highly controllable thickness and also MOF-on-MOF hetero-structured membranes are achievable.[62]

1.3.2. MOF-Based Mixed-Matrix Membrane Systems

Mixed-matrix membranes (MMMs) have some decent advantages over ceramic supported membranes. On the first sight, MMMs should not be considered to be used on the industrial scale, because of the low flux of especially polymeric imine-based glassy polymers. However, the cost efficiency of polymeric membranes is the main advantage and makes them feasible for gas separation tasks. A polymeric membrane that has the same area than a ceramic supported membrane is cheaper by a factor of 3000. This also makes the membrane modules disposable (or recyclable) and additionally, expensive regeneration processes are no longer essential. Through thin-layer fabrication methods like fibre spinning or large area doctor blading the walls of the polymeric membranes can be thinned down to roughly 10-300 nm

and by that give economically interesting fluxes.[63] Focusing on MOF-based MMMs with a minimum wall thickness for maximum flux, the MOF filler material is now the limiting factor for this type of membranes. The MOF has to be in the size range of 10-30 nm to produce defect free layers for industrial utilization.[38,62,64]

As already discussed in chapter 1.2.3., the gas transport in polymeric materials is based on solubility. The separation properties of polymers can be highly tuned by mixing the polymer with MOF materials. Thus, the separation is also relying on the filler properties, such as pore-size, pore-volume and adsorption properties, as well as the amount of filler material, illustrated in Figure 7.[65–67]
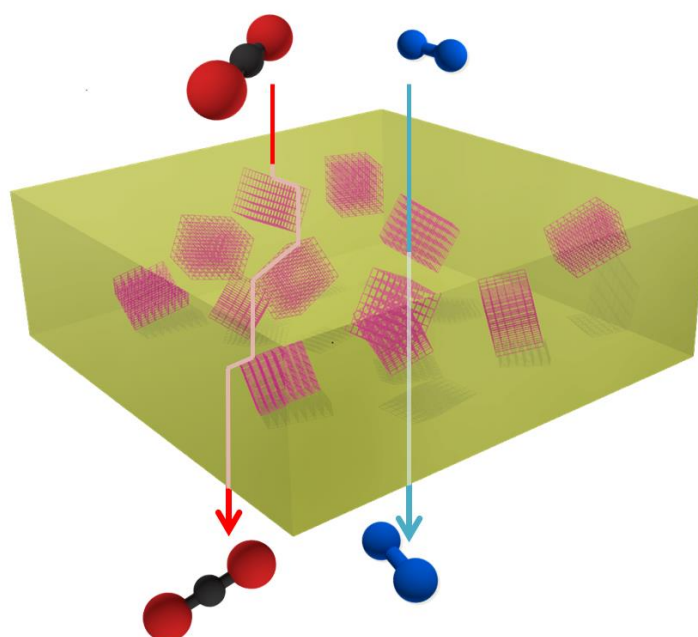
Figure 7 *Illustration of the separation in MMMs. The bigger gas (CO_2) has to go around the porous MOF particle or is adsorbed by entering the pores of the MOF, thus this diffusion pathway is much longer or its diffusion is much slower. The smaller H_2 molecule can pass the pore easily by its size and is not, or only weakly adsorbed, thus moves much faster through the membrane.*

However, the preparation of MOF-based mixed matrix membranes can be very challenging. There are several effects that lead to undesired properties of the MMMs. The ideal way to improve the polymeric material is the increase of both, separation and permeability through the membrane by perfect inclusion of the filler. Nevertheless, there are 3 non-ideal cases that can occur: (i) In the first case the pore of the MOF is clogged, not increasing the separation, only decreasing the permeability; (ii) The second case would be a rigidified polymer layer around the filler, leading to decreased permeability and higher

selectivity, as found by DIESTEL et al.[65]; (iii) The third problem that is likely to occur is bad adhesion between filler and polymer, leading to cavities and voids around the particle, improving permeability drastically, but decrease selectivitiy.[44,68]

1.4. Introduction to Metal-Organic Frameworks

Metal-**O**rganic **F**rameworks (**MOF**s) are porous (or non-porous) hybrid materials consisting of inorganic metal nodes, e.g. metal-ions, metal- or metal-oxide clusters and organic linker molecules. Earlier, MOFs were also referred to as porous coordination polymers (PCPs). The organic linker molecules are bridging the metal nodes by coordination and it can be distinguish between bi-, tri- and poly-dentate linkers, depending on the amount of coordination sides a linker has. The first MOF were invented in 1999[69] and more deeply investigated and described by O. M. YAGHI and published in *Science* in 2002.[70] Since then he, as the MOF pioneer, drafted also a very well-known synthesis principle for these systems, called the reticular synthesis, published in *Nature* in 2003.[71] It was shown that MOF systems can be extended by longer linker chains and that certain metal-ions can be exchanged, obtaining the same crystal structure, but with larger cavities, different pore diameters and a variety of intrinsic properties.[71] The first MOF ever described was MOF-5, which is shown in Figure 8, consisting of terephthalic acid as linker that coordinate Zn_4O_{13} paddle wheel units as inorganic component. The inorganic building block, the paddle wheel unit, consists of tetrahedrons of Zn and O is also often referred to as secondary building unit (SBU). MOF-5 crystallizes in a cubic crystal system with the space group Fm-3m. The structure will become more important, when we look at the light-switchable MOFs, which will be discussed later in this thesis.
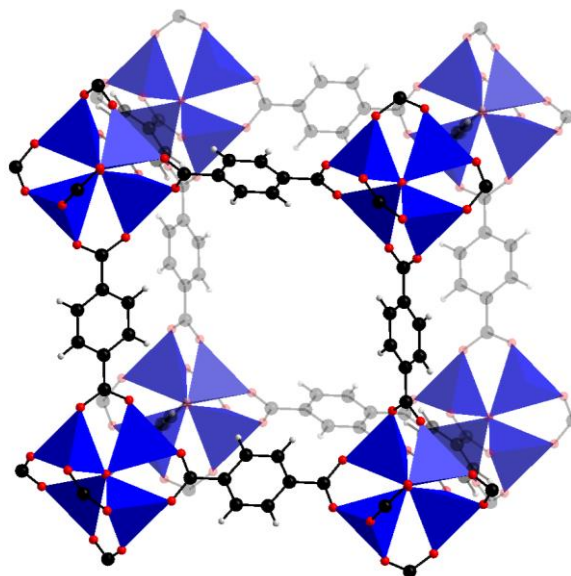
Figure 8 *The crystal structure of MOF-5 or sometimes called IRMOF-1 (isoreticular MOF 1), one of the first MOFs to be found by YAGHI et al.; from CCDC number 256965 (Cambridge Crystallographic Data Centre).[69] Colour code: H grey, C black, O red, Zn-O coordination tetrahedrons blue.*

The different building units of the MOFs allow the introduction of a lot of interesting functionalization. There are three possibilities to improve MOFs without changing the crystal structure significantly (also, c.f. Figure 9):

- *Metal node:* The metal-ions can be exchanged within the frameworks, for example Zn^{2+} ions in the paddle wheel unit, found in several structures, can easily be exchanged to Cu^{2+} improving/decreasing the stability against e.g. moisture and temperature.[72]

- *Linker:* The organic component can be different (isoreticular synthesis), for example terephthalic acid (H$_2$BDC) can be exchanged to 4,4'-biphenyldicarboxylic acid (H$_2$BPDC), changing the physical properties of the MOF; however, also derivatives of the terephthalic acid containing amine, carboxylate, di-carboxylate, or nitrate groups are possible and favour adsorption of different molecules compared to the bare backbone molecule.[67,73] The exchange of the coordinating group from carboxyl to nitrile or thiol groups can lead to electrical conductivity, a property that was introduced to MOFs just recently.[74,75] However, functionalization of the linker can also lead to topological changes in the crystal lattice.[76]

- *Cavity:* The pore or cavity is the empty space inside the MOF, which can take up/release gases or liquids via adsorption/desorption. Of course, MOFs are not only useful for guest uptake, but can also be a host system for functional species, such as azobenzene (AZB) with light switchable functionality.[48,77] Other publications prepared MOFs with metal nanoparticles synthesized inside the pores.[78]
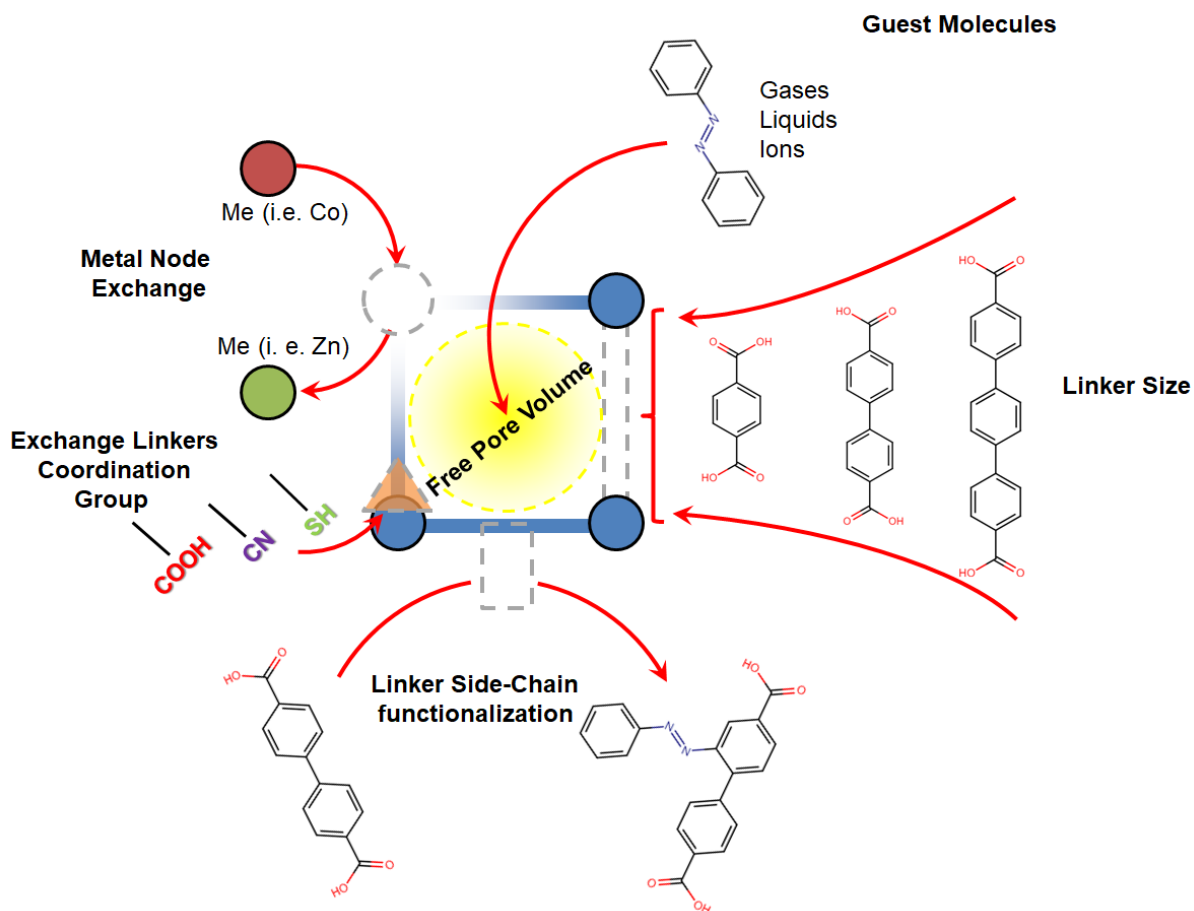
Figure 9 *Stripping the MOF down to its private parts gives us the overview of the functional building units of the MOFs structure that can be utilised to change its properties.*

Additionally, it is possible to do the functionalization of linker and metal-nodes, as well as the introduction of guests into the free pore volume by post-synthetic approaches.[79] However, it was found that a pre-synthetic functionalization of the building units of the crystal lattice, meaning metal-nodes and linkers, is often more beneficial and a lot easier.[80] On the other hand, occupying the free pore volume after the synthesis ensures correct formation of the framework and a lower amount of defects. Sometimes, MOFs are also responsive to guest molecules, which allows determination of the adsorbed molecules or atoms and a use as sensor material.[77,81]

1.5.   Important MOF Structures and their Properties

Within this work, a few MOF structures are of particular interest and it is important to for the understanding of this thesis and the publications it is based on. This chapter will give a deeper insight.

1.5.1. MOF-5 and the IRMOF Series

As already discusses in chapter 1.2., the original pillar-layer structure of the MOF-5 is easy to exchange with different linkers and opens up an easy way to introduce side-chain functionalities to one of the most investigated MOF structures. However, if the Zn from the Zn-paddle wheel is exchanged with Cu, the MOFs stability can increase.[82] The original MOF-5 with Zn as metal-node showed an extremely rapid degradation at humid air, and was destroyed within 3-5 days.[83] The mobility in this framework is high and, for instance rotation, is energetically cheap.[84] This makes it possible to synthesise MOFs with switchable units in its structure without steric hindrance.[60,61] These MOFs are a perfect example for the tailoring of the framework: We exchange Zn in the structure of MOF-5 by Cu, afterwards we use two different length of linker, one as pillar, the other one in the layer, both with a side chain functionality; Obviously, through applying an intelligent synthesis, tailor-made MOFs can be designed for the desired purpose. In Figure 10 the light-switchable pillared-layer MOF Copper-azo-4,4′-benzophenonedicarboxylate-azo-4,4′-bipyridine (Cu-AzoBPDC-AzoBiPy) is shown with a side-chain functionality at each of the linkers and enough space for it to switch between the cis-trans isomers.[48] The windows of the MOFs are cubic shaped with around 8-12 Å diameter and the structure reminds of a cubic primitive cell, too.[61]

trans-AZB   *cis*-AZB
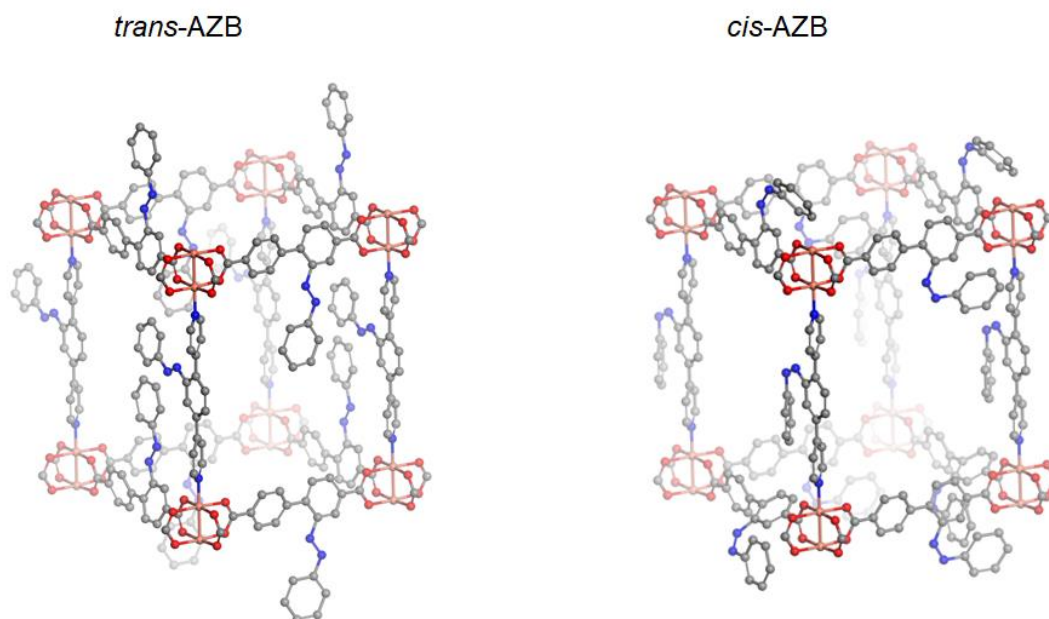
Figure 10 *A 3D image showing the pillared-layer MOFs used for the first photoswitchable MOF membrane with AZB side-chain function, given here in trans and cis conformation (left and right).[61] The structure is the same that the IRMOF series occupies.*

Not many applications for these light-switchable pillared-layer MOFs are reported yet, but there are some: For instance, these photoresponsive MOFs have shown to be interesting for medical application, where light is a source of stimuli easy to apply on a patient. This allows a triggered release of medics from molecular containers.[55] It also not the first switchable example for AZB in porous materials. In zeolites, the photoinduced control over the pore system was achieved with AZB guest and surface-adsorbed molecules.[85,86] With AZB guest molecules, the porosity can also be switched in MOFs, for example in MIL-53 or UiO-67.[48,77]

1.5.2. Zr-Based Metal-Organic Frameworks

MOFs with Zr-ions in their structures, for example MIL-140 and the isoreticular UiO (UiO – Universitetet i Oslo) series, have gained interest due to their extreme high thermal and chemical stability.[87,88] The group of the UiO MOFs are most likely not to exhibiting the freedom of mobility for big side-chains as previously shown for the IRMOFs.[80,88,89] The lattice of UiO-66 and UiO-67 crystallize in the same space group, only the size and volume of the unit cell, and thus the volume of the cavities is different due to the lengths of the linker molecules H_2BDC and H_2BPDC. The unit cells of the MOF are shown in Figure 11. The crystal structure for UiO-66 and UiO-67 have been solved in 2011 and 2014 by researches from the University of Oslo.[90,91] The MOFs are made of SBUs consisting of $Zr_6O_4(OH)_4$ clusters coordinated by 12 $-CO_2$ units each and their pore windows are always trigonally

shaped.[92] The window size of UiO-66 is 5-7 Å due to the linkers rotational freedom, while the trigonal opening of the UiO-67 is around 7-9 Å.[93,94] These MOFs are already deeply investigated and its formation mechanisms were already investigated in an oscillatory chemical clock experiment.[95] Additionally, and probably going hand in hand with the understanding of the crystallization progress, the use of different solvents and additives allow a defect-engineering of the structure during the crystallization of the MOFs, leading to defined doping with missing linker defects.[88,96]
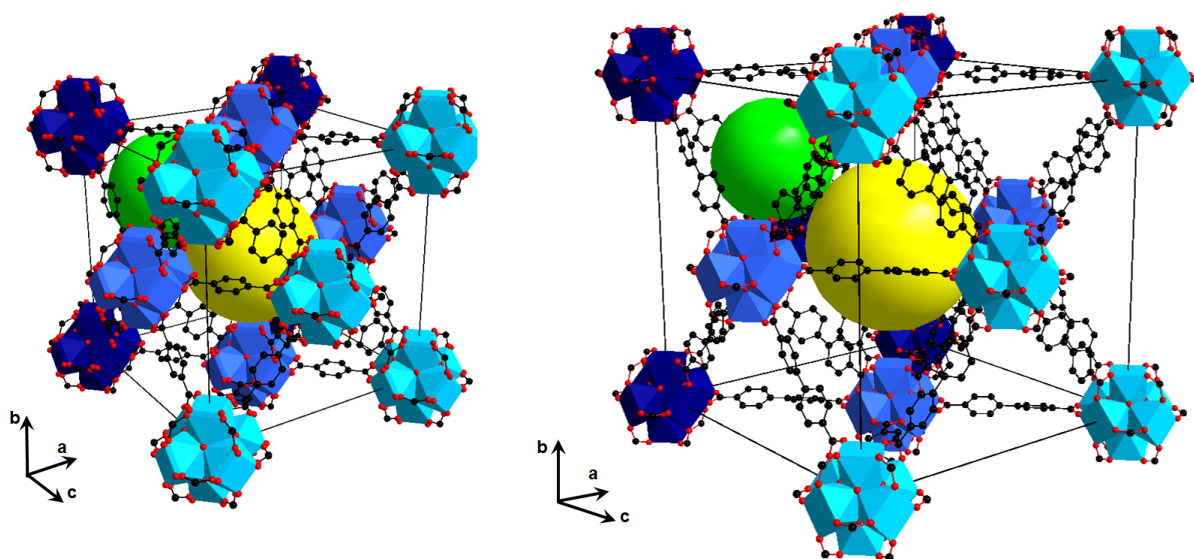
Figure 11 *UiO-66 (left) and UiO-67 (right), the different blue colors of the secondary Zr-building units are chosen to illustrate the lattice planes they are lieing in. The yellow and green balls are used to visualize the cavities, differing volume in each of the MOFs. Color code: O red, C black, H is hidden.*

1.5.3. The Structure of HKUST-1

Another important structure is the structure of HKUST-1 (Hong Kong University of Science and Technology Framework 1), which has Cu^{2+} paddle-wheel units as SBUs again. This MOF is one of the most investigated structures, too. The crystallization of HKUST-1 and the growth can be achieved by self-assembly at room temperature and can form up to mm-sized crystals. Thus, the MOFs crystallization was monitored in situ by atomic force microscopy, revealing real time crystallization and defect incorporation while the crystal is growing.[97] The structure is shown in Figure 12 and was firstly discovered by CHUI and co-workers in 1999.[98] The SBUs are $[Cu_3(BTC)_2(H_2O)_3]_n$ and are bridged via a Cu-Cu couples. The structure in the case of HKUST-1 relies on trimesic acid (H_3BTC) as linker molecule with three caboxyl groups (tri-dentate) coordinating three metal centres at a time, being sufficiently more rigid than bi-dentate linker molecules. In the structure we find honeycomb

arranged hexagonally shaped channels in the (111) direction with a diameter of 18.6 Å and in (100) direction four-fold symmetric channels with 9.5 Å diameter.[98] The HKUST-1 from a solvothermal synthesis always yielded crystals with a blue colour, which is known to originate from defects through the formation. WÖLL et al. could produce defect free layers by liquid phase epitaxy of HKUST-1 which were completely transparent and colourless, not exhibiting any colour centres.[58]
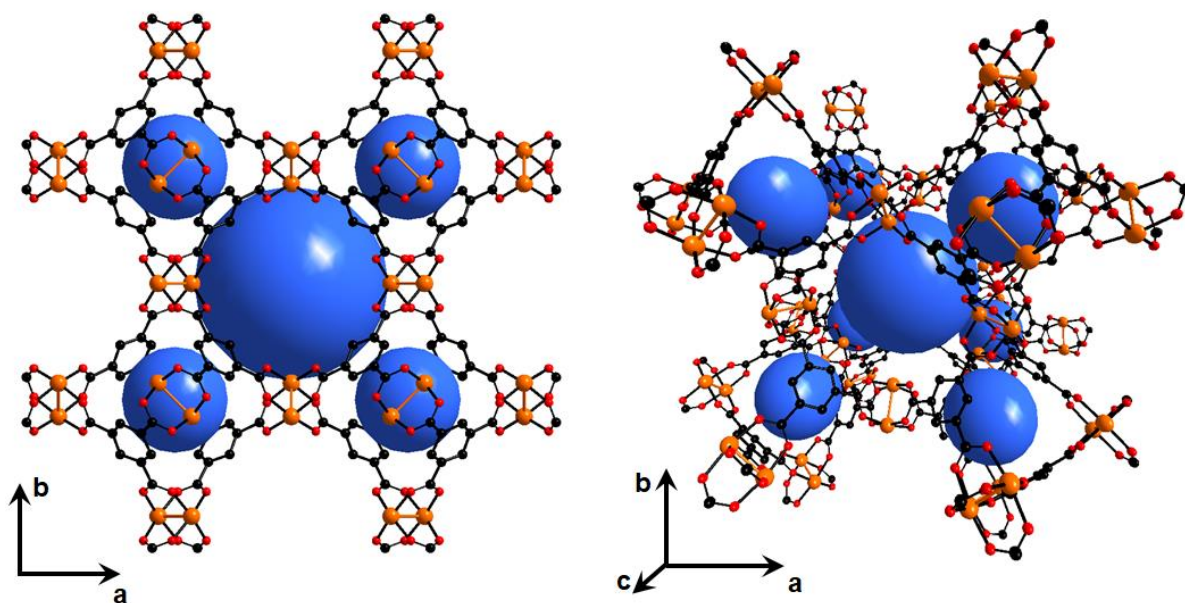
Figure 12 *HKUST-1 structure viewing from the c-direction (111) on the a,b plane (left). On the right a perspective illustration is given. To give a good overview of the pores in the structure the light blue balls were introduced into the structure. The middle ball shows the big cavity, while the eight other balls show the smaller cavities. Colour code: Cu orange, O red, C black, H hidden.*

Even if this structure has a rigid nature, a lot of very interesting findings are reported for the HKUST-1 framework. Recently, it was shown that although this MOF is more rigid compared to other MOFs it still exhibits a decent amount of elasticity, however, no breathing or rotation of linkers is possible.[99] Anyway, flexibility research and "breathing" phenomena[100] are rather new and it is not totally clear how these are affecting the properties of MOFs.

1.5.4. Zeolitic Imidazolate Frameworks – Unique Materials

The last, but probably most important MOF structures within this thesis are the structure of ZIFs, short for zeolitic imidazolate frameworks, first discovered by YAGHI et al. in 2006.[101] In more detail I want to explain the probably most important structure within the ZIFs, which is ZIF-8. The ZIFs in general exhibit very high chemical and thermal stability and additionally the pore sizes of some of them should be capable of molecular sieving.[66,101] The ZIFs make

up a subclass of MOFs and were given their name because of the fact that they are isomorph to Zeolite topologies. The bond angle in ZIF materials of 145 ° between Me-imidazolate-Me is similar to the Si-O-Si bond angle in Zeolites, whereas the Me-ion in ZIFs can be Zn, Co, Cu and some others. The most important ZIF structure is ZIF-8, which is the most investigated ZIF material and crystallizes in the sodalite (SOD) structure with the space group I-43m. ZIF-8 is made of Zn^{2+} and 2-methylimidazole (Hmim) and has a wider, hexagonal pore-window with an average aperture of 3.4 Å and a smaller cubic pore window with an estimated diameter of 1.5-2 Å, whereas the latter one is too small to take part in gas transport. The diameter of the cavity in ZIF-8 is 11.6 Å.[101] The structure is shown in Figure 13.
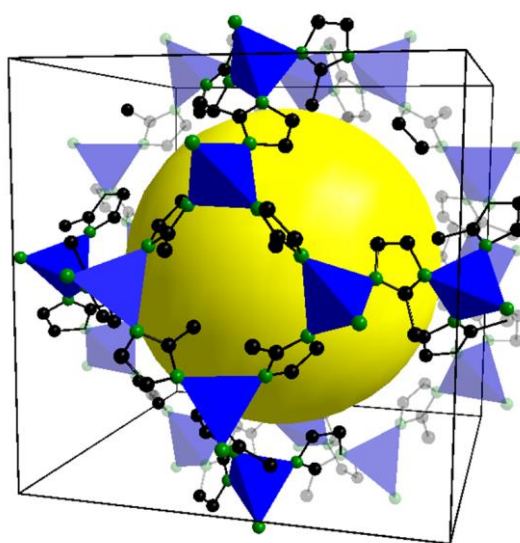
Figure 13 *The ZIF-8 structure. The Zn metal nodes are connected by N atoms from the methyl imidazolate linkers, forming four- and six-membered rings, which are the pore windows. The yellow ball in the middle shows the free pore volume. The space group is I-43m, which is cubic. Colour code: C black, N green, H hidden.*

During the years, people found a lot of anomalous behaviour for ZIF-8. An older example for that would be the phase transformation under high pressure, reported by MOGGACH et al. in 2009.[102] The flexibility of this framework is an outstanding example for the soft-porosity in these crystalline materials in general.[103] RYDER et al. just recently demonstrated shear deformation, soft-modes and gate-opening in THz spectroscopy experiments.[104] The latter effect was already known before and is the reason why ZIF-8 is not a real molecular sieve.[105,106] Later in this thesis the flexibilities will be investigated deeper.

1.6.   Metal-Organic Frameworks Materials – Fields of Innovation

Since 1999 people have started synthesizing a huge amount of MOFs and so far 7 % of the structures deposited in the Cambridge Crystallographic Data Centre, overall 61.000 structures, are MOFs, following the definition of the MOF Commission of the International Zeolite Association (IZA) for the search. Other sources state that there are more than 100.000 synthesised structures known to date.[107] To choose amongst this nearly infinite amount of MOFs, or to decide if it is important to synthesise a new one, it is mainly depending on the desired application:

MOFs are extremely light-weight and highly porous, placing them amongst the materials with the lowest densities known to date. MOFs are also world record holding materials in terms of inner surface areas with up to 7000 m²/g, and theoretically possible inner surface areas of up to 14000 m²/g.[108] Thus, it is no wonder that MOFs are highly interesting for adsorptive processes and one of the first industrial applications is water storage and release, driven by the BASF.[109,110] But also, a lot of research interest was storage of gases, such as H_2[111], and CH_4 in fuel-tanks[112].

But MOFs are also applied in other fields, for example microelectronics.[113] Researchers try to use the properties of high porosity and crystallinity for electronic applications, such as memristors[114], size-selective sensor devices[57], as low κ-dielectrics for capacitors and for capacitive sensing[115], and many other electric applications.[116] For a long time, electronic applications of MOFs have caused big problems, because they are almost only neither conductive materials, nor semi-conductors, which is was clearly shown in band gap calculations.[117] Recent development introduced conductivity to MOFs: Linkers were designed with -CN as coordinative units, where conductivity can be switched between high and low resistance states[75], or with -SH groups along with coordinated π-systems, leading to a conductivity throughout the whole framework.[74]

More and more possible applications are found within the field of MOFs and another example for this is catalysis. In a recent review, possible ways for catalytic centres are described, for instance using open metal-sites, which can be found in MOF-74 or HKUST-1; but also defect sites can be found or intentionally introduced to the frameworks of MOFs, where single-site catalysis can take place. With modern electron microscopy it is also possible to take images and characterize the defect sites.[118] A very prominent example therefore would be the Zr-based framework UiO-66 and its isoreticular analogue UiO-67 and UiO-68, which

are capable of controlled defect engineering as shown in Figure 14.[119,120] However, to perform catalysis with MOFs a better working way is the intentional utilization of the materials' weakness: The carbonization of MOFs leads to very clean and oriented scaffold for the production of catalysts. Very high quality nanoparticle assemblies on carbon support can be derived from MOF networks, for instance from Co containing MOFs, which then serve as amination catalyst.[121]
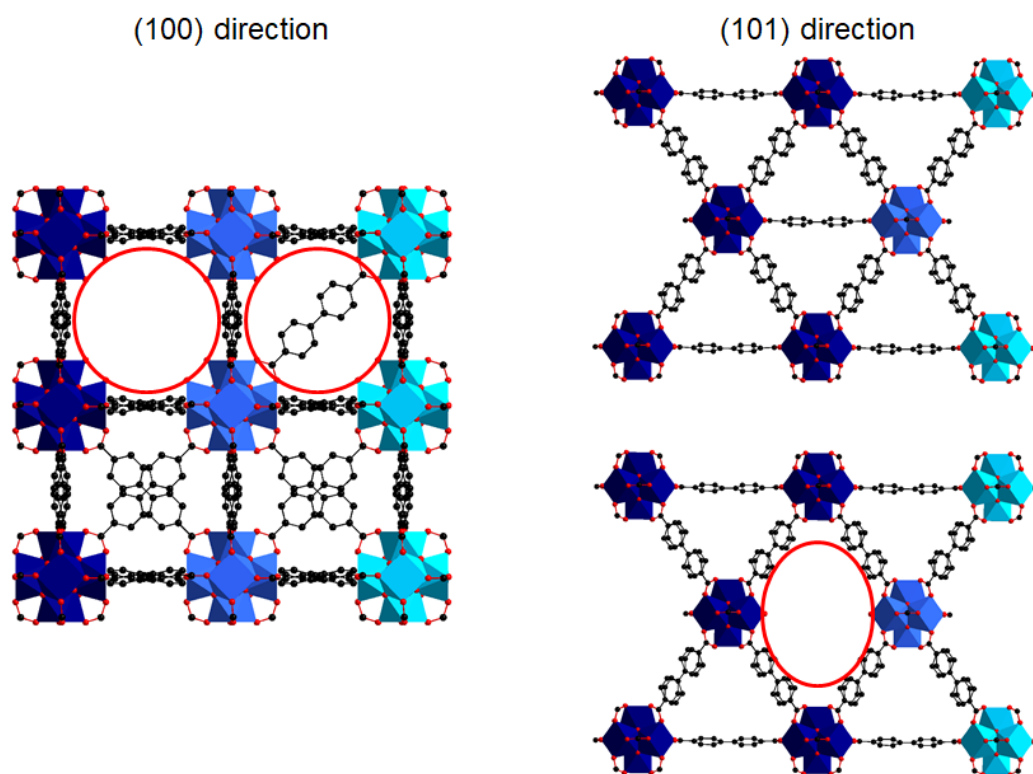
Figure 14 *Possible missing linker defects in UiO-67, which can be shown by TEM imaging.[96,122] The red circles give the positions for the missing linkers. Colour code: O red, C black, H hidden. The different coloured SBUs show the different lattice planes. Using missing linkers can change the electronic properties of the MOF, opens opportunities for electrical applications and brings changes to flexibility.[123]*

Coming back to the scope of this work, the intrinsic material properties are interesting for continuous separation processes, in our case for membrane separation. In membrane technology, MOFs are bridging a gap between pure polymeric membranes and inorganic membranes, for example porous silica or zeolites.[124] On the one side, MOFs have a defined crystal structure and exhibit a constant porosity like inorganic materials, on the other side they are in-between rigid and flexible due to their organic component. These properties make them extremely suitable for being grown on ceramic supports, forming crystalline layers and their use as neat MOF membrane, but their organic component also allows good integration into

polymeric matrices.[125] Different techniques have evolved in the field of membrane production besides the solvothermal synthesis and different coating processes emerged.[51,52] However, especially the flexibility exhibited by many MOF structures is often a hindrance regarding continuous membrane separation. MOFs can have extremely tailored pore opening diameters and they can be tailored in a size range that is capable of molecular sieving of gas molecules and was long believed to actually take place.[66] But they are not reaching the expected values for the separation of gases from their critical diameter.[45,105] The reason for this lies in the flexibility.

1.7. The Flexibility of Metal-Organic Frameworks – A Serious Issue

MOFs were thought to be the ideal crystals for several applications for a long time, especially for separation. They were supposedly tuneable molecular sieves with very narrow pores, such as zeolites, but with more structural possibilities.[126] A lot of publications in the field of gas separation with MOFs were weaving around with phrases like "finally achieved molecular sieving" et cetera.[66,127] Today we know that molecular sieving is not possible with MOFs for a simple reason: They exhibit many lattice motions as for example the linker rotations (see also Figure 15), vibrations, gate-opening, shear deformations, and soft-modes, which were first studied for the Hmim linkers in the ZIF-8 framework by RYDER et al. through THz spectroscopy.[104]
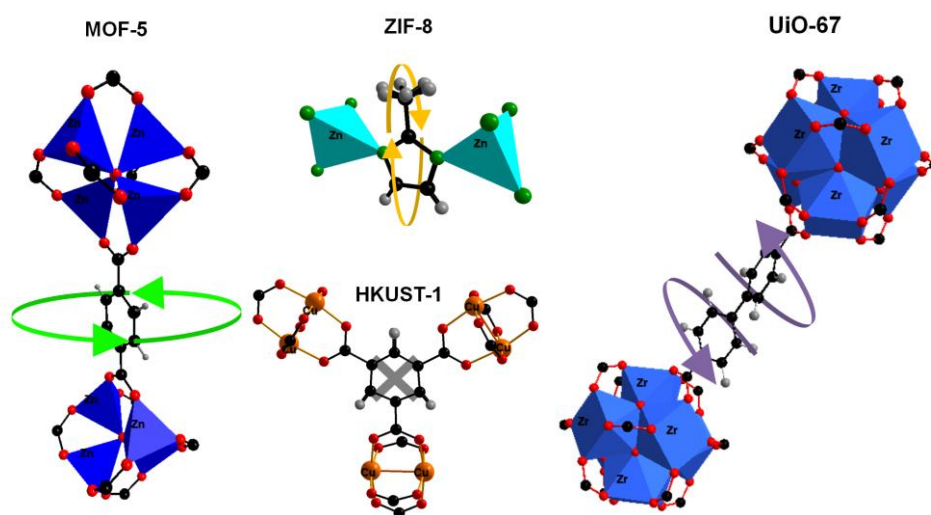
Figure 15 *One of the most unavoidable motions in bi-dentate linked MOFs is the rotation shown here for MOF-5, ZIF-8, UiO-67. In HKUST-1, which has a tri-dentate linker, no rotational motions are possible. However, HKUST-1 shows some very significant elasticity.[99]*

THz spectroscopy is also performed by RYDER et al. for more and more MOFs, amongst them HKUST-1, for which they described the elasticity for the first time in 2016.[99] Also the flexibility in the Zr-based structures could be demonstrated for isoreticular UiO or MIL-140 structures.[88] However, the pore-limiting diameter is at least influenced by 1.5-2 Å through the rotations, which is the length of the ring plus the hydrogen atom attached to it. Often, the rotation also contributes to a gate-opening, like in ZIF-8.[128] Especially looking at separation, the pore-limiting diameter of 3.4 Å in ZIF-8 is almost negligible, because it was found that very big molecules, more than double the pore-limiting diameter, can pass through that pore.[45,105] This emerges through the rotational motion of the linker and the gate-opening[102], sometimes also referred to as breathing, which was investigated deeply by KOLOKOLOV and STEPANOV.[93,106] Of course, up to some point, size selectivity in gas separation is reached by the ZIF SOD structures.[129] Nevertheless, they are not reaching their supposed potential in gas separation.

The effect of "breathing" is defined for huge crystal lattice distortion upon guest-uptake or external stimuli. There are MOFs, like MIL-53, that are highly flexible, as visualized in Figure 16 and their changes induced by guest molecules are visible in the XRD.[130,131] Then, there are MOFs like ZIF-8 that exhibit some sort of breathing, as discussed so far, but this is defined as gate-opening, also known from crystal structural analysis.[102] So far, per definition, ZIF-8 is rather doing a "gate-opening" than "breathing" effect, but the definition is not completely clear. What we conclude is that all sorts of flexibility have a high impact on the separation also in rigid metal-organic frameworks.[132]

Nevertheless, external stimuli are rarely used to trigger breathing. As explained earlier, pressure could be used, but just recently a theoretical study reports that electric fields could lead to breathing in MIL-53[133], which was published while our paper on experimental evidence "*Defibrillation of soft-porous metal-organic frameworks with electric fields*" was still under review.[134]

MIL-53(Al) closed pores   MIL-53(Al) open pores
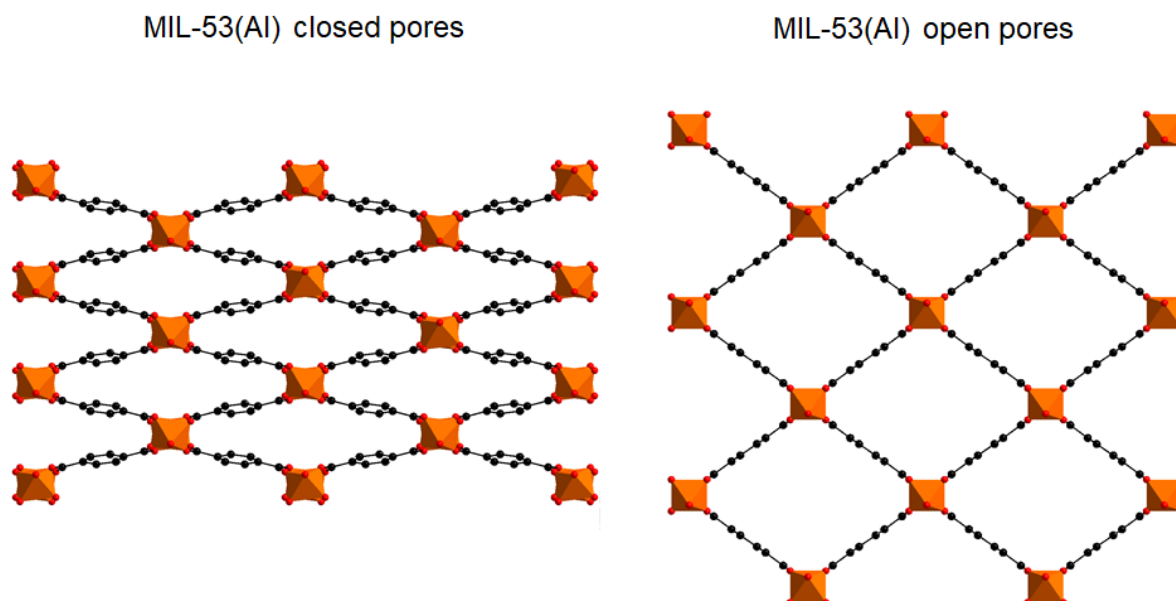
Figure 16 *A crystallographic visualization of the breathing from the pore-closed (left, CCDC 1004911) to the pore-open form (right, CCDC 1004912) of the one dimension porous MIL-53 (Al). View from the c-direction. Colour code: O red, C black, Al octahedral orange, H is hidden.*

This is a good example on how to alter intrinsic properties of MOFs with external stimuli, in this case the gate-opening or the breathing behaviour. There are papers reporting also phase transitions of MOFs under the influence of an electrical current, for example using Cu(TCNQ), a two dimension non-porous coordination polymer (CP).[135] However, this is a slightly different case, but still proves the hypothesis: This CP switches its conductivity under an electrical current by phase transition.[75] The flexibility is an issue that limits the materials properties, especially for application in separation, and external stimuli like light and electric fields could be the key to make bad effects positive. Anyways, in case of Cu(TCNQ), but also in our case of the "defibrillation" of ZIF-8 it is possible to exploit the flexibility.

1.8.   Switchable MOF Materials – Smart Properties

Many smart materials have been developed so far and are widely applied in our everyday life, for instance shape memory alloys in medical applications[136] such as stents[137] or chromogenic windows that change their transparency by applying an electrical current.[138] Applying smart properties to MOFs is a tough challenge, but is recently finding much attention in the MOF research community.[139] External stimuli are used to modify the properties of MOFs, utilizing the different building units and can lead to different types of switching as illustrated in Figure 17.
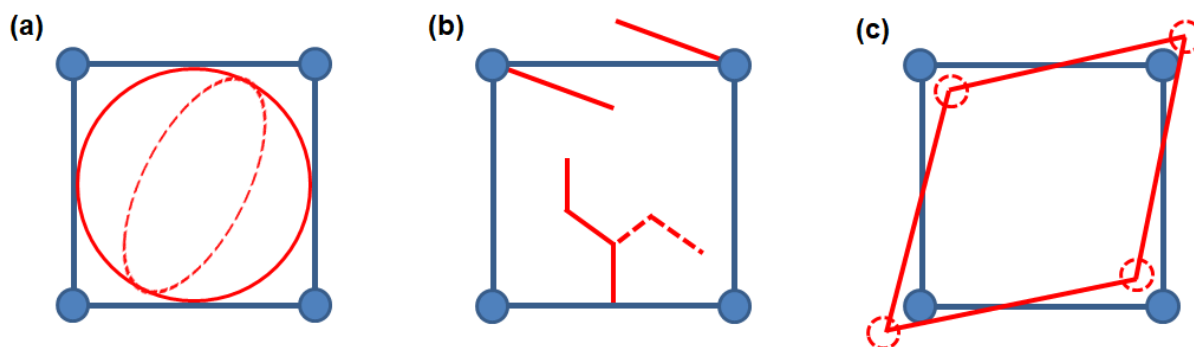
Figure 17 *The three common ways of how to utilize the MOF through applying of external stimuli. In (a) the guest control over the pore is imaged, (b) molecular switches in the MOF linkers and in (c) possible lattice distortions are shown.*

Using light as external stimuli, all of the above mention ways on controlling the porosity of the MOF are possible. There are MOFs with azobenzene linkers in the backbone, but these were not switchable by light.[140] Nevertheless, not all of the MOFs with side-chain functionality were switchable by light, even if the linker molecule itself shows switchability.[141] However, when using the right crystalline structure of the MOF, the steric hindrance reported for the other systems could be overcome and switching was achieved.[55,56,60,61] Also using guest molecules with lightswitching abilities led to switching of the types (a)[48] and (c)[77]. With post-synthetic functionalization of the MOFs backbone, there is the possibility to literally introduce light-switches, which work by breaking and forming bonds through UV/Vis-irradation.[142]

When using electrical stimuli, for example electrical currents, MOFs can be switched in their crystal structure, in conjunction with type (c) of switching abilities. Exemplarily, the non-porous coordination polymer Cu(TCNQ) - upon applying an electrical field and current - undergoes a bistable switching between its more and less conductive phases, leading to possible applications in memory devices.[135] Thinking of crystals in an electric field, the most obvious possible idea is piezo- or more general ferroelectricity, which can be achieved by applying chiral linker molecules, forming non-centrosymmetric unit cells.[143] But also guest molecules acting as molecular rotors inside the pore of a 1D MOF (MOF-74) can be aligned in an electric field, then acting as molecular gates. The gate is closed, when the electric field is not applied, and opens when the electric field is sufficiently strong enough to align the dipolar molecule inside the MOF.[144] However, through the fact, that MOFs are often porous, the unit cell is free to be distorted also without a non-centrosymmtric unit cell. With electric fields, the ions in the MOF structure can be distorted, which was shown by theoretical

calculations to the breathing of the MOF MIL-53.[133] There is only one problem: The calculated values are much higher than the breakthrough voltage: The voltage where a dielectric medium get so strongly polarized and ionised that the arc breaks through. We conducted the first study towards the behaviour of the porous structure of a MOF in an electric field, which will certainly lead to more and more research in this topic.[134] This leads us to the main part of this thesis, starting with a review to the external stimuli responsive materials, especially for separation purposes. Chapter 2 will give a deep insight into all kind of smart materials in gas separation with special focus on smart MOF systems.

REFERENCES

1. Figueroa, J. D., Fout, T., Plasynski, S., McIlvried, H. & Srivastava, R. D. Advances in CO_2 capture technology—The U.S. Department of Energy's Carbon Sequestration Program. *Int. J. Greenh. Gas Con.* **2,** 9–20 (2008).

2. Baker, R. W. Future Directions of Membrane Gas Separation Technology. *Ind. Eng. Chem. Res.* **41,** 1393–1411 (2002).

3. Awad, A. H. & Veziroglu, T. N. Hydrogen versus Synthetic Fossil Fuels. *Int. J. Hydrog. Energy* **9,** 355–366 (1983).

4. Kreuer, K. D. On the development of proton conducting polymer membranes for hydrogen and methanol fuel cells. *J. Mem. Sci.* **185,** 29–39 (2001).

5. Bennaceur, K. *et al.* Hydrogen: A Future Energy Carrier? *Oilfield Rev.* (2005).

6. Dunn, S. Hydrogen futures: toward a sustainable energy system. *Int. J. Hydrog. Energy* **27,** 235–264 (2002).

7. Haszeldine, R. S. Carbon Capture and Storage: How Green can Black Be? *Science* **325,** 1647–1652 (2009).

8. Kanniche, M. *et al.* Pre-combustion, post-combustion and oxy-combustion in thermal power plant for CO_2 capture. *Appl. Therm. Eng.* **30,** 53–62 (2010).

9. Sanz-Pérez, E. S., Murdock, C. R., Didas, S. A. & Jones, C. W. Direct Capture of CO_2 from Ambient Air. *Chem. Rev.* **116,** 11840–11876 (2016).

10. Kenarsari, S. D. *et al.* Review of recent advances in carbon dioxide separation and capture. *RSC Adv.* **3,** 22739 (2013).

11. Dyer, P. Ion transport membrane technology for oxygen separation and syngas production. *Solid State Ion.* **134,** 21–33 (2000).

12. Lackner, K. S. A Guide to CO_2 Sequestration. *Science* **300,** 1677–1678 (2003).

13. Alders, M., Winterhalder, D. & Wessling, M. Helium recovery using membrane processes. *Sep. Purif. Technol.* **189,** 433–440 (2017).

14. Schrier, J. Helium Separation Using Porous Graphene Membranes. *J. Phys. Chem. Lett.* **1,** 2284–2287 (2010).

15. Robeson, L. M. The upper bound revisited. *J. Mem. Sci.* **320,** 390–400 (2008).

16. Zakaria, Z. & Kamarudin, S. K. Direct conversion technologies of methane to methanol: An overview. *Renew. Sust. Energ. Rev.* **65,** 250–261 (2016).

17. Rabelo, S. C., Carrere, H., Maciel Filho, R. & Costa, A. C. Production of bioethanol, methane and heat from sugarcane bagasse in a biorefinery concept. *Biores. Technol.* **102,** 7887–7895 (2011).

18. U.S. Department of Energy, Office of Energy Efficiency and Renewable Energy. Materials for Separation Technologies: Energy and Emission Reduction Opportunities, 2005.

19. Worrell, E., Phylipsen, D., Einstein, D. & Martin, N. Energy use and energy intensity of the U.S. chemical industry, 2000.

20. Alcántara-Avila, J. R., Gómez-Castro, F. I., Segovia-Hernández, J. G., Sotowa, K.-I. & Horikawa, T. Optimal design of cryogenic distillation columns with side heat pumps for the propylene/propane separation. *Chem. Eng. Process.* **82,** 112–122 (2014).

21. Sircar, S. Pressure Swing Adsorption. *Ind. Eng. Chem. Res.* **41,** 1389–1392 (2002).

22. Baker, R. W. & Low, B. T. Gas Separation Membrane Materials: A Perspective. *Macromolecules* **47,** 6999–7013 (2014).

23. Krishna, R. & Wesselingh, J. A. The Maxwell-Stefan approach to mass transfer. *Chem. Eng. Sci.* **52,** 861–911 (1997).

24. Troeh, F. R., Jabro, J. D. & Kirkham, D. Gaseous diffusion equations for porous materials. *Geoderma* **27,** 239–253 (1982).

25. Scott, D. S. & Dullien, F. A. L. Diffusion of ideal gases in capillaries and porous solids. *AIChE J.* **8,** 113–117 (1962).

26. Malek, K. & Coppens, M.-O. Knudsen self- and Fickian diffusion in rough nanoporous media. *J. Chem. Phys.* **119,** 2801–2811 (2003).

27. Bosch, A. T. Kinetic theory of gas separation in a nanopore and comparison to molecular dynamics simulation. *J. Chem. Phys.* **122,** 84711 (2005).

28. Barrer, R. M. Porous crystal membranes. *Faraday Trans.* **86,** 1123 (1990).

29. Millington, R. J. Gas Diffusion in Porous Media. *Science* **130,** 100–102 (1959).

30. Wu, T. & Zhang, D. Impact of Adsorption on Gas Transport in Nanopores. *Sci. Rep.* **6,** 23629 (2016).

31. Gunn, R. D. & King, C. J. Mass transport in porous materials under combined gradients of composition and pressure. *AIChE J.* **15,** 507–514 (1969).

32. Shelekhin, A. B., Dixon, A. G. & Ma, Y. H. Theory of gas diffusion and permeation in inorganic molecular-sieve membranes. *AIChE J.* **41,** 58–67 (1995).

33. Kapteijn, F., Moulijn, J. A. & Krishna, R. The generalized Maxwell–Stefan model for diffusion in zeolites. *Chem. Eng. Sci.* **55,** 2923–2930 (2000).

34. Leonardi, E. & Angeli, C. On the Maxwell-Stefan approach to diffusion: a general resolution in the transient regime for one-dimensional systems: A general resolution in the transient regime for one-dimensional systems. *J. Phys. Chem. B* **114,** 151–164 (2010).

35. Koros, W. L., Ma, Y. H. & Shimidzu, T. Terminology for Membranes and Membrane Processes. *Pure & Appl. Chem.* **68,** 1479–1489 (1996).

36. Chen, Y., Jia, M., Xu, H., Cao, Y. & Fan, H. Counterintuitive Gas Transport through Polymeric Nanocomposite Membrane: Insights from Molecular Dynamics Simulations. *J. Phys. Chem. C* **118,** 28179–28188 (2014).

37. Dechnik, J., Gascon, J., Doonan, C. J., Janiak, C. & Sumby, C. J. Mixed-Matrix Membranes. *Angew. Chem. Int. Ed.* **56,** 9292–9310 (2017).

38. Noble, R. D. Perspectives on mixed matrix membranes. *J. Mem. Sci.* **378,** 393–397 (2011).

39. George, S. C. & Thomas, S. Transport phenomena through polymeric systems. *Prog. Poly. Sci.* **26,** 985–1017 (2001).

40. Ghosal, K. & Freeman, B. D. Gas separation using polymer membranes: An overview. *Polym. Adv. Technol.* **5,** 673–697 (1994).

41. Javaid, A. Membranes for solubility-based gas separation applications. *Chem. Eng. J.* **112,** 219–226 (2005).

42. Wijmans, J. G. & Baker, R. W. The solution-diffusion model: A review. *J. Mem. Sci.* **107,** 1–21 (1995).

43. Bétard, A. *et al.* Fabrication of a CO_2-selective membrane by stepwise liquid-phase deposition of an alkylether functionalized pillared-layered metal-organic framework [Cu2L2P]n on a macroporous support. *Micropor. Mesopor. Mater.* **150,** 76–82 (2012).

44. Knebel, A. *et al.* Comparative Study of MIL-96(Al) as Continuous Metal-Organic Frameworks Layer and Mixed-Matrix Membrane. *ACS Appl. Mater. Interfaces* **8,** 7536–7544 (2016).

45. Diestel, L., Bux, H., Wachsmuth, D. & Caro, J. Pervaporation studies of n-hexane, benzene, mesitylene and their mixtures on zeolitic imidazolate framework-8 membranes. *Micropor. Mesopor. Mater.* **164,** 288–293 (2012).

46. Kwon, H. T. & Jeong, H.-K. Improving propylene/propane separation performance of Zeolitic-Imidazolate framework ZIF-8 Membranes. *Chem. Eng. Sci.* **124,** 20–26 (2015).

47. Li, W. *et al.* Ultrathin metal-organic framework membrane production by gel-vapour deposition. *Nat. Commun.* **8,** 406 (2017).

48. Knebel, A. *et al.* Azobenzene Guest Molecules as Light-Switchable CO_2 Valves in an Ultrathin UiO-67 Membrane. *Chem. Mater.* **29,** 3111–3117 (2017).

49. Fan, L., Xue, M., Kang, Z., Li, H. & Qiu, S. Electrospinning technology applied in zeolitic imidazolate framework membrane synthesis. *J. Mater. Chem.* **22,** 25272 (2012).

50. Jiang, D., Burrows, A. D., Xiong, Y. & Edler, K. J. Facile synthesis of crack-free metal–organic framework films on alumina by a dip-coating route in the presence of polyethylenimine. *J. Mater. Chem. A* **1,** 5497 (2013).

51. Chernikova, V., Shekhah, O. & Eddaoudi, M. Advanced Fabrication Method for the Preparation of MOF Thin Films: Liquid-Phase Epitaxy Approach Meets Spin Coating Method. *ACS Appl. Mater. Interfaces* **8,** 20459–20464 (2016).

52. Hurrle, S. *et al.* Sprayable, Large-Area Metal-Organic Framework Films and Membranes of Varying Thickness. *Chem. Eur. J.* **23,** 2294–2298 (2017).

53. Shekhah, O. *et al.* The liquid phase epitaxy approach for the successful construction of ultra-thin and defect-free ZIF-8: Pure and mixed gas transport studymembranes. *Chem. Commun.* **50,** 2089–2092 (2014).

54. Summerfield, A., Cebula, I., Schröder, M. & Beton, P. H. Nucleation and Early Stages of Layer-by-Layer Growth of Metal Organic Frameworks on Surfaces. *J. Phys. Chem. C* **119,** 23544–23551 (2015).

55. Heinke, L. *et al.* Photoswitching in two-component surface-mounted metal-organic frameworks: Optically triggered release from a molecular container. *ACS Nano* **8,** 1463–1467 (2014).

56. Heinke, L., Gu, Z. & Wöll, C. The surface barrier phenomenon at the loading of metal-organic frameworks. *Nat. Commun.* **5,** 4562 (2014).

57. Heinke, L., Tu, M., Wannapaiboon, S., Fischer, R. A. & Wöll, C. Surface-mounted metal-organic frameworks for applications in sensing and separation. *Micropor. Mesopor. Mater.* **216,** 200–215 (2015).

58. Müller, K. *et al.* Defects as Color Centers: The Apparent Color of Metal-Organic Frameworks Containing Cu^{2+}-Based Paddle-Wheel Units. *ACS Appl. Mater. Interfaces* **9,** 37463–37467 (2017).

59. Valadez Sánchez, E. P., Gliemann, H., Haas-Santo, K., Wöll, C. & Dittmeyer, R. ZIF-8 SURMOF Membranes Synthesized by Au-Assisted Liquid Phase Epitaxy for Application in Gas Separation. *Chem. Ing. Tech.* **88,** 1798–1805 (2016).

60. Müller, K. *et al.* Switching Thin Films of Azobenzene-Containing Metal-Organic Frameworks with Visible Light. *Chem. Eur. J.* **23,** 5434–5438 (2017).

61. Wang, Z. *et al.* Tunable molecular separation by nanoporous membranes. *Nat. Commun.* **7,** 13872 (2016).

62. Knebel, A. *et al.* Hierarchical Nanostructures of Metal-Organic Frameworks Applied in Gas Separating ZIF-8-on-ZIF-67 Membranes. *Chem. Eur. J.* **24**, 5728–5733 (2018).

63. Baker, R. W. *Membrane Technology and Applications,* John Wiley & Sons, Ltd, Chichester, UK, 2nd Edition, ISBN 9780470854457 (2012).

64. Livingston, A. & Baker, R. Membranes from academia to industry. *Nat. Mater.* **16,** 280–282 (2017).

65. Diestel, L., Wang, N., Schulz, A., Steinbach, F. & Caro, J. Matrimid-Based Mixed Matrix Membranes: Interpretation and Correlation of Experimental Findings for

Zeolitic Imidazolate Frameworks as Fillers in H_2 /CO_2 Separation. *Ind. Eng. Chem. Res.* **54,** 1103–1112 (2015).

66. Ordoñez, M. J. C., Balkus, K. J., Ferraris, J. P. & Musselman, I. H. Molecular sieving realized with ZIF-8/Matrimid® mixed-matrix membranes. *J. Mem. Sci.* **361,** 28–37 (2010).

67. Friebe, S., Mundstock, A., Unruh, D., Renz, F. & Caro, J. NH_2-MIL-125 as membrane for carbon dioxide sequestration: Thin supported MOF layers contra Mixed-Matrix-Membranes. *J. Mem. Sci.* **516,** 185–193 (2016).

68. Moore, T. T. & Koros, W. J. Non-ideal effects in organic–inorganic materials for gas separation membranes. *J. Mol. Struc.* **739,** 87–98 (2005).

69. Li, H., Eddaoudi, M., O'Keeffe, M. & Yaghi, O. M. Design and synthesis of an exceptionally stable and highly porous metal-organic framework. *Nature* **402,** 276–279 (1999).

70. Eddaoudi, M. *et al.* Systematic Design of Pore Size and Functionality in Isoreticular MOFs and Their Application in Methane Storage. *Science* **295,** 469–472 (2002).

71. Yaghi, O. M. *et al.* Reticular synthesis and the design of new materials. *Nature* **423,** 705–714 (2003).

72. Bhunia, M. K., Hughes, J. T., Fettinger, J. C. & Navrotsky, A. Thermochemistry of paddle wheel MOFs: Cu-HKUST-1 and Zn-HKUST-1. *Langmuir* **29,** 8140–8145 (2013).

73. Yang, J., Grzech, A., Mulder, F. M. & Dingemans, T. J. The hydrogen storage capacity of mono-substituted MOF-5 derivatives: An experimental and computational approach. *Micropor. Mesopor. Mater.* **171,** 65–71 (2013).

74. Sun, L., Campbell, M. G. & Dincă, M. Electrically Conductive Porous Metal-Organic Frameworks. *Angew. Chem. Int. Ed.* **55,** 3566–3579 (2016).

75. Fernandez, C. A. *et al.* An electrically switchable metal-organic framework. *Sci. Rep.* **4,** 6114 (2014).

76. Cai, Y., Kulkarni, A. R., Huang, Y.-G., Sholl, D. S. & Walton, K. S. Control of Metal–Organic Framework Crystal Topology by Ligand Functionalization: Functionalized HKUST-1 Derivatives. *Cryst. Growth Des.* **14,** 6122–6128 (2014).

77. Hermann, D., Emerich, H., Lepski, R., Schaniel, D. & Ruschewitz, U. Metal-organic frameworks as hosts for photochromic guest molecules. *Inorg. Chem.* **52,** 2744–2749 (2013).

78. Aijaz, A. & Xu, Q. Catalysis with Metal Nanoparticles Immobilized within the Pores of Metal-Organic Frameworks. *J. Phys. Chem. Lett.* **5,** 1400–1411 (2014).

79. Modrow, A., Zargarani, D., Herges, R. & Stock, N. Introducing a photo-switchable azo-functionality inside Cr-MIL-101-NH_2 by covalent post-synthetic modification. *Dalton Trans.* **41,** 8690–8696 (2012).

80. Castellanos, S. *et al.* Structural Effects in Visible-Light-Responsive Metal-Organic Frameworks Incorporating ortho-Fluoroazobenzenes. *Chem. Eur. J.* **22,** 746–752 (2016).

81. Yanai, N. *et al.* Guest-to-host transmission of structural changes for stimuli-responsive adsorption property. *J. Am. Chem. Soc.* **134,** 4501–4504 (2012).

82. Tan, K. *et al.* Stability and Hydrolyzation of Metal Organic Frameworks with Paddle-Wheel SBUs upon Hydration. *Chem. Mater.* **24,** 3153–3167 (2012).

83. Ming, Y. *et al.* Kinetic Stability of MOF-5 in Humid Environments: Impact of Powder Densification, Humidity Level, and Exposure Time. *Langmuir* **31,** 4988–4995 (2015).

84. Morris, W., Taylor, R. E., Dybowski, C., Yaghi, O. M. & Garcia-Garibay, M. A. Framework mobility in the metal–organic framework crystal IRMOF-3: Evidence for aromatic ring and amine rotation. *J. Mol. Struc.* **1004,** 94–101 (2011).

85. Weh, K., Noack, M., Hoffmann, K., Schröder, K.-P. & Caro, J. Change of gas permeation by photoinduced switching of zeolite-azobenzene membranes of type MFI and FAU. *Micropor. Mesopor. Mater.* **54,** 15–26 (2002).

86. Marlow, F., Hoffmann, K. & Caro, J. Photoinduced switching in nanocomposites of azobenzene and molecular sieves. *Adv. Mater.* **9,** 567–570 (1997).

87. Taddei, M. When defects turn into virtues: The curious case of zirconium-based metal-organic frameworks. *Coord. Chem. Rev.* **343,** 1–24 (2017).

88. Ryder, M. R., Civalleri, B. & Tan, J.-C. Isoreticular zirconium-based metal-organic frameworks: Discovering mechanical trends and elastic anomalies controlling chemical structure stability. *PCCP* **18,** 9079–9087 (2016).

89. Castellanos, S., Kapteijn, F. & Gascon, J. Photoswitchable metal organic frameworks: turn on the lights and close the windows. *CrystEngComm* **18,** 4006–4012 (2016).

90. Valenzano, L. *et al.* Disclosing the Complex Structure of UiO-66 Metal Organic Framework: A Synergic Combination of Experiment and Theory. *Chem. Mater.* **23,** 1700–1718 (2011).

91. Øien, S. *et al.* Detailed Structure Analysis of Atomic Positions and Defects in Zirconium Metal–Organic Frameworks. *Cryst. Growth Des.* **14,** 5370–5372 (2014).

92. Furukawa, H. *et al.* Water adsorption in porous metal-organic frameworks and related materials. *J. Am. Chem. Soc.* **136,** 4369–4381 (2014).

93. Kolokolov, D. I. *et al.* Probing the Dynamics of the Porous Zr Terephthalate UiO-66 Framework Using ^{2}H NMR and Neutron Scattering. *J. Phys. Chem. C* **116,** 12131–12136 (2012).

94. Zhu, X. *et al.* Zr-based metal–organic frameworks for specific and size-selective enrichment of phosphopeptides with simultaneous exclusion of proteins. *J. Mater. Chem. B* **3,** 4242–4248 (2015).

95. Goesten, M. G. *et al.* Evidence for a chemical clock in oscillatory formation of UiO-66. *Nat. Commun.* **7,** 11832 (2016).

96. Wu, H. *et al.* Unusual and highly tunable missing-linker defects in zirconium metal-organic framework UiO-66 and their important effects on gas adsorption. *J. Am. Chem. Soc.* **135,** 10525–10532 (2013).

97. Shoaee, M., Anderson, M. W. & Attfield, M. P. Crystal growth of the nanoporous metal-organic framework HKUST-1 revealed by in situ atomic force microscopy. *Angew. Chem. Int. Ed.* **47,** 8525–8528 (2008).

98. Chui, Lo Charmant, Orpen & Williams. A chemically functionalizable nanoporous material. *Science* **283,** 1148–1150 (1999).

99. Ryder, M. R., Civalleri, B., Cinque, G. & Tan, J.-C. Discovering connections between terahertz vibrations and elasticity underpinning the collective dynamics of the HKUST-1 metal–organic framework. *CrystEngComm* **18,** 4303–4312 (2016).

100. Férey, G. & Serre, C. Large breathing effects in three-dimensional porous hybrid matter: Facts, analyses, rules and consequences. *Chem. Soc. Rev.* **38,** 1380–1399 (2009).

101. Park, K. S. *et al.* Exceptional chemical and thermal stability of zeolitic imidazolate frameworks. *Proc. Natl. Acad. Sci. U.S.A* **103,** 10186–10191 (2006).

102. Moggach, S. A., Bennett, T. D. & Cheetham, A. K. The effect of pressure on ZIF-8: Increasing pore size with pressure and the formation of a high-pressure phase at 1.47 GPa. *Angew. Chem. Int. Ed.* **48,** 7087–7089 (2009).

103. Horike, S., Shimomura, S. & Kitagawa, S. Soft porous crystals. *Nat. Chem.* **1,** 695–704 (2009).

104. Ryder, M. R. *et al.* Identifying the role of terahertz vibrations in metal-organic frameworks: From gate-opening phenomenon to shear-driven structural destabilization. *Phys. Rev. Lett.* **113,** 215502 (2014).

105. Kolokolov, D. I., Diestel, L., Caro, J., Freude, D. & Stepanov, A. G. Rotational and Translational Motion of Benzene in ZIF-8 Studied by ^{2}H NMR: Estimation of Microscopic Self-Diffusivity and Its Comparison with Macroscopic Measurements. *J. Phys. Chem. C* **118,** 12873–12879 (2014).

106. Kolokolov, D. I., Stepanov, A. G. & Jobic, H. Mobility of the 2-Methylimidazolate Linkers in ZIF-8 Probed by ^{2}H NMR: Saloon Doors for the Guests. *J. Phys. Chem. C* **119,** 27512–27520 (2015).

107. Moghadam, P. Z. *et al.* Development of a Cambridge Structural Database Subset: A Collection of Metal-Organic Frameworks for Past, Present, and Future. *Chem. Mater.* **29,** 2618–2625 (2017).

108. Farha, O. K. *et al.* Metal-organic framework materials with ultrahigh surface areas: Is the sky the limit? *J. Am. Chem. Soc.* **134,** 15016–15021 (2012).

109. Furukawa, H., Müller, U. & Yaghi, O. M. "Heterogeneity within order" in metal-organic frameworks. *Angew. Chem. Int. Ed.* **54,** 3417–3430 (2015).

110. Czaja, A. U., Trukhan, N. & Müller, U. Industrial applications of metal-organic frameworks. *Chem. Soc. Rev.* **38,** 1284–1293 (2009).

111. Rosi, N. L. *et al.* Hydrogen Storage in Microporous Metal-Organic Frameworks. *Science* **300,** 1127–1129 (2003).

112. Yang, Q. *et al.* CH4 storage and CO_2 capture in highly porous zirconium oxide based metal-organic frameworks. *Chem. Commun.* **48,** 9831–9833 (2012).

113. Stavila, V., Talin, A. A. & Allendorf, M. D. MOF-based electronic and opto-electronic devices. *Chem. Soc. Rev.* **43,** 5994–6010 (2014).

114. Yoon, S. M., Warren, S. C. & Grzybowski, B. A. Storage of electrical information in metal-organic-framework memristors. *Angew. Chem. Int. Ed.* **53,** 4437–4441 (2014).

115. Eslava, S. *et al.* Metal-Organic Framework ZIF-8 Films As Low-κ Dielectrics in Microelectronics. *Chem. Mater.* **25,** 27–33 (2013).

116. Allendorf, M. D., Schwartzberg, A., Stavila, V. & Talin, A. A. A roadmap to implementing metal-organic frameworks in electronic devices: Challenges and critical directions. *Chem. Eur. J.* **17,** 11372–11388 (2011).

117. Butler, K. T., Hendon, C. H. & Walsh, A. Electronic structure modulation of metal-organic frameworks for hybrid devices. *ACS Appl. Mater. Interfaces* **6,** 22044–22050 (2014).

118. Zhu, Y. *et al.* Unravelling surface and interfacial structures of a metal-organic framework by transmission electron microscopy. *Nat. Mater.* **16,** 532–536 (2017).

119. Rogge, S. M. J. *et al.* Metal-organic and covalent organic frameworks as single-site catalysts. *Chem. Soc. Rev.* **46,** 3134–3184 (2017).

120. Vandichel, M. *et al.* Active site engineering in UiO-66 type metal–organic frameworks by intentional creation of defects: A theoretical rationalization. *CrystEngComm* **17,** 395–406 (2015).

121. Chen, L.-F. & Xu, Q. Converting MOFs into amination catalysts. *Science* **358,** 304–305 (2017).

122. Zhang, D. *et al.* Atomic-resolution transmission electron microscopy of electron beam-sensitive crystalline materials. *Science* (2018).

123. Vos, A. de, Hendrickx, K., van der Voort, P., van Speybroeck, V. & Lejaeghere, K. Missing Linkers. An Alternative Pathway to UiO-66 Electronic Structure Engineering. *Chem. Mater.* **29,** 3006–3019 (2017).

124. Rangnekar, N., Mittal, N., Elyassi, B., Caro, J. & Tsapatsis, M. Zeolite membranes - a review and comparison with MOFs. *Chem. Soc. Rev.* **44,** 7128–7154 (2015).

125.   Seoane, B. *et al.* Metal-organic framework based mixed matrix membranes: A solution for highly efficient CO_2 capture? *Chem. Soc. Rev.* **44,** 2421–2454 (2015).

126.   Caro, J. *et al.* Aligned molecular sieve crystals. *Adv. Mater.* **4,** 273–276 (1992).

127.   Wang, Y. & Zhao, D. Beyond Equilibrium. Metal–Organic Frameworks for Molecular Sieving and Kinetic Gas Separation. *Crystal Growth Des.* **17,** 2291–2308 (2017).

128.   Fairen-Jimenez, D. *et al.* Opening the Gate: Framework Flexibility in ZIF-8 Explored by Experiments and Simulations. *J. Am. Chem. Soc.* **133,** 8900–8902 (2011).

129.   Huang, A., Wang, N., Kong, C. & Caro, J. Organosilica-functionalized zeolitic Imidazolate framework ZIF-90 membrane with high gas-separation performance. *Angew. Chem. Int. Ed.* **51,** 10551–10555 (2012).

130.   Trung, T. K. *et al.* Hydrocarbon adsorption in the flexible metal organic frameworks MIL-53(Al, Cr). *J. Am. Chem. Soc.* **130,** 16926–16932 (2008).

131.   Bolinois, L. *et al.* Breathing-induced new phase transition in an MIL-53(Al)-NH2 metal-organic framework under high methane pressures. *Chem. Commun.* **53,** 8118–8121 (2017).

132.   Henke, S., Schmid, R., Grunwaldt, J.-D. & Fischer, R. A. Flexibility and sorption selectivity in rigid metal-organic frameworks: The impact of ether-functionalised linkers. *Chem. Eur. J.* **16,** 14296–14306 (2010).

133.   Ghoufi, A., Benhamed, K., Boukli-Hacene, L. & Maurin, G. Electrically Induced Breathing of the MIL-53(Cr) Metal-Organic Framework. *ACS cent. sci.* **3,** 394–398 (2017).

134.   Knebel, A. *et al.* Defibrillation of soft porous metal-organic frameworks with electric fields. *Science* **358,** 347–351 (2017).

135.   Potember, R. S., Poehler, T. O. & Cowan, D. O. Electrical switching and memory phenomena in Cu-TCNQ thin films. *Appl. Phys. Lett.* **34,** 405–407 (1979).

136.   van Humbeeck, J. Shape Memory Alloys. A Material and a Technology. *Adv. Eng. Mater.* **3,** 837 (2001).

137.   Morgan, N.B. Medical shape memory alloy applications—the market and its products. *Mat. Sci. Eng. A* **378,** 16–23 (2004).

138.   Lampert, C. M. Chromogenic smart materials. *Mater. Today* **7,** 28–35 (2004).

139.   Knebel, A. *et al.* Smart Metal-Organic Frameworks (MOFs): Switching Gas Permeation through MOF Membranes by External Stimuli. *Chem. Eng. Technol.* **41,** 224–234 (2018).

140.   Schaate, A. *et al.* A Novel Zr-Based Porous Coordination Polymer Containing Azobenzenedicarboxylate as a Linker. *Eur. J. Inorg. Chem.* **2012,** 790–796 (2012).

141.   Modrow, A., Zargarani, D., Herges, R. & Stock, N. The first porous MOF with photoswitchable linker molecules. *Dalton Trans.* **40,** 4217–4222 (2011).

142. Furlong, B. J. & Katz, M. J. Bistable Dithienylethene-Based Metal-Organic Framework Illustrating Optically Induced Changes in Chemical Separations. *J. Am. Chem. Soc.* **139,** 13280–13283 (2017).

143. Fu, D.-W., Zhang, W. & Xiong, R.-G. The first metal-organic framework (MOF) of Imazethapyr and its SHG, piezoelectric and ferroelectric properties. *Dalton Trans.,* 3946–3948 (2008).

144. Tam, B. & Yazaydin, O. Design of electric field controlled molecular gates mounted on metal–organic frameworks. *J. Mater. Chem. A* **5,** 8690–8696 (2017).

2. The Pioneering Field of Switchable MOF Membranes in Detail

2.1. Summary

The field of switchable MOFs and MOF membranes is a very new field and is emerging from a niche to an area of high research interest and more and more publications are popping up. Switchable membranes, however, are not limited to MOFs and papers have been published, e.g. about switchable membranes containing polymeric brushes, liquid crystalline polymers and many more. We show a lot of different ways that were reported to influence gas-transport and selectivity through porous materials by external stimuli: Thermally driven pore-changes, pressure influence on pore-geometries, mechanically induced stress that induces molecular gating mechanisms as well as the type of adsorbed species that is introduced into a pore and switches the properties of the whole material.

In chapter 2.2 the mechanisms that can induce pore changes are described and we give an overview of the almost infinite possibilities that MOF materials have. For example, experimental MOF struts can switch between pore-open to pore-close forms that react to external pressures and show reverse adsorption. One of the most important external stimuli to switch MOFs is the optical switching that can be achieved similar to the switching of AZB, stilbenes and many other organic molecules, such as thioindigo or dithienylethene. These struts can be brought into the MOF lattice by mounting them, before synthesis, post-synthetic to the linker molecules or as a guest into the cavity the MOF. It is possible to introduce the light-switchable moieties as side-chain to the backbone of the linker molecule. We were the pioneers using light-switchable MOFs to switch the separation properties of membranes. The switching by light is reported to be relying on adsorptive or gating mechanisms.

In the last part of the paper, we highlight the importance of electrically switchable MOFs and coordination polymers. There is not much reported so far: Coordination polymers from TCNQ are reported to switch between conductive and isolating phases upon poling. Regarding porous MOFs, our work to the polymorphic switching of a ZIF-8 membrane is upon the pioneering works towards electric field influencing pore-geometries and diffusion. The prominent MIL-53 was described by theoretical DFT calculations to be switchable with electrical fields between its open and closed pore forms by e-field induced breathing. Furthermore, guest-molecules adsorbed into the pores of MOFs can be influenced through e-field induced dipolar alignment showing gating mechanisms.

It is expected that a lot of research will be conducted to this interesting field in the future, as it is interesting for many reasons to influence the pores of MOFs by switching. The holy grail of separation technology can be imagined to be the fine-tuning of the materials properties during a continuous technical process.

2.2. Smart Metal-Organic Frameworks (MOFs): Switching Gas Permeation through MOF Membranes by External Stimuli

A. Knebel, C. Zhou, A. Huang, J. Zhang, L. Kustov, J. Caro

Alexander Knebel[1]
Chen Zhou[2]
Aisheng Huang[2]
Jian Zhang[2]
Leonid Kustov[3]
Juergen Caro[1,*]

Smart Metal-Organic Frameworks (MOFs): Switching Gas Permeation through MOF Membranes by External Stimuli

The switching of gas permeation and adsorption on polymers, zeolites, and metal-organic frameworks (MOFs) by external stimuli like temperature, pressure, light, and electric fields is discussed. Especially MOFs as soft porous crystals are suitable candidates for switching gas transport. If the linker of a MOF contains a *cis-trans* switchable azo moiety, switching of the *trans* state into the *cis* state reduces gas transport through a MOF membrane. On the other hand, MOFs with dipolar or ionic components can be switched upon polarization with an electric field into polymorphs of the starting MOF. A ZIF-8 membrane can be switched into a polymorph with a rather stiff lattice, which sharpens the molecular sieving effect of the membrane, and, as an example, the propene/propane selectivity increases.

1   Thermal and Mechanical Switching of Gas Permeation – State of the Art

Switching the selectivity of gas transport through a membrane by external stimuli is highly desired in chemical engineering. There are first attempts to develop smart interactive organic polymer membranes that can be switched by external stimuli [1–3]. Polymers can change their physicochemical properties upon external stimuli like electromagnetic fields [4] and light [5], temperature [6], and pH value [7].

There are some pioneering studies on the thermal switching of gas transport through membranes. As an example, the permeation of ionic molecules through parallel nanopores functionalized with amine-terminated polymer brushes can be thermally controlled [8]. In a first step, the nanopores are prepared through heavy ion irradiation of polyethylene terephthalate followed by chemical track-etching. In a second step, the surface of the pore walls has been functionalized with amine-terminated poly(*N*-isopropylacrylamide) brushes. By manipulating the temperature, due to swelling/shrinking of the polymer brushes at the inner pore walls, the ionic transport through the membrane is increased/decreased as schematically shown in Fig. 1.

Another example for thermal switching is the thermal tuning of oxygen transport through a supported liquid crystalline polymer (LCP) layer. The LCPs show temperature-triggered phase transformations between smectic ↔ nematic ↔ isotropic. Increasing crystallinity in the smectic phase reduces the gas permeability. Switching the LCP membrane from a liquid crystalline smectic to a less crystalline isotropic state by heating the LCP film above the T_c results in a 10-fold increase of the

oxygen transport through the isotropic phase as illustrated schematically in Fig. 2 [9].

A mechanical switching of gas transport is also possible. Stress can convert a microporous molecular crystal into an active fluidic device through a mechanical reorientation of the nanoporous channels. Stress induces a new orientation of the channel geometry of $[Cu(II)_2(bza)_4(pyz)]_n$ (bza = benzoate, pyz = pyrazine) [10]. As illustrated in Fig. 3, in the α-phase the gases permeate through the (100) surface, whereas there is no transport through the (001) plane. However, by mechanical treatment, an α'-phase is formed inside the α-phase, which acts as a barrier for gas transport.

Metal-organic frameworks (MOFs) or sometimes referred to as porous coordination polymers (PCPs) are a new class of nanoporous materials and promising candidates for switchable materials, including switching of gas adsorption and permeation. MOFs are hybrid materials and represent a self-assembly of organic linker molecules interconnected by metal ions or metal oxide clusters. Possible switchable physical properties are

[1]Alexander Knebel, Prof. Dr. Juergen Caro
juergen.caro@pci.uni-hannover.de
Leibniz University Hannover, Institute for Physical Chemistry and Electrochemistry, Callinstrasse 3A, 30167 Hannover, Germany.

[2]Dr. Chen Zhou, Prof. Dr. Aisheng Huang, Prof. Dr. Jian Zhang
Ningbo Institute of Materials Technology and Engineering, CAS, Institute of New Energy Technology, 1219 Zhongguan Road, 315201 Ningbo, China.

[3]Prof. Dr. Leonid Kustov
Russian Academy of Sciences, N. D. Zelinsky Institute of Organic Chemistry, Leninsky Prospect, 47, 119991 Moscow, Russia.

Review 225
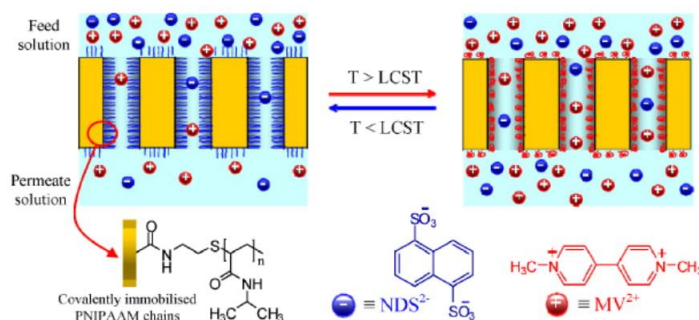
Figure 1. Thermally driven changes of the conformation of the polymer brushes anchored at the inner pore wall surface and the results for the transport of ionic molecules through the pores [8]. LCST, lower critical solubility temperature.

Figure 2. Switching of oxygen transport from a gas mixture through a liquid crystalline polymer (LCP) by phase switching of the supported LCP film [9]. There is almost no oxygen transport through the crystalline smectic phase (oxygen permeability $P_{O_2} = 0.013 \times 10^{-13}$ cm^{3}cm(m^2 Pa)$^{-1}$), but a high oxygen flux through the isotropic LCP phase ($P_{O_2} = 0.493 \times 10^{-13}$ cm^{3}cm(m^2 s Pa)$^{-1}$) [9].
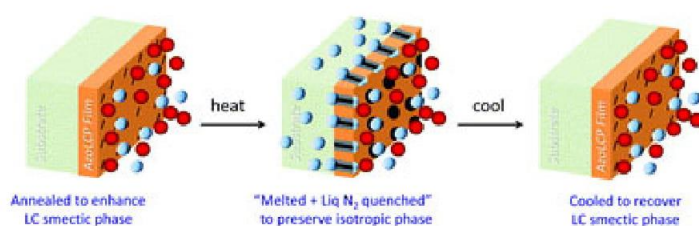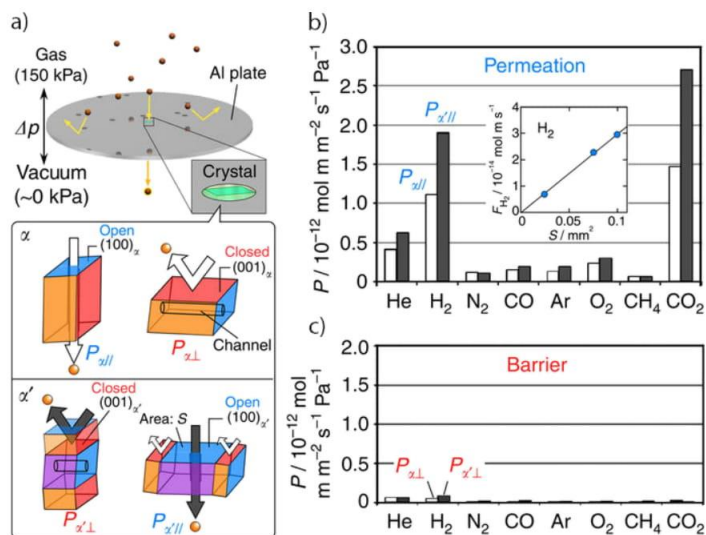

Figure 3. (a) Switching of gas transport by mechanical stress-induced reorientation of the channel geometry. (b) Gas permeation through an undisturbed [Cu(II)$_2$(bza)$_4$(pyz)]$_n$ crystal (α-phase), and (c) blocked gas transport (barrier case) after channel reorientation, as a result of stress (α'-phase is formed inside the α-phase) [10].

reviewed in [11]. The variety of structural changes which a MOF structure can undergo as a response to the external stimuli, including light absorption, temperature, adsorption of guest molecules, mechanical pressure etc. are reviewed in [12, 13]. One of the unique properties for PCPs/MOFs is their "flexible" nature of crystalline frameworks which adapt their structures to environmental changes [14, 15]. The ultrafast structural fluctuations of MOFs could be detected by 2D IR spectroscopy [16].

Several switching properties of MOFs can be potentially used for electronic and optoelectronic devices [17] or in sensors [18, 19]. Breathing, however, is a specific type of framework flexibility only exhibited by a limited number of MOFs. It can be described as the ability to undergo large structural deformations associated with great changes of the unit cell volume upon external stimuli such as pressure [20, 21], temperature [22], adsorption [23], extreme transformations induced by changes in temperature, mechanical constraints, and guest adsorption. This gated adsorption and breathing [24, 25] can be beneficial or limiting to applications in gas separations and sensing.

The organic linker can have a variety of functional groups which respond to external stimuli like pressure, temperature, light, E-field, or guest molecules. Also, the metal ions/oxide clusters can change their oxidation state and/or alter between high and low spin state, thus changing their ionic radii. These interactions can trigger structural changes of the MOFs which alter their permeation properties and make them more or less soft nanoporous crystals [26, 27].

In a classical paper combining different experimental techniques with molecular simulations it has been demonstrated that the ZIF-8 structure is modified by gas adsorption in the same way as it is modified by a very high external pressure of 14.7 kbar [28]. Another rather new pressure-induced transformation of a tailored MOF lattice resulted in negative gas adsorption. At a threshold pressure, the MOF framework contracts and the formerly adsorbed guest molecules become desorbed which leads to a spontaneous pressure increase as indicated in Fig. 4 [29].

In the following, the switching of gas transport through molecular sieve membranes (zeolite, MOF) will be treated using electromagnetic stimuli such as light and electric fields.
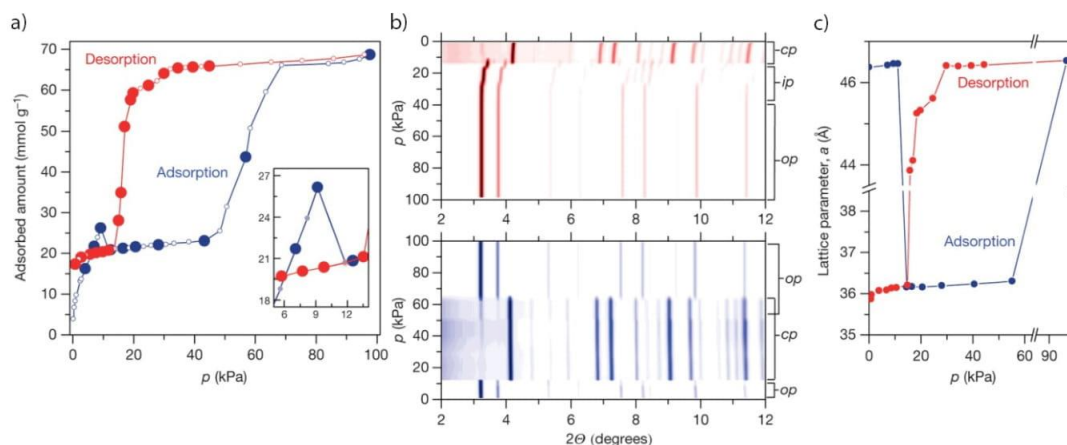
Figure 4. In situ measured methane adsorption and desorption isotherms on the MOF DUT-49 at 111 K. (a) At about 80 kPa, the further increase of the methane pressure results in a lower amount adsorbed. (b) Powder XRD pattern evolution during adsorption (blue) and desorption (red). *op*, open-pore phase; *cp*, contracted-pore phase; *ip*, intermediate pore phase. (c) Evolution of the lattice parameters during adsorption (blue) and desorption (red) of methane on the MOF DUT-49 at 111 K; for details see [29].

2 Optical Switching of Gas Permeation

Under irradiation of light with a certain wavelength, molecules can change their shape. Well-known are the *trans-cis* photo-isomerization of azo groups or stilbene derivatives [30], the twisted intramolecular charge transfer (TICT) states [31], or the photoisomerization of thioindigo [32]. Fig. 5 presents examples for the molecular photo-switching. There are a few papers describing the modulation of adsorption properties of MOFs upon photoswitching [33–35].

A bistable MOF with pores that can be optically changed has been prepared on the basis of dithienylethene-containing linker molecules [36]. This MOF has been prepared by solvent-assisted linker exchange starting with ZIF-70 (consisting of Zn(II) and imidazole and 2-nitroimidazole) and substituting it by an imidazolate-based dithienylethene linker. Dithienylethene undergoes photoswitching as illustrated in Fig. 6. The open and closed conformers have been evaluated in the separation of toluene/naphthalene/pyrene mixtures.

Also MOFs with mixed photoresponsive linkers have been synthesized and evaluated in the switching of adsorption. Fig. 7 illustrates an MOF with diarylethene and azobenzene as photochromic units [37].

A further example how to control adsorption by MOFs is given in Fig. 8.

Here, a zwitterionic pyridinium 4-carboxylate unit has been used as photoreactive MOF material [38]. UV light irradiation causes the photoreactive units to form radical triplets permitted by intramolecular electron transfer from the anionic
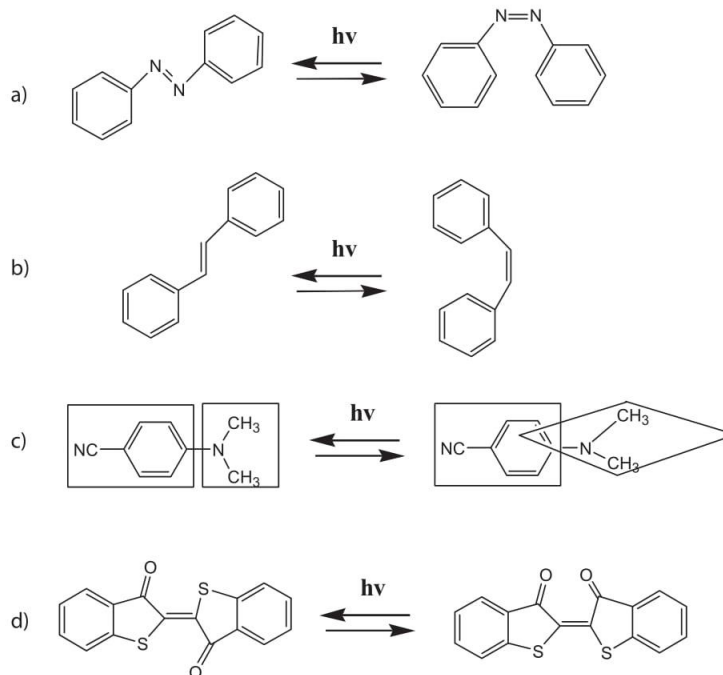
Figure 5. Examples for the change of the molecule structure as a result of photo-switching: (a) azobenzene, (b) stilbene, (c) dimethylaminobenzonitrile, (d) thioindigo.
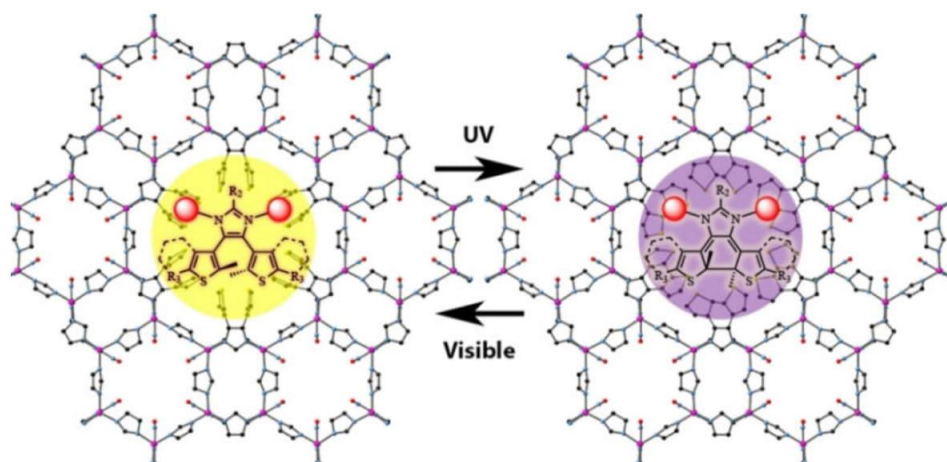
www.cet-journal.com

Figure 6. Open (left) and closed (right) conformation of a photo-switchable MOF containing diethienylethene-based linker [36].
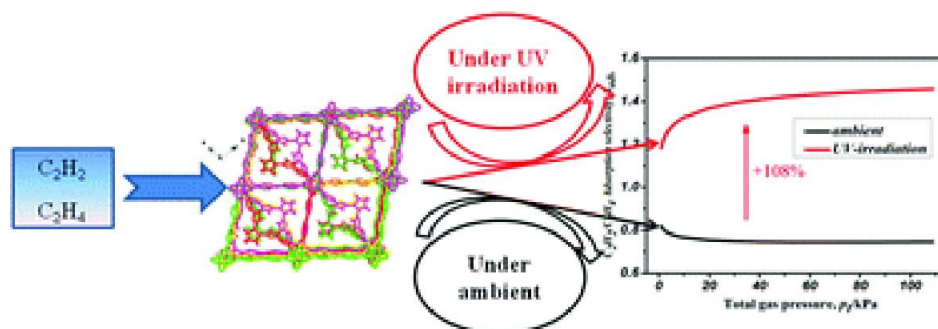

Figure 7. Influence of photo-switching on the gas adsorption of ethine and ethane [37].

carboxylate to the cationic pyridinium ions. As a result, a reversible charge gradient is created which influences the adsorption of guest molecules. The effect has been demonstrated experimentally for CO_2 adsorption: After irradiation, the amount of CO_2 adsorbed was reduced and the heat of adsorption decreased to about 20 % of its starting value without photoactivation.

In a pioneering study, about 20 years ago in this journal Chemical Engineering & Technology, the control of gas permeation through polymethacrylate membranes by azobenzene (AZB) as a switching unit was reported [39], but the switching effects of gas transport were found to be moderate and remained behind the expectations. It has been concluded, therefore, to bring AZB as a switchable valve in the pores of molecular sieve membranes such as zeolites or MOFs. In a first paper, supported nanoporous zeolite-type MFI and FAU membrane layers have been modified by adsorption of AZB, and gas permeation through the zeolite/AZB composite membranes has been studied for AZB switched reversibly between its *trans* and *cis* states [40].

Fig. 9 displays the permeance of different probe molecules through a FAU membrane containing AZB guest molecules which are reversibly photo-switched between *trans* and *cis* states. By illuminating the supported FAU membrane with AZB guest molecules via an optical fiber with the light of 365 nm and 436 nm wavelength, respectively, the switching could be successfully achieved. It follows from Fig. 9 that switching of AZB from the thermodynamically most stable *trans* into *cis* state by using UV light reduces the gas permeation. This decrease of permeation through the membrane for the *cis* state of AZB is different for the various gas molecules. The gas permeation of large molecules (SF_6) is more reduced than that one of smaller molecules (H_2). At first sight, this reduction of the permeance in the *cis* state compared with the *trans* state seems to correlate with the kinetic diameter which means that the switching is based on a steric effect caused by the bulky *cis* state of AZB. However, when calculating the *trans* to *cis* selectivity as the ratio of the permeances of a certain probe gas for *trans* and *cis* state as a measure of the switching efficiency (right ordinate in Fig. 9), one can see that the ideal
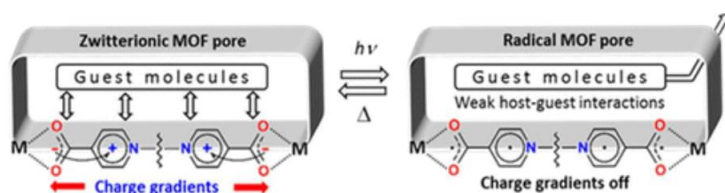
Figure 8. Control of gas adsorption in zwitterionic MOFs by influencing the interaction energy of the adsorptive with the host through reversible optical switching [38]. In the starting state (left), large charge gradients form a high intramolecular electric field which in turn causes a strong adsorption through host-guest interaction. Optical switching leads to intramolecular electron transfer which weakens adsorption (right).

trans to *cis* selectivity does not correlate with the kinetic diameter of the permeating molecules. In addition to only steric effects – which would slow down the diffusion of the probe molecules – an adsorptive retardation seems to exist, especially for CO_2. This combined adsorption-diffusion model for the explanation of gas transport through membranes with AZB switching has been confirmed for MOF membranes containing AZB groups, as will be shown later in this paper.

However, the modification of a molecular sieve membrane by physisorbed AZB guest molecules as shown in Fig. 9 is not long-time stable since there is a continuous slight desorption of AZB from the pore system of the zeolite membrane into the feed or sweep gas streams. Another problem of physisorbed AZB in molecular sieve membranes is the fact that the AZB loading is difficult to control and AZB cannot be switched at complete pore fillings in constraint systems [41, 42] since the photoisomerization requires sufficient free volume. This impossible *trans-cis* switching of AZB at a high loading is in complete agreement with the finding that compact AZB crystals cannot be also switched. To solve these problems, AZB has

to be attached covalently in defined distances to the wall of a membrane pore. This concept can be realized relatively easily for MOF membranes by chemical modification of the organic linker molecules. Photo-switchable linkers can be inserted in MOFs either as an integral part of the scaffold or as a guest [43]. Nevertheless, we had to learn that MOFs with an AZB moiety in the backbone of the scaffold can be synthesized [44], but these MOFs do not undergo *trans-cis* photoisomerization, i.e., they cannot be switched [45]. For the photochemical *trans/cis* switching of the AZO group inside a MOF structure, it must be a side group of the linker and not in the backbone of the linker as illustrated in Fig. 10.

Fig. 10 demonstrates the effect of *trans/cis* switching of a nanoporous MOF membrane with AZO groups in the side group of the linker and the impact of in situ switching on the separation of H_2/CO_2 and N_2/CO_2 mixtures. It follows from this figure that switching of the AZO groups from *trans* to *cis* (i) does not alter the permeance of H_2 and N_2, but (ii) the CO_2 permeance is much lower in the *cis* state of AZB in comparison with the *trans* state [46]. Thus, this switching of the gas permeances leads to an up and down variation of the membrane selectivity (see Fig. 10). This experimental finding is surprising since the kinetic diameters of CO_2 (3.3 Å) and N_2 (3.7 Å) are comparable (see Tab. 1), but these probe molecules show quite a different reaction on AZB switching. AZB can change its molecular size upon *trans* → *cis* switching from 9 to 5.5 Å, its geometry from planar to a more spherical one, and the dipole moment from 0.5 to 3.1 Debye [47]. We propose, therefore,
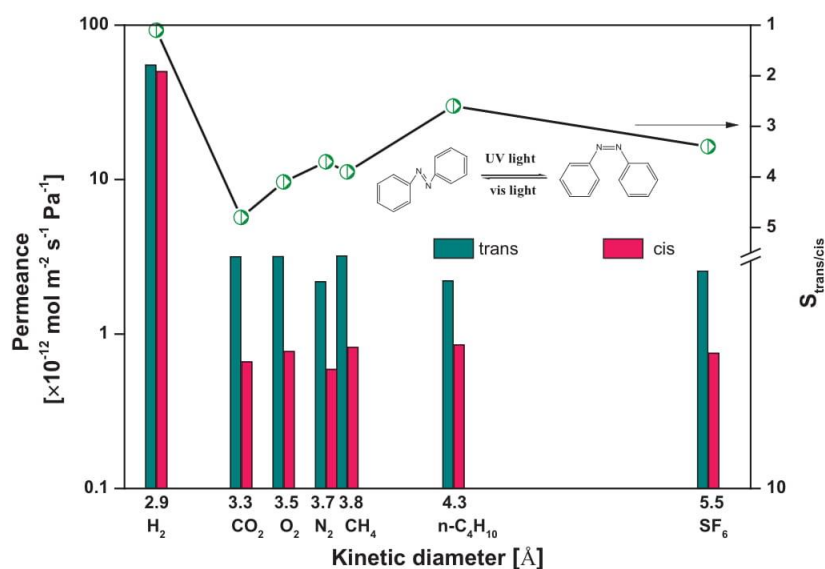
Figure 9. Single gas permeances of probe molecules through a supported FAU (NaX) membrane with adsorbed AZB guest molecules as a function of the kinetic diameter of the permeating gases at room temperature. By a fiber optic, the AZB could be switched from *trans* to *cis* (360 nm) and back from *cis* to *trans* (436 nm). The right ordinate gives the ideal selectivities $S_{trans/cis}$ calculated as the *trans/cis* permeances; redesigned using the data from [40].

- 47 -
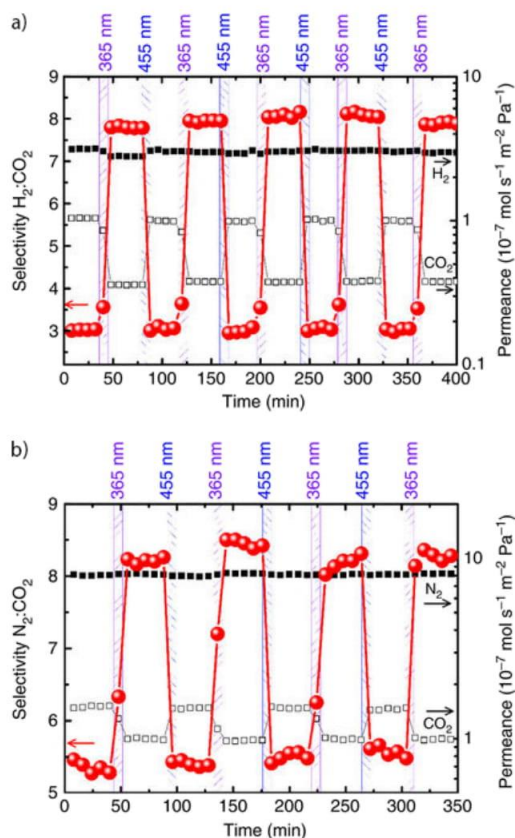
Figure 10. AZB can be covalently attached to the organic linker molecule. AZB in the side group can be reversibly *trans* ⇌ *cis* switched by light. Photo-switchable membrane separation of (a) H_2/CO_2 and (b) N_2/CO_2. The membrane is irradiated by light of 365 and 455 nm for 5 min each. The prepared SURMOF films have a pillared-layer structure of type $Cu_2(AzoBPDC)_2(AzoBiPyB)$. The samples used in this study were prepared by 90 cycles of immersing the sample in ethanolic 1 mM copper(II) acetate solution and in ethanolic 0.1 mM AzoBiPyB and 0.1 mM AzoBPDC solution at 60 °C; for details see [46].

Table 1. Selected physical constants of gases [50].

Gas	Kinetic diameter [Å]	Polarizability [10^{25} cm^3]	Quadrupole moment [10^{-26} esu cm^2]
Ar	3.5	16.4	0
H_2	2.9	8.0	0.66
N_2	3.7	17.4	1.52
CO_2	3.3	29.1	4.30
C_2H_4	4.2	38.4	0
C_3H_6	4.7	62.6	0.4

that the permeation of gas through AZB-modified membranes is both adsorption- and diffusion-controlled. AZB in the *cis* state shows a strong dipole moment and permeating molecules such as CO_2 (with a quite strong quadrupole moment) that can interact with the *cis*-AZB, are additionally retarded.

This assumption of a combined adsorption-diffusion mechanism is in complete agreement with the finding of [48]. The *cis*-switching of an AZO-MOF powder reduced the sorption uptake rate of CO_2 with a kinetic diameter of 3.3 Å remarkably, whereas Ar with a similar kinetic diameter (3.4 Å) showed no influence of *trans-cis* AZO switching. CO_2 and Ar are both apolar, but CO_2 exhibits a high quadrupole moment. Also the polarizability of CO_2 is higher than that of Ar. In [49], the sorption uptake of butanediol was reduced by a factor of 15 if the MOF layer is switched from *trans* to *cis*.

Fig. 11 provides another example for the photo-switching of an MOF with AZO moieties in the side group of the linker. The same AZO linker has been used as for the azo membrane as indicated in Fig. 10, but the linker has been fluorinated. Because of this linker fluorination, the switching of *trans* to *cis* could be shifted in the visible region [51]. In addition to a steric hindrance, the olefins like ethylene and propylene will additionally interact with the dipole moment of *cis* AZB and become, therefore, additionally retarded (see Tab. 1).

3 Electric Switching of Gas Permeation

An MOF structure could be switched electrically reversibly from a high-resistance to a conducting state by an applied potential as illustrated in Fig. 12 [52].

There are only a few studies describing the influence of electric fields on adsorption. Examples are the enhanced binding of H_2 to Li-doped carbon nanotubes [53] or to N-doped graphene [54] via an electric field through dissociative adsorption and diffusion mechanisms. Several theoretical studies predict interesting adsorption effects upon switching MOFs by using electric fields [55]. In another study, external electric fields have been applied to switch the direction of electric polarization in the MOF DMAMnF (dimethyl-ammonium-Mn-formate) and to control the magnitude of the electric polarization with a magnetic field [56].

However, in advanced molecular simulations, an accurate force field was used to describe the flexibility of the MOF MIL-53(Cr) in a strong electric field [57]. It was predicted that under the influence of an electric field the large-pore MIL-53(Cr) is transformed into a narrow-pore MIL-53(Cr) as schematically displayed in Fig. 13. Simulated adsorption isotherms show that the narrow-pore MIL-53(Cr) can only adsorb CO_2 (kinetic diameter 3.3 Å) but not CH_4 (3.4 Å); see Fig. 13. However, it has to be noted that the field strengths of 2 V nm^{-1} are unrealistically high.

In a following theoretical paper, the molecular mechanism of the change of the pore size and shape was explained in detail as presented in Fig. 14 [58]. It was found that for a strength of the *E*-field of 1.75 V nm^{-1}, the MOF closes in the same fashion like under pressure or guest molecule adsorption. It has to be stated, however, that these fields lay orders of magnitude above the breakthrough voltage in air of about 3×10^{-3} V nm^{-1}.
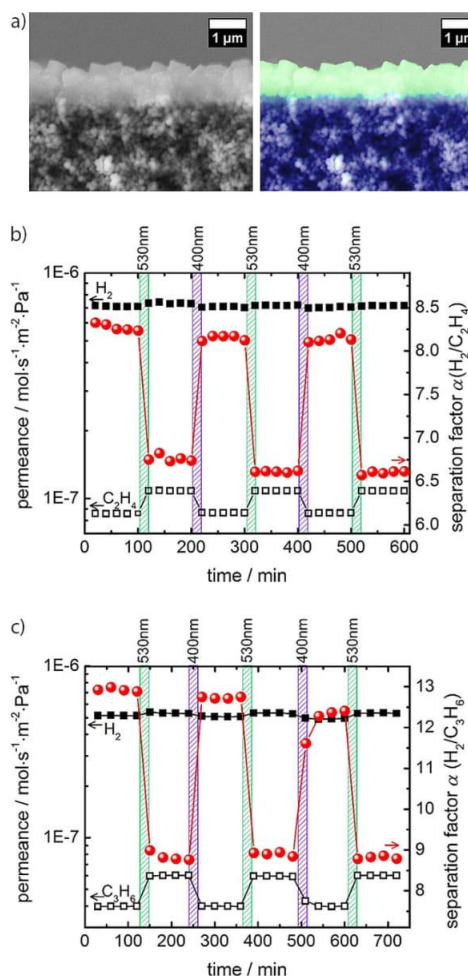
Figure 11. Visible light photo-switching of a supported SURMOF membrane with fluorinated AZO-containing linkers [49]. (a) SEM of the SURMOF membrane on a porous α-Al_2O_3 support. Membrane selectivities of (b) H_2:C_2H_4 and (c) H_2:C_3H_6 gas mixtures, switched in situ via illumination by 400 and 530 nm light for three cycles. Each illumination time was 20 min. The permeances of H_2 (solid square) and C_2H_4 or C_3H_6 (open squares) are shown on the left, while the resulting separation factors (red spheres) are shown on the right. The MOF under study is $Cu_2(F_2AzoBDC)_2(dabco)$ SURMOF; for details see [51].
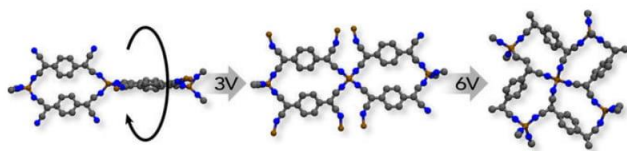
Figure 12. Electric switching of the MOF Cu(TCNQ) from a high-resistance state to a conducting state by an electric potential [52].

Interestingly, this switching between a large-pore and a narrow-pore architecture of MIL-53(Al) could be also realized via increasing the mechanical stress applied for pelletizing a commercial MIL-53(Al) powder as indicated in Fig. 15 [59].

The concept of electric field-controlled pore openings with molecular rotors has been computationally demonstrated for molecular gates mounted on the open metal coordination sites of the Mg-MOF-74 [60]. The hexagonal channels of Mg-MOF-74 are proposed to become open and closed under the effect of an electric field. The gate molecule contains carboxy groups to coordinate to the open metal sites and a permanent dipole moment for the interaction with the electric field. The electric field is expected to orientate the dipolar gate molecule dimethyl-bis(trifluoromethyl)pyrene-dicarboxylic acid as displayed in Fig. 16.

Just recently, it has been proven that the control of gas transport through a MOF membrane by switching the MOF layer by electric fields is possible [61]. As shown in Fig. 17 a, a ZIF-8 (zeolitic imidazolate framework) with a thickness of 1 μm has been prepared by the counter-diffusion technique [62, 63]. Above and below the membrane metal nets were attached and by applying a voltage, a DC electric field is built up utilizing the MOF membrane as a capacitor. Fig. 17 b indicates that the CO_2 flux through the membrane drops by about 75 % after switching on the E-field of 500 V mm^{-1}. Interestingly, after the field was shut down, the permeance kept its value for almost 1 h in the switched state until the permeance instantaneously jumped back in the former state before switching. This switching behavior was found to be reversible.

At first sight, one could assume that the dipolar linker molecules of ZIF-8 (methylimidazolate anions) have lost their rotational freedom since they become "frozen" by the E-field. There are tough studies on the energy barriers of the flip-flop motion of the methylimidazolate linker in ZIF-8 that opens the gate [64]. However, a quantitative evaluation proved that this interaction energy of the dipolar linker methylimidazolate with the external electric field is too weak to stop the thermally triggered linker rotation completely [58]. That case of the MOF ZIF-8 is different to the 180° flip-flop motion of the m-fluoroanilinium cation in a molecular single crystal, which could be switched by an electric field [65].

By applying ab initio density functional theory calculations as theoretical tool and experimental techniques like XRD with Rietveld refinement, dielectric spectroscopy, deuterium NMR, and polarization spectroscopy, it was found that the complex interactions of the Zn^{2+} ions and of the dipolar methylimidazolate linker with the E-field causes deformation of the ZIF-8 structure into a metastable polymorph. This ZIF-8 polymorph has indeed a rigid framework with reduced lattice flexibility. The permeation through the rigid ZIF-8 membrane is slowed down in any case. However, this reduced lattice flexibility in the polarized state sharpens the molecular sieving effect of this MOF membrane. Fig. 17 c reveals the improvement of the propene/propane separation under the E-field. The rigid ZIF-8 framework reduces the gas transport of the slightly larger propane molecule more than that of the slightly smaller propene. As a
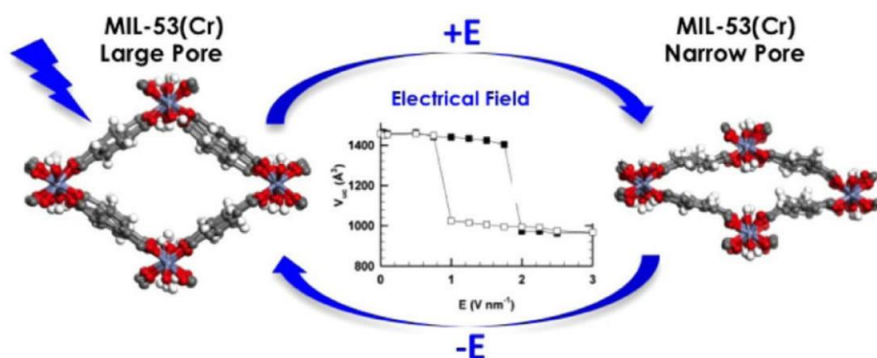
Figure 13. Change of the unit cell volume for increasing (full symbols) and decreasing (empty symbols) electric field strengths. The final structures for $E < 1\,V\,nm^{-1}$ and for $E > 2\,V\,nm^{-1}$ correspond to the large- and narrow-pore state of MIL-53(Cr) [57].
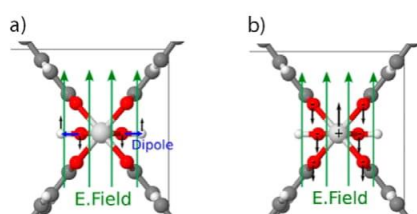
Figure 14. Deformation of the MIL-53(Cr) lattice in a homogeneous electric field, which leads to an induced polarization. (a) Orientation of the OH groups, (b) deformation of the coordination environment [58].

result, the separation factor α(propene/propane) increases under the E-field.

4   Conclusions

Gas transport through supported MOF membranes can be switched by using soft MOF structures that can be addressed by either electric fields or undergo a photochemical *trans/cis* isomerization. Interestingly, the life time of an optically switched AZO MOF membrane in the *cis* state and of an electrically switched MOF state in the polarized state can be several hours even in the absence of any light or electrical field as external stimuli. This pioneering work on switching a supported ZIF-8 membrane by external stimuli will trigger further work on switching MOF and other membranes.

However, the way of such smart switchable membranes into the industrial practice will be long because of some additional critical issues. UV light has a limited penetration depth and it can damage the MOF. Usually, much less than 50 % of the *trans* state can be switched into *cis* state. Electric switching is expensive, to build up an electric field, a certain amount of charge carriers is necessary.

Nevertheless, if the transport of a gas through an MOF membrane can be influenced by light or an electric field, also
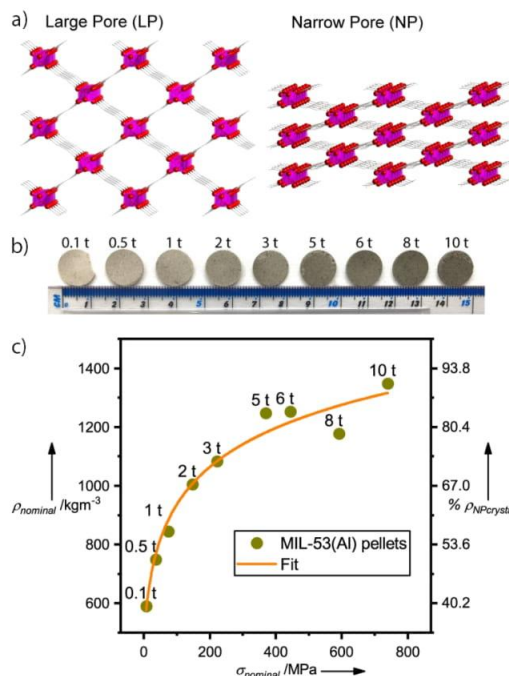
Figure 15. Switching of the large-pore modification of MIL-53(Al) into the narrow-pore modification by the mechanical pressure in pellet pressing. (a) Schematic illustration. (b) Photographs of the pressed pellets. (c) Pellet density and narrow-pore phase content in the MIL-53(Al) sample as a function of the pressure in pelletizing [59].

the adsorption/desorption kinetics of gases on MOF adsorbents can be modulated. We expect, therefore, intense R&D activities on switching adsorption on MOFs in next future.
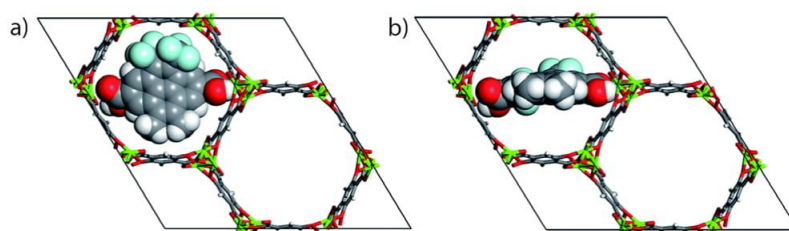
Figure 16. Schematic drawing showing how the gate molecule (a) closes and (b) opens the hexagonal pore of Mg-MOF-74 [60].
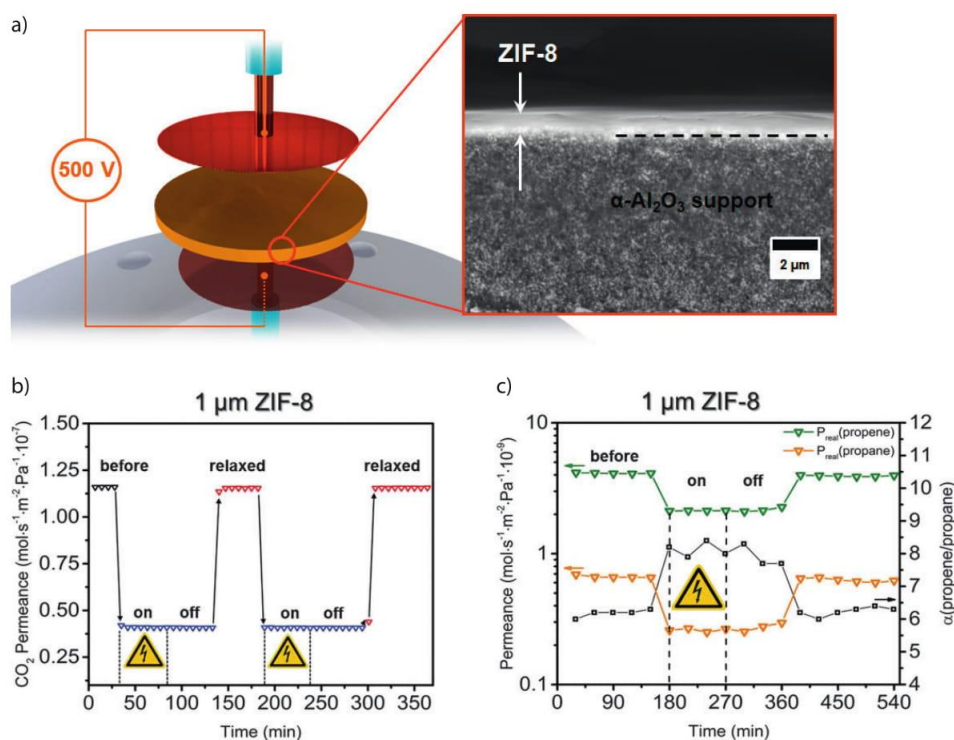
Figure 17. Switching of gas transport through a supported MOF membrane by an electric field [61]. (a) Polished cross-sectional SEM of a supported 1-μm thick ZIF-8 layer on a porous asymmetric α-Al$_2$O$_3$ support. Between the metal nets on top and bottom a DC voltage of 500 V is applied. (b) Reduction of the single gas CO$_2$ permeance upon electrical switching. (c) Influence of the electrical switching on mixed gas propene/propane separation. Since the propane permeance drops more than the propene one, the separation factor α (propene/propane) increases from 6 to 8 upon E-field switching.

Acknowledgment

Review

Abbreviations

AZB	azobenzene
LCP	liquid crystalline polymer
LCST	lower critical solubility temperature
MOF	metal-organic framework
PCP	porous coordination polymer

References

[1] M. A. C. Stuart, W. T. S. Huck, J. Genzer, M. Müller, C. Ober, M. Stamm, G. B. Sukhorukov, I. Szleifer, V. V. Tsukruk, M. Urban, F. Winnik, S. Zauscher, I. Luzinov, S. Minko, *Nat. Mater.* **2010**, *9*, 101–113. DOI: 10.1038/nmat2614

[2] P. Schattling, F. D. Jochum, P. Theato, *Polym. Chem.* **2014**, *5*, 25–36. DOI: 10.1039/C3PY00880K

[3] D. Wandera, S. R. Wickramasinghe, S. M. Husson, *J. Membr. Sci.* **2010**, *357*, 6–35. DOI: 10.1016/j.memsci.2010.03.046

[4] J. Thevenot, H. Oliveira, O. Sandre, S. Lecommandoux, *Chem Soc. Rev.* **2013**, *42*, 7099–7166. DOI: 10.1039/C3CS60058K

[5] Y. Zhao, *Macromolecules* **2012**, *45*, 3647–3657. DOI: 10.1021/ma300094t

[6] D. Roy, W. L. Brooks, B. S. Sumerlin, *Chem. Soc. Rev.* **2013**, *42*, 7214–7243. DOI: 10.1039/c3cs35499g

[7] J. J. Li, Y. N. Zhou, Z. H. Luo, *Chem. Eng. J.* **2017**, *322*, 693–701. DOI: 10.1016/j.cej.2017.04.074

[8] S. Nasir, M. Ali, W. Ensiger, *Nanotechnology* **2012**, *23*, 225502. DOI: 10.1088/0957–4484/23/227225502

[9] S. Hassan, R. Anandakathir, M. J. Sobkowicz, B. M. Budhlall, *Polym. Chem.* **2016**, *7*, 1452–1460. DOI: 10.1039/c5py01640a

[10] Y. Takasaki, S. Takamizawa, *Nat. Commun.* **2015**, *6*, 8934. DOI: 10.1038/ncomms9934

[11] O. Sato, *Nat. Chem.* **2016**, *8*, 644–656. DOI: 10.1038/NCHEM.2547

[12] F.-X. Coudert, *Chem. Mater.* **2015**, *27*, 1905–1916. DOI: 10.1021/acs.chemmater.5b00046

[13] S. S. Nagarkar, A. V. Desai, S. K. Ghosh, *Chem. Asian J.* **2014**, *9*, 2358–2376. DOI: 10.1002/asia.201402004

[14] H. Sato, W. Kosaka, R. Matsuda, A. Hori, Y. Hijikata, R. V. Belosludov, S. Sakaki, M. Takat, S. Kitagawa, *Science* **2014**, *343*, 167–170. DOI: 10.1126/science.1246423

[15] S. Shimomura, M. Higuchi, R. Matsuda, K. Yoneda, Y. Hijikata, Y. Kubota, Y. Mita, J. Kim, M. Takata, S. Kitagawa, *Nat. Chem.* **2010**, *2*, 633–637. DOI: 10.1038/nchem.684

[16] J. Nishida, A. Tamimi, H. Fei, S. Pullen, S. Ott, S. M. Cohen, M. D. Fayer, *PNAS* **2014**, *111*, 18442–18447. DOI: 10.1073/pnas.1422194112

[17] V. Stavila, A. A. Talin, M. D. Allendorf, *Chem. Soc. Rev.* **2014**, *43*, 5994–6010. DOI: 10.1039/c4cs00096

[18] L. E. Kreno, K. Leong, O. K. Farha, M. Allendorf, R. P. Van Duyne, J. T. Hupp, *Chem. Rev.* **2012**, *112*, 1105–1125. DOI: 10.1021/cr200324t

[19] F.-Y. Yi, D. Chen, M.-K. Wu, L. Han, H.-L. Jiang, *ChemPlusChem* **2016**, *81*, 675–690. DOI: 10.1002/cplu.201600137

[20] P. Yot, L. Vanduyfhuys, E. Alvarez, J. Rodriguez, J.-P. Itié, P. Fabry, N. Guillou, T. Devic, I. Beurroies, P. L. Llewellyn, V. Van Speybroeck, C. Serre, G. Maurin, *Chem. Sci.* **2016**, *7*, 446–450. DOI: 10.1039/C5SC02794B

[21] S. M. J. Rogge, L. Vanduyfhuys, A. Ghysels, M. Waroquier, T. Verstraelen, G. Maurin, V. Van Speybroeck, *J. Chem. Theory Comput.* **2015**, *11*, 5583–5597. DOI: 10.1021/acs.jctc.5b00748

[22] Y. Liu, J.-H. Her, A. Dailly, A. J. Ramirez-Cuesta, D. A. Neumann, C. M. Brown, *J. Am. Chem. Soc.* **2008**, *130*, 11813–11818. DOI: 10.1021/ja803669w

[23] L. Vanduyfhuys, A. Ghysels, S. M. J. Rogge, R. Demuynck, V. Van Speybroeck, *Mol. Simul.* **2015**, *41*, 1311–1328. DOI: 10.1080/08927022.2015.1048512

[24] S. Kitagawa, R. Kitaura, S.-I. Noro, *Angew. Chem., Int. Ed.* **2004**, *43*, 2334–2375. DOI: 10.1002/anie.200300610.

[25] G. Férey, C. Serre, *Chem. Soc. Rev.* **2009**, *38*, 1380–1399. DOI: 10.1039/B804302G

[26] S. Horike, S. Shimomura, S. Kitagawa, *Nat. Chem.* **2009**, *1*, 695–704. DOI: 10.1038/NCHEM.444

[27] A. Schneemann, V. Bon, I. Schwedler, I. Senkovska, S. Kaskel, R. A. Fischer, *Chem. Soc. Rev.* **2014**, *43*, 6062–6096. DOI: 10.1039/c4cs00101j

[28] D. Fairen-Jimenez, S. A. Moggach, M. T. Wharmby, P. A. Wright, S. Parsons, T. Düren, *J. Am. Chem. Soc.* **2011**, *133*, 8900–8902. DOI: 10.1021/ja202154j

[29] S. Krause, V. Bon, I. Senkovska, U. Stoeck, D. Wallacher, D. M. Többens, S. Zander, R. S. Pillai, G. Maurin, F.-X. Coudert, S. Kaskel, *Nature* **2016**, *532*, 348–352. DOI: 10.1038/nature17430

[30] F. Leysser, S. Hagen, L. Ovari, J. Dokic, P. Saalfrank, M. V. Peters, S. Hecht, T. Klamroth, P. Tegeder, *J. Phys. Chem. C* **2010**, *114*, 1231–1239. DOI: 10.1021/jp909684x

[31] S. Sasaki, G. P. C. Drummen, G. Konishi, *J. Mater. Chem. C* **2016**, *4*, 2731–2743. DOI: 10.1039/c5tc03933a

[32] Y. Yan, M. E. Mariott, C. Petchprayoon, G. Mariott, *Biochem. J.* **2011**, *433*, 411–422. DOI: 10.1042/BJ20100992

[33] Z. Wang, S. Grosjean, S. Bräse, L. Heinke, *ChemPhysChem* **2015**, *16*, 3779–3783. DOI: 10.1002/cphc.201500829

[34] A. Modrow, D. Zargarani, R. Herges, N. Stock, *Dalton Trans.* **2012**, *41*, 8690–8696. DOI: 10.1039/C2DT30672G

[35] J. Park, D. Q. Yuan, K. T. Pham, J. R. Li, A. Yakovenko, H. C. Zhou, *J. Am. Chem. Soc.* **2012**, *134*, 99–102. DOI: 10.1021/ja209197f

[36] B. J. Furlong, M. J. Katz, *J. Am. Chem. Soc.* **2017**, *139*, 13280–13283. DOI: 10.1021/jacs.7b07856.

[37] C. B. Fan, Z. Q. Liu, L. L. Gong, A. M. Zheng, L. Zhang, C. S. Yan, H. Q. Wu, X. F. Feng, F. Luo, *Chem. Commun.* **2017**, *4*, 763–766. DOI: 10.1039/C6CC08982H

[38] W. An, D. Aulakh, X. Zhang, W. Verdegaal, K. R. Dunbar, M. Wriedt, *Chem. Mater.* **2016**, *28*, 7825–7832. DOI: 10.1021/acs.chemmater.6b03224

[39] K. Weh, M. Noack, R. Ruhmann, K. Hoffmann, P. Toussaint, J. Caro, *Chem. Eng. Technol.* **1998**, *5*, 408–412.

[40] K. Weh, M. Noack, K. Hoffmann, K.-P. Schröder, J. Caro, *Microporous Mesoporous Mater.* **2002**, *54*, 15–26.

[41] A. Knebel, L. Sundermann, A. Mohmeyer, I. Strauß, S. Friebe, P. Behrens, J. Caro, *Chem. Mater.* **2017**, *29*, 3111–3117. DOI: 10.1021/acs.chemmater.7b00147

[42] K. Hoffmann, F. Marlow, J. Caro, *J. Fluoresc.* **1994**, *4*, 75–77.

[43] S. Castellanos, F. Kapteijn, J. Gascon, *CrystEngComm* **2016**, *18*, 4006–4012. DOI: 10.1039/c5ce02543e

[44] R. Lyndon, K. Konstas, B. P. Ladewig, P. D. Southon, C. J. Kepert, M. R. Hill, *Angew. Chem., Int. Ed.* **2013**, *52*, 3695–3698. DOI: 10.1002/anie.201206359

[45] A. B. Kanj, K. Müller, L. Heinke, *Macromol. Rapid Commun.* **2018**, *39*, 1700239. DOI: 10.1002/marc.201700239

[46] Z. Wang, A. Knebel, S. Grosejean, D. Wagner, S. Bräse, C. Wöll, J. Caro, L. Heinke, *Nat. Commun.* **2017**, *7*, 13872. DOI: 10.1038/ncomms13827

[47] H. Rau, in *Photochemistry and Photophysics* (Eds: J. F. Rabek, G. W. Scott), CRC Press, Boca Raton, FL **1990**, Vol. 4, 120–141.

[48] H. Huang, H. Sato, T. Aida, *J. Am. Chem. Soc.* **2017**, *139*, 8784–8787. DOI: 10.1021/jacs.7b02979

[49] Z. Wang, L. Heinke, J. Jelik, M. Cakici, M. Dommaschk, R. J. Maurer, H. Oberhofer, S. Grosejean, R. Herges, S. Bräse, K. Reuter, C. Wöll, *Phys. Chem. Chem. Phys.* **2015**, *17*, 14582–14587. DOI: 10.1039/c5cp01372k

[50] J.-R. Li, R. J. Kuppler, H.-C. Zhou, *Chem. Soc. Rev.* **2009**, *38*, 1477–1504. DOI: 10.1039/b802426j

[51] K. Müller, A. Knebel, F. Zhao, D. Bleger, J. Caro, L. Heinke, *Chem. – Eur. J.* **2017**, *23*, 5434–5438. DOI: 10.1002/chem. 201700989

[52] C. A. Fernandez, P. C. Martin, T. Schaef, M. E. Bowden, P. K. Thallapally, L. Dang, W. Xu, X. Chen, P. McGrail, *Sci. Rep.* **2014**, *4*, 6114. DOI: 10.1038/srep06114

[53] Z. M. Ao, A. D. Hernandez–Nieves, F. M. Peeters, S. Li, *Phys. Chem. Chem. Phys.* **2012**, *14*, 1463–1467. DOI: 10.1039/ c1cp23153g

[54] W. Liu, Y. H. Zhao, Y. Li, E. J. Lavernia, Q. Jiang, *Phys. Chem. Chem. Phys.* **2009**, *11*, 9233–9240. DOI: 10.1039/B907591G

[55] B. Tam, O. Yazaydin, *J. Mater. Chem. A* **2017**, *5*, 8690–8696. DOI: 10.1039/c7ta00101k

[56] P. Jain, A. Stroppa, D. Nabok, A. Marino, A. Rubano, D. Paparo, M. Matsubara, H. Nakotte, M. Fiebig, S. Picozzi, E. S. Choi, A. K. Cheetham, C. Draxl, N. S. Dalal, V. S. Zapf, *npj Quantum Mater.* **2016**, *1*, 16012. DOI: 10.1038/npjquantmats. 2016.12

[57] A. Ghoufi, K. Benhamed, L. Boukli-Hacene, G. Maurin, *ACS Cent. Sci.* **2017**, *3*, 394–398. DOI: 10.1021/acscentsci. 6b00392

[58] R. Schmid, *ACS Cent. Sci.* **2017**, *3*, 369–371. DOI: 10.1021/ acscentsci.7b00162

[59] K. Titov, Z. Zheng, M. R. Ryder, A. K. Chaudhari, B. Civalleri, C. S. Kelley, M. D. Frogley, G. Cinque, J.-C. Tan, *J. Phys. Chem. Lett.* **2017**, *8*, 5035–5040. DOI: 10.1021/acs.ipclett. 7b02003

[60] B. Tam, O. Yazaydin, *J. Mater. Chem. A* **2017**, *5*, 8690–8696. DOI: 10.1039/c7ta00101k

[61] A. Knebel, B. Geppert, K. Volgmann, D. I. Kolokolov, A. G. Stepanov, P. Twiefel, P. Heitjans, D. Volkmer, J. Caro, *Science* **2017**, *358*, 347–351. DOI: 10.1126/science.aal2456

[62] H. T. Kwon, H.-K. Jeong, *Chem. Commun.* **2013**, *49*, 3854–3856. DOI: 10.1039/c3cc41039k

[63] M. Shah, H. T. Kwon, V. Tran, S. Sachdeva, H.-K. Jeong, *Microporous Mesoporous Mater.* **2013**, *165*, 63–69. DOI: 10.1016/j.micromeso.2012.07.046

[64] F.-X. Coudert, *ChemPhysChem* **2017**, *18*, 2732–2738. DOI: 10.1002/cphc.201700463

[65] T. Akutagawa, T. Akutagawa, H. Koshinaka, D. Sato, S. Takeda, S.-I. Noro, H. Takahashi, R. Kumai, Y. Tokura, T. Nakamura, *Nat. Mater.* **2009**, *8*, 342–347. DOI: 10.1038/ nmat2377

- 53 -

3. Thin-Layer Preparation Techniques for MOF-Based Membranes

3.1. Summary

MOF-based membranes began to develop almost immediately after the invention of MOFs. Nowadays, the state-of-the-art membranes are very thin and have high fluxes and high separation factors. To achieve these properties advanced preparation methods have widely developed. In the following chapter a layer-by-layer approach towards the synthesis of nanosized MOF heterostructures is shown in a paper published in *Chemistry – A European Journal*. As it was highly interesting to a broad readership and received very good reviews it was featured as a hot paper with a cover picture.

The layer-by-layer technique allows a very controlled growth of nanostructures as particles and layers by self-assembly and we could transfer this to the thin layer membrane fabrication. Those heterostructures are made of a ZIF-8-on-ZIF-67 material combination and were applied as neat, thin layer MOF membrane or as particles in mixed-matrix membranes. The combination of the two MOFs in the MOF-on-MOF membranes show additive properties improving the gas separation compared to the single ZIF-8 and ZIF-67, but also compared to other MOF materials. Especially in H_2 purification and CO_2 capture applications this heterostructures perform surprisingly well.

We show that the increased performance and the preparation techniques are highly interesting when industrial application is planned: The self-assembly and layer-by-layer techniques allow a fast and easy approach with the potential to upscale. The size on the nanometre scale of the produced layers could be determined by a combination of XRD, SEM and EDXS. More interesting is the nanoparticle core-shell approach. Industrial scaled polymeric membrane walls are in the range of 10-300 nm and the presented heterostructured particles are 35 nm in diameter. Thus, it would be possible to produce defect free MMMs with a utilizable size range.

We could show that the easy approach of self-assembly, either as thin layer in neat MOF-on-MOF membranes or as heterostructured nanoparticles for the preparation of MMMs gives increased separation performance that outperform the single materials and comparable other MOFs membrane systems. Especially for H_2/CO_2 separation these membranes are highly interesting.

3.2. Hierarchical Nanostructures of Metal-Organic Frameworks Applied in Gas Separating ZIF-8-on-ZIF-67 Membranes

A. Knebel, P. Wulfert-Holzmann, S. Friebe, J. Pavel, I. Strauß, A. Mundstock, F. Steinbach, J. Caro

- 56 -

CHEMISTRY
A European Journal

www.chemeurj.org

A Journal of
ChemPubSoc
Europe
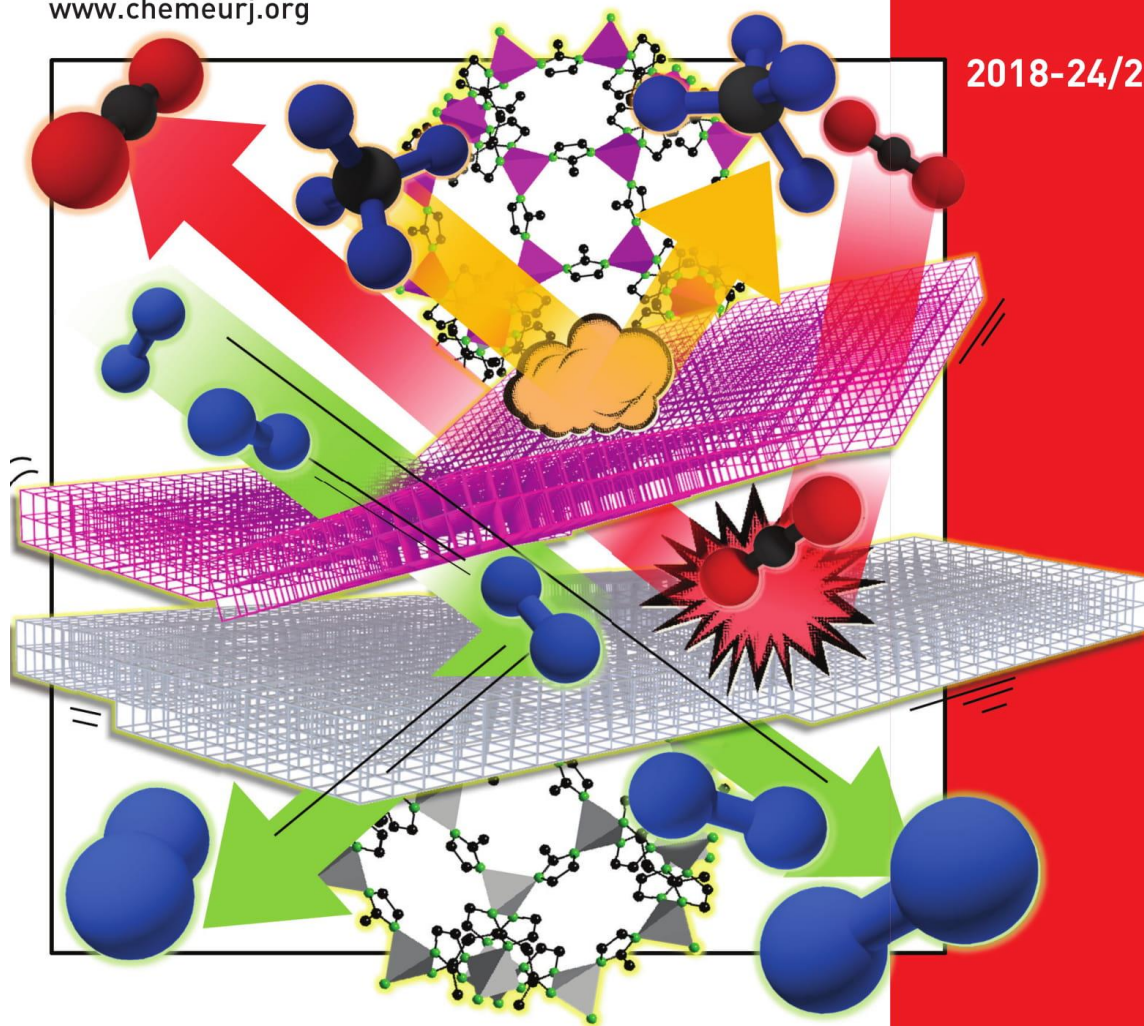
2018-24/22

Cover Feature:
A. Knebel et al.
Hierarchical Nanostructures of Metal-Organic Frameworks Applied
in Gas Separating ZIF-8-on-ZIF-67 Membranes

Supported by
ACES Asian Chemical Editorial Society

WILEY-VCH

COVER PICTURE

A. Knebel,* P. Wulfert-Holzmann, S. Friebe,
J. Pavel, I. Strauß, A. Mundstock,
F. Steinbach, J. Caro

■■ – ■■

Hierarchical Nanostructures of Metal–Organic Frameworks Applied in Gas-Separating ZIF-8-on-ZIF-67 Membranes

Hierarchical ZIF-8-on-ZIF-67 gas separation membranes: It is possible to synthesize hierarchical thin layers and nanoparticles with precise growth control on the nanometer scale by self-assembly. The neat ZIF-8-on-ZIF-67 layers are supported α-Al_2O_3, while nanoparticles are embedded in free-standing mixed-matrix membranes. The ZIF-8-on-ZIF-67 membranes show increased performance compared with membranes with only ZIF-8 or ZIF-67. More information can be found in the Communication by A. Knebel et al. (DOI: 10.1002/chem.201705562).

▌Metal-Organic Frameworks ┃Hot Paper┃

Hierarchical Nanostructures of Metal-Organic Frameworks Applied in Gas Separating ZIF-8-on-ZIF-67 Membranes

Alexander Knebel+,*[a] Paul Wulfert-Holzmann+,[a] Sebastian Friebe,[a] Janet Pavel,[a] Ina Strauß,[a, b] Alexander Mundstock,[a] Frank Steinbach,[a] and Jürgen Caro[a, b]

Abstract: Membranes from metal-organic frameworks (MOFs) are highly interesting for industrial gas separation applications. Strongly improved performances for carbon capture and H$_2$ purification tasks in MOF membranes are obtained by using highly reproducable and very accuratly, hierarchically grown ZIF-8-on-ZIF-67 (ZIF-8@ZIF-67) nanostructures. To forgo hardly controllable solvothermal synthesis, particles and layers are prepared by self-assembling methods. It was possible for the first time to confirm ZIF-8-on-ZIF-67 membrane growth on rough and porous ceramic supports using the layer-by-layer deposition. Additionally, hierarchical particles are made in a fast RT synthesis with high monodispersity. Characterization of the hierarchical and epitaxial grown layers and particles is performed by SEM, TEM, EDXM and gas permeation. The system ZIF-8@ZIF-67 shows a nearly doubled H$_2$/CO$_2$ separation factor, regardless of whether neat membrane or mixed-matrix-membrane in comparison to other MOF materials.

For membranes consisting of neat metal-organic framework (MOFs) layers or mixed-matrix-membranes (MMMs) containing MOFs as filler materials a reduction of the layer thickness and filler size is crucially important to meet industrial requirements. MOF particles should reach average particle sizes below 100 nm-not for the separative purpose of MMMs,[1] but when thinking of industrial upscaling. Neat MOF layers should also be prepared as thin as possible to provide state of the art properties: good separation factors at high flux. MOF thin layers have been developed widely, for example, preparation on conducting and semiconducting substrates were invent-

ed.[2] Reasearchers found a lot of different applications, for example guest release,[3] optical coatings,[4] and microelectronics[5] such as memristors[6] or optoelectronic hybrid devices.[7] Nucleation and growth mechanisms of MOFs have been investigated a lot[8] and this also included thin layer formation,[9] which was helpful regarding the transfer to membrane synthesis. Looking at the production of thin layered MOF membranes, very complicated techniques have set new hights, such as gel-vapour deposition[10] and counter diffusion in microfluidic processing of membranes.[11] However, liquid phase epitaxy is an excellent technique for thin film coatings on flat substrates, often supported by self assembled monolayers which are chemically or physically bound to the original surface, laying the foundation for "surface anchored metal-organic frameworks" (SURMOFs).[12] With liquid phase epitaxy, it is possible to synthesize MOFs layer-by-layer with extremely defined thickness.[13] However, synthesis of these SURMOFs needs conditions for self-assembly. This is possible, for example for HKUST-1 that can be spray-coated[14] or spin-coated.[15] The liquid phase epitaxy can fabricate MOF membranes, for instance ZIF-8[16] or light switchable MOFs with tailored linker molecules in a pillar-layer fashion.[17] These membranes either showed defects or could not be prepared thinner than 1 μm originating from the rough surface from porous ceramic substrates. For our study we used ZIF-8 and ZIF-67,[18] two nearly identical MOFs, but consisting of Zn-metal nodes in case of ZIF-8 and Co-metal nodes in case of ZIF-67. Conventional membranes prepared of these materials by solvothermal synthesis were reported before.[19] However, we achieved to prepare ZIF-67 and a ZIF-8-on-ZIF-67 membranes only by self assembly and with exactly controlled layer thickness of 180 nm by layer-by-layer growth. By functionalization we could decisevely improve the preparation on rough surfaces, such as porous α-Al$_2$O$_3$.[20] The hierarchical membanes were tested in gas separation, especially hydrogen purification tasks, such as pre-combustion, where H$_2$ needs to be removed from a mixture with CO$_2$. In the pre-combustion process, H$_2$ is burned with O$_2$ to H$_2$O as green waste gas, CO$_2$ is captured in the underground.[21] Further, separating hydrogen from other system is mandatory when using natural gas or oil for the combustive production of hydrogen.[22] The neat ZIF-8@ZIF-67 membrane showed very good results, especially for H$_2$/CO$_2$ separation. We wanted to prepare comparable MMMs, thus inventing a novel synthesis for ZIF-8@ZIF-67 hybrid nanoparticles with extremely small particle sizes of 55 nm at complete monodispersity. The hybrid particles reported from literature were micrometer sized[23] and

[a] A. Knebel,+ P. Wulfert-Holzmann,+ Dr. S. Friebe, J. Pavel, I. Strauß,
    A. Mundstock, F. Steinbach, Prof. Dr. J. Caro
    Institute for Physical Chemistry and Electrochemistry
    Leibniz University Hannover
    Callinstrasse 3A, 30167 Hannover (Germany)
    E-mail: E-malexander.knebel@pci.uni-hannover.de

[b] I. Strauß, Prof. Dr. J. Caro
    Laboratory of Nano and Quantum Engineering (LNQE)
    Leibniz University Hannover
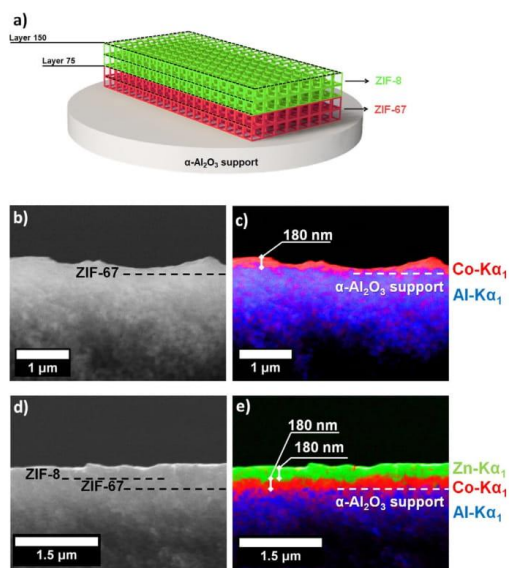   Schneiderberg 39, 30167 Hannover (Germany)

[+] These authors contributing equally to this work.

    Supporting information and the ORCID identification number(s) for the author(s) of this article can be found under:
    https://doi.org/10.1002/chem.201705562.

thereby nonrelevant for industrial useful MMMs with 0.1–0.2 μm wall thickness.[24] MMM's performance, especially H_2/CO_2 separation, is strongly increased compared to both single materials, as found also for the neat ZIF-8-on-ZIF-67 system.

Ultrathin ZIF-67 and ZIF-8-on-ZIF-67 layers have been prepared defect-free on ceramic α-Al_2O_3 discs by 75 cycles of layer-by-layer growth. One cycle means that we immerse the support consecutively in the linker-solution and metal-solution for a certain time period to allow self-assembly of the layer. Each step is followed by a washing step with pure solvent to remove residual chemicals (c.f. Supporting Information). A very beneficial aspect of the SURMOF process is that only very low amounts of metal-salt and linker are needed, but on the expense of high solvent consumption. For expensive chemicals such as Co-salts in our case, a recovery of salt and solvent is a realistic possibility when thinking of high throughput synthesis and large area coatings. In Figure 1 a the principle of the layer-by-layer growth is shown. The SEM image and corresponding EDX mapping (EDXM) of the ZIF-67 (c.f. Figure 1 b, c) and the ZIF-8-on-ZIF-67 membrane (Figure 1 c, d) show a layer thickness of 180 nm.

Through the characteristic X-ray wavelengths ZIF-8 and ZIF-67 could be identified successfully. The layer formation for ZIF-67 and ZIF-8 is defect-free and yields an identical layer thickness of 180 nm each for the ZIF-8-on-ZIF-67 membrane. How-ever, a SURMOF membrane, when preparing the layer with 75 cycles, should yield-assuming the cubic unit cell side length of ZIF-8 and ZIF-67 of a,b,c ≈1.7 nm-a 127.5 nm thick layer.[25, 26] Here we found thicknesses of around 180 nm, which is attributed to the roughness of the support, but assuming a cube of 127.5 nm is standing on its edge, its height is exactly 180 nm, we conclude that the crystals start growing from their edges, thus a layer-by-layer grown SURMOF membrane. Another point that supports this argument is that the ZIF-8 layer, under the exact same synthetic conditions, yields the exact same thickness as the ZIF-67 layer, shown in Figure 1 d. Crystal structure analysis was performed by X-ray diffraction, given in Figure 2, allowing a determination that ZIF-8 was grown hierarchically on ZIF-67. New reflexes and higher reflex intensities are found, which is corresponding to a further crystal growth and in conjunction with the SEM results in Figure 1, we can proof the success of our heteroepitaxial SURMOF growth.
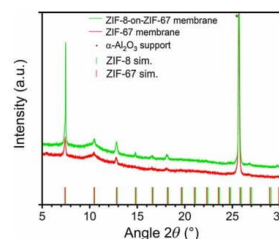
Figure 2. XRD of the ZIF-67 (black) and ZIF-8-on-ZIF-67 (red) membranes and corresponding simulated reflexes (CCDC 671073 (ZIF-67, red line),[25] 963856 (ZIF-8, green line)[26] contain the supplementary crystallographic data for this paper. These data can be obtained free of charge from The Cambridge Crystallographic Data Centre. The reflex positions of ZIF-8 and ZIF-67 are nearly the same. Higher reflex intensities on all positions in the ZIF-8@ZIF-67 membrane and emerging reflexes (c.f. 14.8, 22.2°2θ) give evidence for layer-on-layer growth.[27] The asterisk gives the reflex of the supporting α-Al_2O_3 disc. The overall crystallinity of the layers is well and reflex broadening is visible, because of the only very few layers.

Figure 1. SEM analysis of the ZIF-67 and ZIF-8-on-ZIF-67 membranes at 20 kV accelerating voltage. (a) Gives a simple schematic view on how the self-assembly of the membranes works for layer-by-layer deposition. (b) and (c) show SEM and EDXM of the ZIF-67 membrane cross-section. ZIF-8-on-ZIF-67 membrane: (d) and (e) show the SEM and EDXM cross-section picture of the dual layer. It can be seen that the procedure results in exactly defined layer thicknesses, corresponding to the number of cycles. Color code of EDXS: $Zn_{Kα1}$ green, $Co_{Kα1}$ red, $Al_{Kα1}$ blue.

For gas permeation experiments the separation through the neat ZIF-67 and ZIF-8-on-ZIF-67 membranes with binary mixtures of the probe gases was tested in a Wicke-Kallenbach setup under ambient conditions. The results are shown in Figure 3. To proof that the membranes separation is the same when permeating from the ZIF-8 to ZIF-67 side, and vice versa, the membrane was flipped in the gas flow direction. Very comparable results were collected for different gas mixtures H_2/CO_2, H_2/CH_4, H_2/N_2, H_2/ethane, H_2/ethylene, H_2/propane and H_2/propylene (c.f. Figure 3 b–h).

No direction dependency on the gas permeation means ZIF-8 is not growing on the expense of ZIF-67 and vice versa. Also, we do not find direction dependent adsorption effects on the separation, excluding defects in one of the layers. This further proofs the epitaxial growth: The ZIF-8 does not introduce defects into the ZIF-67 membrane, thus we find additional adsorptive separation behaviour in the material and both layers are separating additionally. The membrane performs very well
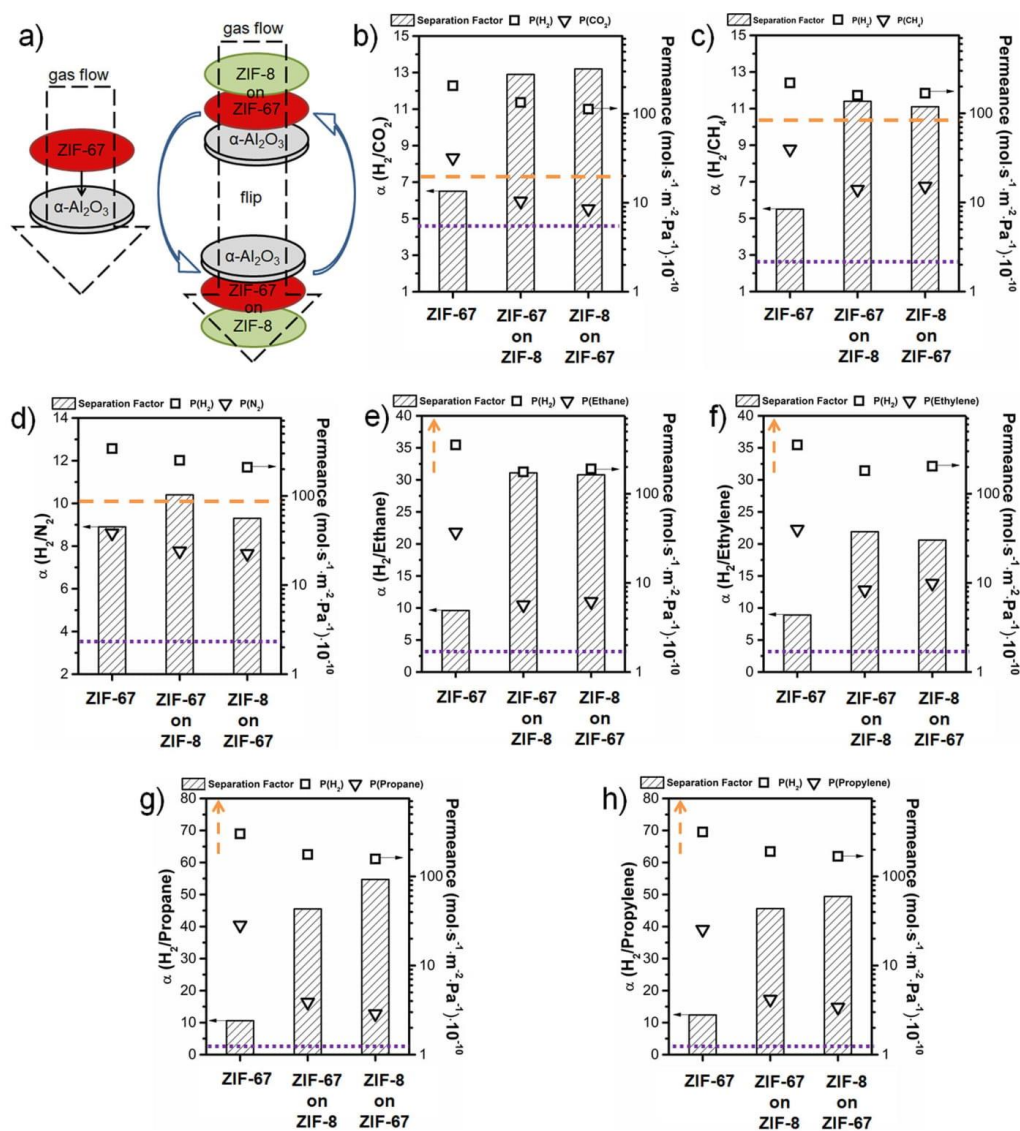
Figure 3. (a) Schematically measuring principle to clarify the permeation data in both directions of the neat, supported ZIF-67, ZIF-67-on-ZIF-8 and ZIF-67-on-ZIF-8 layers (c.f. Figure 1). (b) Permeation data for H_2/CO_2, (c) for H_2/CH_4, (d) for H_2/N_2, (e) for $H_2/ethane$, (f) for $H_2/ethylene$, (g) for $H_2/propane$, and (h) for $H_2/propylene$. All membranes show clearly a separation factor α above Knudsen (purple, dotted line). The orange dashed line shows the performance of conventionally prepared neat ZIF-8 membrane taken from comparable literature data.[28–31]

for the separation of smaller gases like H_2/CO_2, H_2/CH_4 and H_2/N_2. In case of the H_2/N_2 separation in Figure 3c, the performance of the ZIF-67 membrane is nearly as good as of the ZIF-8-on-ZIF-67 membrane, being close to the literature values for ZIF-8 membranes without significant improvement.[28] In

case of H_2/CH_4 (c.f. Figure 3b) the ZIF-67 membrane performs far above Knudsen but loses compared to the conventional ZIF-8 membrane. Even though, the combination of ZIF-67 and ZIF-8 in the epitactically grown membrane yields an improved separation performance.[29] Finally the H_2/CO_2 separation

- 61 -

(Figure 3 b) values are comparable between ZIF-67 and ZIF-8, but when in combination, the separation performance is nearly doubled and exceeds the best values found in literature by a factor of two.[30] In case of H_2/ethane, H_2/ethylene, H_2/propane and H_2/propylene (Figure 3 e–h) the membranes are far above the values for Knudsen diffusion, however staying also far behind the literature values. A deeper look behind growth mechanisms[32] explains the low H_2/C_2 and H_2/C_3 separation: Using smaller pores and thereby decreasing the roughness of the support would probably be a benefit to the layer-by-layer method and could yield an even better crystal-support interface. The interface on which crystallization takes place is important for the separation of olefin/paraffin and this membranes probably suffer from infiltration, as stated by Kwon et al.[32]

The ZIF-8@ZIF-67 hybrid core–shell particles were prepared in a self-assembly synthesis at RT for application in MMMs, as the H_2/CO_2 separation was found to be a benchmark application for this heterostructures. Synthesis times are with 5 minutes extremely short. The cleaned but not dry ZIF-8 particles were used as seed crystals for the synthesis of the ZIF-67 shell. The particles show very good crystallinity and are highly monodisperse. XRD analysis and SEM pictures can be found in the SI. From the size of the core and shell layer, determined from STEM pictures in Figure 4 a, we find a 60:40 volume ratio of ZIF-67 to ZIF-8.

The EDXM of the ZIF-8@ZIF-67 particles (c.f. Figure 4 b) shows a distribution of Co at a higher concentration at the particles edges, which was expected for a core@shell morphology. The element maps in Figure 4 c–e show clearly the distribution of Zn in the core, meaning ZIF-8, whereas high intensity of Co (therefore ZIF-67) is found in the shell. The $N_{K\alpha 1,2}$ signal is found over the whole range of the particle corresponding to methylimidazole (Hmim) (Figure 4 e). Therefore, we conclude that a self-assembled core@shell particle has been synthesized, given in Figure 4 f.

MMMs with Matrimid were prepared using 10 wt.% of the hybrid particles in a solution of dichloromethane (DCM) casted on a glass substrate. The membranes were slowly dried in a DCM atmosphere and afterwards cured at 100 °C and 50 mbar for 72 h (c.f. Supporting Information). SEM pictures of the used membranes shown in Figure 5 a and b give a closer look at the microstructure of these freestanding MMMs. No visible defects can be found, the surface is smooth. The membranes show high fluxes and good separation factors in the corresponding gas permeation measurements, meaning they were completely dense. Photos of the as prepared membranes are shown in Figure 5 c, d. The membranes are extremely thin and transparent and allow reading of the logo of the Leibniz University Hannover. Thus, they are extremely flexible and not brittle.

The gas permeation results are given in the Robeson plots at RT and 150 °C (c.f. Figure 5 e and f) where the upper bound is corresponding to the state-of-the-art polymeric membranes performance throughout literature data.[33] As the polymer membranes upper bound was updated the last time in 2008[33] we added several data points, which are directly comparable to our data sets in terms of temperature, pressure, wt.% filler and the used polymer Matrimid.

The prepared MMM with the ZIF-8@ZIF-67 hybrid particles shows an increased selectivity for H_2/CO_2 precombustion carbon capture application at both RT and 150 °C with $\alpha = 5.5$ and 7, respectively. The flux through the ZIF-8@ZIF-67 membrane is also increased, exceeding those of all other compared particles. At RT the MMM has a permeability of 100 Barrer, whereas at 150 °C the membranes permeability is further increased to 120 Barrer. Comparing selectivity and permeability in all cases, the used material is upon the best MOF filler particle reported for use in a Matrimid matrix.

In conclusion, ultrathin supported membranes of ZIF-67 or hierarchically grown ZIF-8-on-ZIF-67, as well as free standing MMMs containing ZIF-8@ZIF-67 nanoparticles, have shown to be promising candidates for H_2/CO_2 separation. Hierarchical
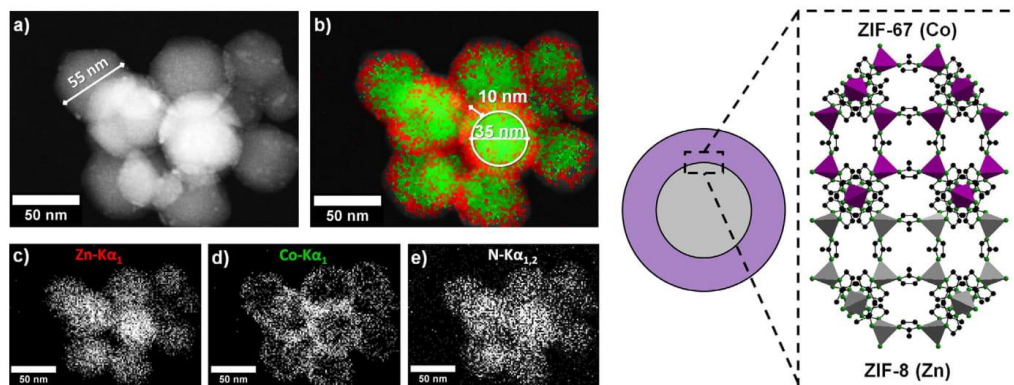
Figure 4. (a) STEM image of ZIF-8 core and ZIF-67 shell particles with particle sizes of 55 nm. (b) TEM-EDXM of core and shell are given as colorized mix of $Zn_{K\alpha 1}$ and $Co_{K\alpha 1}$ element maps (c), (d). The ZIF-8 core has 35 nm diameter, wheras the shell is around 10 nm. Element maps in (c), (d) and (e) show the detailed elemental distribution of the core (Zn), shell (Co) and the linker (N) over the whole particle. (f) Shows the assumed crystal structure of ZIF-8@ZIF-67, grey for Zn^{2+}, purple for Co^{2+} coordinating tetrahedral units. N is green, C is black, H is hidden.
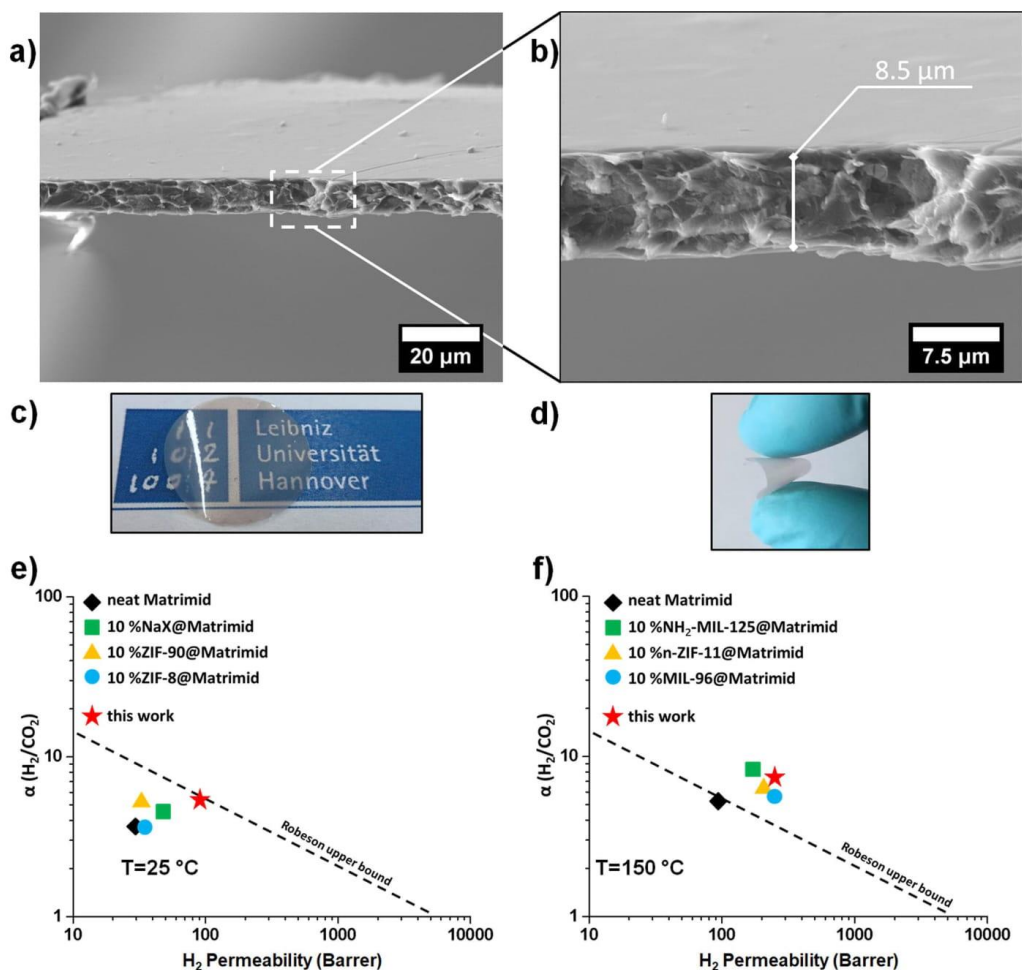
Figure 5. (a) and (b) SEM images of the freestanding MMM cointaining 10 wt.% ZIF-8@ZIF-67 particles in Matrimid prepared by doctor blading. The membrane surface is smooth without visible defects. (c) and (d) are two photographs of the membranes. The membrane permeation data (e) at RT and (f) at 150°C for precombustion is compared to the Robson upper bound and exceeds gas separation values of other Matrimid MMMs containing MOF materials. Studies used for the materials in Matrimid, comparison at RT and 1 bar, NaX,[34] ZIF-90,[35] ZIF-8[35] and at 150°C for nano-ZIF-11,[36] NH2-MIL-125,[37] MIL-96,[38] neat Matrimid.[38]

structures of both, neat MOF layers and particles, have been characterized by SEM and TEM imaging and the hierarchical growth could be confirmed. The neat supported ZIF-67 and ZIF-8-on-ZIF-67 membranes were evaluated in H_2 gas separation tasks and showed an improved performance compared to solvothermally prepared membranes. The ZIF-8-on-ZIF-67 double layer shows additive adsorption effects resulting in improved selectivity. Nanoparticles of ZIF-8@ZIF-67 have been prepared with a size of 55 nm, and were embedded into a Matrimid matrix. Also the MMMs containing the hierarchically grown ZIF-8@ZIF-67 nanoparticles were tested in H_2/CO_2 separation at RT and 150°C and atmospheric pressure, exceeding flux and selectivity of different MOFs (MIL-125-NH_2 to ZIF-90, NaX zeolites, and ZIF-8). The MMMs' H_2/CO_2 separation lies above the Robeson upper bound, which makes them relevant candidates for industrial application. Thus, the main advantage of hierarchical MOF membranes is the additive adsorption, improving specific separation tasks, in neat MOF membranes, as well as in MMMs.

ChemPubSoc
Europe

- 64 -

CHEMISTRY
A European Journal
Communication

Conflict of interest

The authors declare no conflict of interest.

Keywords: carbon capture · hydrogen purification · metal-organic frameworks · membranes · mixed-matrix-membrane (MMM)

[1] J. Dechnik, J. Gascon, C. J. Doonan, C. Janiak, C. J. Sumby, *Angew. Chem. Int. Ed.* **2017**, *56*, 9292; *Angew. Chem.* **2017**, *129*, 9420.
[2] O. Shekhah, J. Liu, R. A. Fischer, C. Wöll, *Chem. Soc. Rev.* **2011**, *40*, 1081.
[3] L. Heinke, M. Tu, S. Wannapaiboon, R. A. Fischer, C. Wöll, *Microporous Mesoporous Mater.* **2015**, *216*, 200.
[4] C.-Y. Sun, X.-L. Wang, X. Zhang, C. Qin, P. Li, Z.-M. Su, D.-X. Zhu, G.-G. Shan, K.-Z. Shao, H. Wu, J. Li, *Nat. Commun.* **2013**, *4*, 2717.
[5] M. D. Allendorf, A. Schwartzberg, V. Stavila, A. A. Talin, *Chem. Eur. J.* **2011**, *17*, 11372.
[6] S. M. Yoon, S. C. Warren, B. A. Grzybowski, *Angew. Chem. Int. Ed.* **2014**, *53*, 4437; *Angew. Chem.* **2014**, *126*, 4526.
[7] a) G. Lu, O. K. Farha, W. Zhang, F. Huo, J. T. Hupp, *Adv. Mater.* **2012**, *24*, 3970; b) V. Stavila, A. A. Talin, M. D. Allendorf, *Chem. Soc. Rev.* **2014**, *43*, 5994.
[8] M. Shoaee, M. W. Anderson, M. P. Attfield, *Angew. Chem. Int. Ed.* **2008**, *47*, 8525; *Angew. Chem.* **2008**, *120*, 8653.
[9] A. Summerfield, I. Cebula, M. Schröder, P. H. Beton, *J. Phys. Chem. C* **2015**, *119*, 23544.
[10] W. Li, P. Su, Z. Li, Z. Xu, F. Wang, H. Ou, J. Zhang, G. Zhang, E. Zeng, *Nat. Commun.* **2017**, *8*, 406.
[11] A. J. Brown, N. A. Brunelli, K. Eum, F. Rashidi, J. R. Johnson, W. J. Koros, C. W. Jones, S. Nair, *Science* **2014**, *345*, 72.
[12] J.-L. Zhuang, A. Terfort, C. Wöll, *Coord. Chem. Rev.* **2016**, *307*, 391.
[13] O. Shekhah, H. Wang, D. Zacher, R. A. Fischer, C. Wöll, *Angew. Chem. Int. Ed.* **2009**, *48*, 5038; *Angew. Chem.* **2009**, *121*, 5138.
[14] S. Hurrle, S. Friebe, J. Wohlgemuth, C. Wöll, J. Caro, L. Heinke, *Chem. Eur. J.* **2017**, *23*, 2294.
[15] V. Chernikova, O. Shekhah, M. Eddaoudi, *ACS Appl. Mater. Interfaces* **2016**, *8*, 20459.
[16] E. P. Valadez Sánchez, H. Gliemann, K. Haas-Santo, C. Wöll, R. Dittmeyer, *Chem. Ing. Tech.* **2016**, *88*, 1798.
[17] Z. Wang, A. Knebel, S. Grosjean, D. Wagner, S. Bräse, C. Wöll, J. Caro, L. Heinke, *Nat. Commun.* **2016**, *7*, 13872.
[18] P. Krokidas, M. Castier, S. Moncho, D. N. Sredojevic, E. N. Brothers, H. T. Kwon, H.-K. Jeong, J. S. Lee, I. G. Economou, *J. Phys. Chem. C* **2016**, *120*, 8116.
[19] a) H. T. Kwon, H.-K. Jeong, A. S. Lee, H. S. An, J. S. Lee, *J. Am. Chem. Soc.* **2015**, *137*, 12304; b) C. Wang, F. Yang, L. Sheng, J. Yu, K. Yao, L. Zhang, Y. Pan, *Chem. Commun.* **2016**, *52*, 12578; c) F. Cacho-Bailo, I. Matito-Martos, J. Perez-Carbajo, M. Etxeberría-Benavides, O. Karvan, V. Sebastián, S. Calero, C. Téllez, J. Coronas, *Chem. Sci.* **2017**, *8*, 325.
[20] A. Bétard, H. Bux, S. Henke, D. Zacher, J. Caro, R. A. Fischer, *Microporous Mesoporous Mater.* **2012**, *150*, 76.
[21] M. Kanniche, R. Gros-Bonnivard, P. Jaud, J. Valle-Marcos, J.-M. Amann, C. Bouallou, *Appl. Therm. Eng.* **2010**, *30*, 53.
[22] N. Jusoh, Y. F. Yeong, T. L. Chew, K. K. Lau, A. M. Shariff, *Sep. Purif. Rev.* **2016**, *45*, 321.
[23] J. Yang, F. Zhang, H. Lu, X. Hong, H. Jiang, Y. Wu, Y. Li, *Angew. Chem. Int. Ed.* **2015**, *54*, 10889; *Angew. Chem.* **2015**, *127*, 11039.
[24] A. Livingston, R. Baker, *Nat. Mater.* **2017**, *16*, 280.
[25] R. Banerjee, A. Phan, B. Wang, C. Knobler, H. Furukawa, M. Keeffe, O. M. Yaghi, *Science* **2008**, *319*, 939.
[26] O. Shekhah, R. Swaidan, Y. Belmabkhout, M. Du Plessis, T. Jacobs, L. J. Barbour, I. Pinnau, M. Eddaoudi, *Chem. Commun.* **2014**, *50*, 2089.
[27] O. Shekhah, K. Hirai, H. Wang, H. Uehara, M. Kondo, S. Diring, D. Zacher, R. A. Fischer, O. Sakata, S. Kitagawa S. Furukawa, C. Wöll, *Dalton Trans.* **2011**, *40*, 4954.
[28] H. Bux, A. Feldhoff, J. Cravillon, M. Wiebcke, Y.-S. Li, J. Caro, *Chem. Mater.* **2011**, *23*, 2262.
[29] H. Bux, F. Liang, Y. Li, J. Cravillon, M. Wiebcke, J. Caro, *J. Am. Chem. Soc.* **2009**, *131*, 16000.
[30] L. Fan, M. Xue, Z. Kang, H. Li, S. Qiu, *J. Mater. Chem.* **2012**, *22*, 25272.
[31] S. Qiu, M. Xue, G. Zhu, *Chem. Soc. Rev.* **2014**, *43*, 6116.
[32] H. T. Kwon, H.-K. Jeong, *Chem. Eng. Sci.* **2015**, *124*, 20.
[33] L. M. Robeson, *J. Membr. Sci.* **2008**, *320*, 390.
[34] A. Mundstock, S. Friebe, J. Caro, *Int. J. Hydrogen Energy* **2017**, *42*, 279.
[35] L. Diestel, N. Wang, A. Schulz, F. Steinbach, J. Caro, *Ind. Eng. Chem. Res.* **2015**, *54*, 1103.
[36] J. Sánchez-Laínez, B. Zornoza, Á. Mayoral, Á. Berenguer-Murcia, D. Cazorla-Amorós, C. Téllez, J. Coronas, *J. Mater. Chem. A* **2015**, *3*, 6549.
[37] S. Friebe, A. Mundstock, D. Unruh, F. Renz, J. Caro, *J. Membr. Sci.* **2016**, *516*, 185.
[38] A. Knebel, S. Friebe, N. C. Bigall, M. Benzaqui, C. Serre, J. Caro, *ACS Appl. Mater. Interfaces* **2016**, *8*, 7536.

- 65 -

4. Light-Switchable Metal-Organic Framework Membranes

4.1. Summary

Control over the pores of a material is a highly interesting field of invention that makes a direct process and application control possible. The control of gas transport with a contactless method in membrane separation can be achieved by the switching with light, implementing a highly versatile smart material to a highly desired technology. Additionally, our development aims towards multi-function switchable membranes using a single, switchable material for different separation tasks.

In the chapter 4.2. a pioneering work on *"Tunable molecular separation with nanoporous membranes"* is presented that allows selectivity control over CO_2 mixtures with a tailor-made MOF membrane: Through the irradiation with light, the cis-trans isomerism of AZB in the MOFs linker changes the composition of the gases on the permeate side. This achievement leads to diverse applications, such as a composition control between flammable or explosive gas mixtures of H_2, which would be interesting for pre-combustion processes. In addition, it was shown to be applicable for post-combustion tasks, separating N_2 from CO_2 with remotely tuneable separation.

The next work in chapter 4.3. shows how the exchange of the AZB group in such a light-switchable MOF is useful for a different separation: By introducing fluoro-AZB into a similar MOF strut (c.f. 4.2.), the materials switching can be achieved by only using visible light. Thereby, the material is protected from bleaching effects through the UV-irradiation that was earlier necessary for the switching. Nevertheless, the separation was investigated for mixtures of H_2/ethylene and H_2/propylene, which are interesting in H_2 generation processes from natural gas sources.

In chapter 4.4. another work on light-switchable membranes is presented where a UiO-67 membrane was loaded with AZB guest molecules. The preparation of the material represented is way easier than the previously shown membranes, because commercially available chemicals could be used. Control over the molecular separation was achieved and we could investigate and formulate a mechanism of the switching. As the separation of the AZB@UiO-67 membrane was completely different, comparing the impact on CO_2 permeability in cis and trans to the previous tailored membrane, we found that the separation is relying on gating mechanisms.

4.2.   Tunable Molecular Separation by Nanoporous Membranes

- 68 -

ARTICLE

Tunable molecular separation by nanoporous membranes

Zhengbang Wang[1,*], Alexander Knebel[2,*], Sylvain Grosjean[3], Danny Wagner[4], Stefan Bräse[3,4,5], Christof Wöll[1], Jürgen Caro[2] & Lars Heinke[1]

Metal-organic frameworks offer tremendous potential for efficient separation of molecular mixtures. Different pore sizes and suitable functionalizations of the framework allow for an adjustment of the static selectivity. Here we report membranes which offer dynamic control of the selectivity by remote signals, thus enabling a continuous adjustment of the permeate flux. This is realized by assembling linkers containing photoresponsive azobenzene-side-groups into monolithic, crystalline membranes of metal-organic frameworks. The azobenzene moieties can be switched from the *trans* to the *cis* configuration and *vice versa* by irradiation with ultraviolet or visible light, resulting in a substantial modification of the membrane permeability and separation factor. The precise control of the *cis:trans* azobenzene ratio, for example, by controlled irradiation times or by simultaneous irradiation with ultraviolet and visible light, enables the continuous tuning of the separation. For hydrogen:carbon-dioxide, the separation factor of this smart membrane can be steplessly adjusted between 3 and 8.

[1] Institute of Functional Interfaces (IFG), Karlsruhe Institute of Technology (KIT), Hermann-von-Helmholtz-Platz 1, 76344 Eggenstein-Leopoldshafen, Germany. [2] Institute for Physical Chemistry and Electrochemistry, Leibniz University Hanover, Callinstraße 3a, 30167 Hannover, Germany. [3] Soft Matter Synthesis Lab, Institute of Biological Interfaces 3 (IBG 3), Karlsruhe Institute of Technology (KIT), Hermann-von-Helmholtz-Platz 1, 76344 Eggenstein-Leopoldshafen, Germany. [4] Institute of Organic Chemistry (IOC), Karlsruhe Institute of Technology (KIT), Fritz-Haber-Weg 6, 76131 Karlsruhe, Germany. [5] Institute of Toxicology and Genetics (ITG), Karlsruhe Institute of Technology (KIT), Hermann-von-Helmholtz-Platz 1, D-76344 Eggenstein-Leopoldshafen, Germany. * These authors contributed equally to this work. Correspondence and requests for materials should be addressed to A.K. (email: alexander.knebel@pci.uni-hannover.de) or to L.H. (email: Lars.Heinke@kit.edu).

Many sustainable applications require an efficient and energy-saving separation of molecular mixtures[1]. In this context, membrane technologies hold substantial potential for the separation of gas or liquid mixtures, since they offer an economic, energy-saving and ecological alternative to energy-intensive distillation or cryogenic separations. To reach high efficiencies, compelling research efforts are undertaken to develop novel materials allowing the fabrication of membranes with high permeation fluxes and high molecular separation factors. Ultrathin polymer[2] and porous carbon[3] membranes as well as two-dimensional materials, like graphene and graphene oxide[4,5], are considered to be auspicious materials in this context, since they offer high permeation fluxes, chemical stability, extensive mechanical strength and flexibility. However, a remaining major challenge is the precise control over the chemical functionality and over the pore size. Recently, metal-organic frameworks (MOFs)[6], crystalline solids composed of metal nodes connected by organic linker molecules, demonstrated large potential for membrane separation processes[7–12]. MOFs possess an abundance of unique properties like well-defined, periodic nanoporous structures, large specific surface areas and large structural and chemical variety, with more than 20,000 different MOF structures published before 2013 (ref. 6). Furthermore, the structure or chemical functionality of MOFs can be modified by different pre- and post-synthetic methods[13], which allow to further adjust the specific properties of these porous materials.

Of particular interest with respect to membrane fabrication is remote control, that is, the ability to switch crucial membrane parameters, like permeance or selectivity, by external stimuli without direct contact. Integrating such smart membranes into separation systems is expected to lead to a major break-through in overall performance. Light is a particularly simple, handy and (usually) non-invasive signal. Thus, photosensitive molecules, which undergo reversible isomerization when irradiated with light of a certain wavelength, attract a lot of attention[14–16]. Photoisomerization processes are typically very fast and

can be repeated many times. By incorporating photoswitchable molecular groups in molecular compounds like polymers and liquid crystals, some properties of these materials can be modified by illumination. Photoswitchable azobenzene-containing polymers and liquid crystals have been used as actuators[17,18] and light-driven motors[19]. Furthermore, photoswitchable molecular scaffolds[20] and gel assemblies[21] were realized utilising azobenzene photoisomerization. Also, for MOFs in the form of powders or thin films, photoswitchable moieties[22–24] were used to demonstrate the remote-control of the MOF properties like colour[25], release[26–28] and adsorption[29–33] of the guest molecules, in particular of CO_2 (refs 32,33). While in most cases illumination with ultraviolet-light was needed, linker molecules that can be switched with visible light were used for the MOF preparation recently[34].

Here, we describe the design of a nanoporous, photoswitchable MOF membrane, where the azobenzene moieties are incorporated as side groups into the framework. By controlling the isomerization state of the photosensitive groups by light, the flux and the separation factor of a molecular, gaseous mixture permeating the membrane can be switched. In addition to varying the permeability, the separation factor (also referred to as (perm-)selectivity) can be continuously tuned by adjusting the ratio of the *trans* and *cis* isomers of the photochromic moieties. As a result, the molecular composition of the permeate flux can be precisely tuned in a fully remote-controlled way, see Fig. 1.

Results

Photoswitchable SURMOF films. The membranes are fabricated by growing MOF thin films in a layer-by-layer fashion, employing liquid-phase epitaxy by alternatively immersing the sample in solutions containing the MOF components, that is, in (separate) solutions of the metal nodes and of the organic linker molecules. This technique yields monolithic, crystalline, continuous MOF films, referred to as surface-mounted MOFs (SURMOFs)[35–38]. The prepared SURMOF films have a pillared-layer structure of type $Cu_2(AzoBPDC)_2(AzoBiPyB)$ (Fig. 2; AzoBPDC: 2-phenyldiazenyl-4,4′-biphenyldicarboxylic acid[26], and AzoBiPyB: (*E*)-4,4′-(2-(phenyldiazenyl)-1,4-phenylene) dipyridine (or dipyridylazobenzene)[30]. The samples used in this study were prepared by 90 (or 60) cycles of immersing the sample in ethanolic 1 mM copper(II)acetate solution and in ethanolic 0.1 mM AzoBiPyB and 0.1 mM AzoBPDC solution at 60 °C. Uptake experiments with butanol as guest molecule using a quartz crystal microbalance[39,40] indicate that the used MOF structure, that is, $Cu_2(AzoBPDC)_2(AzoBiPyB)$ with three azobenzene moieties per unit cell, results in large effects of the *trans-cis* switching, see Supplementary Fig. 1. The SURMOF films were prepared on quartz glass and on gold thin films on silicon supports for ultraviolet–vis (UV-vis) and infrared reflection absorption spectroscopy (IRRAS), respectively. For the membrane separation, the SURMOF films were prepared on asymmetric mesoporous aluminium oxide supports, which have a pore size of 70 nm on the top surface. Before the synthesis, the gold substrates were functionalized by 11-mercapto-1-undecanol (MUD) self-assembled monolayers (SAMs), while the quartz and porous aluminium oxide substrates were functionalized by oxygen plasma treatment[41].

From the IRRAS (Fig. 2b) and ultraviolet–vis spectra (Supplementary Fig. 2), it is clearly visible that the azobenzene (or phenyldiazenyl) side groups in the MOF can be switched by irradiation with light of 365 nm from *trans* (*E*) to *cis* (*Z*) and *vice versa* with light of 455 nm. The X-ray diffractograms of the SURMOF (Fig. 2c) indicate that the crystalline MOF (lattice) structure is not affected by the irradiation with ultraviolet or
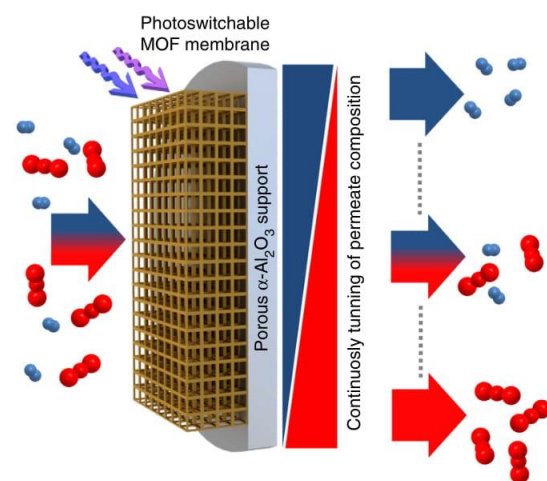
Figure 1 | Switchable membrane separation. Schematic illustration of tunable, remote-controllable molecular selectivity by a photoswitchable MOF membrane. The molecular feed mixture (left-hand side), where the molecules are depicted in red and blue, is separated by the nanoporous membrane. The molecular separation factor, giving the composition of the permeation flux (right-hand side), can be continuously tuned by light irradiation.

ARTICLE
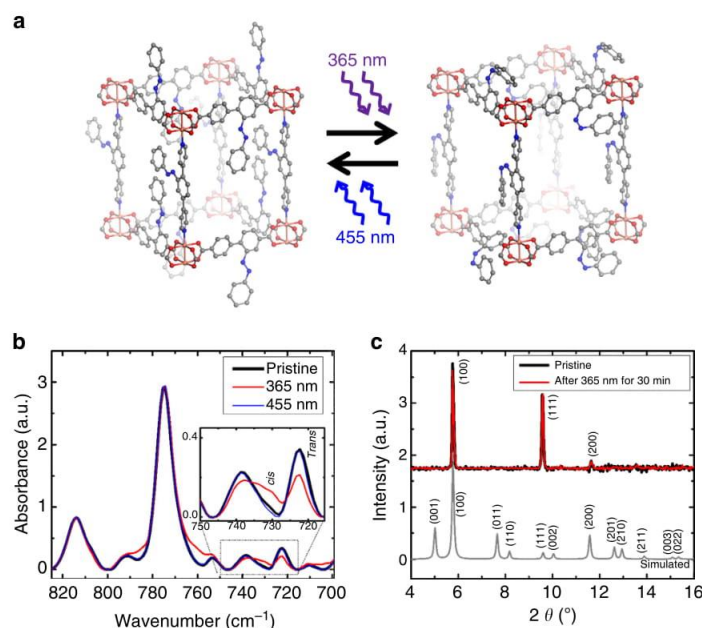
Figure 2 | Photoswitchable SURMOFs of type Cu$_2$(AzoBPDC)$_2$(AzoBiPyB). (**a**) The structure of Cu$_2$(AzoBPDC)$_2$(AzoBiPyB) with the azobenzene groups in the (basic) *trans* state, left, and in the *cis* state, right. The photoisomerization from *trans* to *cis* is performed by irradiation with ultraviolet-light of 365 nm, while the *cis*-to-*trans* isomerization is performed by irradiation with blue light of 455 nm. (Different view points of the MOF structure are shown in Supplementary Fig. 3.) (**b**) Infrared spectra of the Cu$_2$(AzoBPDC)$_2$(AzoBiPyB) SURMOF in the pristine *trans* state (black), after ultraviolet irradiation with light of 365 nm (red) and after irradiation with visible light of 455 nm (blue). The inset shows the magnification of the *trans* and *cis* azobenzene bands at about 720 and 730 cm^{-1}, respectively. An infrared spectrum with a larger range is shown in Supplementary Fig. 4. (**c**) Out-of-plane X-ray diffractogram of Cu$_2$(AzoBPDC)$_2$(AzoBiPyB) SURMOF before (black) and after (red) ultraviolet irradiation.
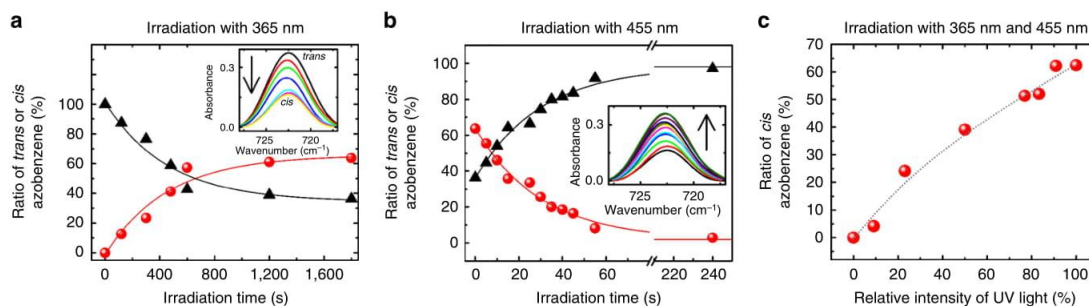
Figure 3 | Photoswitching of the SURMOF films. Amount of *trans* azobenzene (black triangles) and *cis* azobenzene (red spheres) of the Cu$_2$(AzoBPDC)$_2$(AzoBiPyB) SURMOF. (**a**) The sample is initially in the (100%) *trans* state and is irradiated with 365 nm. (**b**) The sample is initially in the *cis* state (that is, 63% *cis*) and is irradiated with 455 nm. The insets show the infrared *trans* azobenzene peak at 720 cm^{-1} during the irradiation with 365 and 455 nm, respectively. (**c**) The sample is simultaneously irradiated with light of 365 and 455 nm. The irradiation time of each point is 30 min, resulting in a photostationary state. The ratio of *cis* azobenzene, determined from the infrared peak at 720 cm^{-1}, is shown as a function of intensity of 365 nm relative to the total light intensity (365 and 455 nm). The light intensities are (roughly) adjusted by the potentiometers of the LEDs.

visible light, this means, by the photoisomerization of the azobenzene-side-groups.

For a detailed understanding of the photoswitching in the MOF film, the photoisomerization during irradiation with ultraviolet or visible light or their mixture was studied by using IRRAS. By analysing the intensity of the infrared vibrational band at about 720 cm^{-1}, which can be assigned to *trans* azobenzene[42], the percentage of *trans* azobenzene and therefore of *cis*

azobenzene in the MOF structure was determined. This band may be assigned to the γ(CH) and τ(ring) vibration of the *trans* azobenzene side group, which, because of the bonding to the framework, is red shifted in comparison to the vibration band of the isolated azobenzene[43,44].

The maximum yield of *cis* azobenzene, this means, the photostationary state under irradiation by light of 365 nm wavelength, was determined to be ~63%, Fig. 3a. The percentage of *cis* and
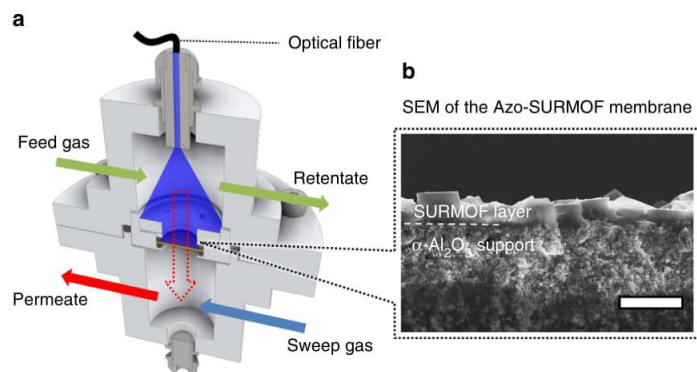
Figure 4 | Membrane separation setup. (**a**) Sketch of the setup for the photoswitchable membrane permeation experiments. The feed-retentate gas flow is above the membrane, while the sweep-permeate gas flow is below the membrane. A fiber-coupled LED is used for *in situ* irradiation of the SURMOF-covered top-side of the alumina membrane. (**b**) SEM cross-section image of the SURMOF membrane on the mesoporous α-alumina support. A dense SURMOF layer with a thickness of roughly 2 μm is observed. The length of the white scale bar is 5 μm.
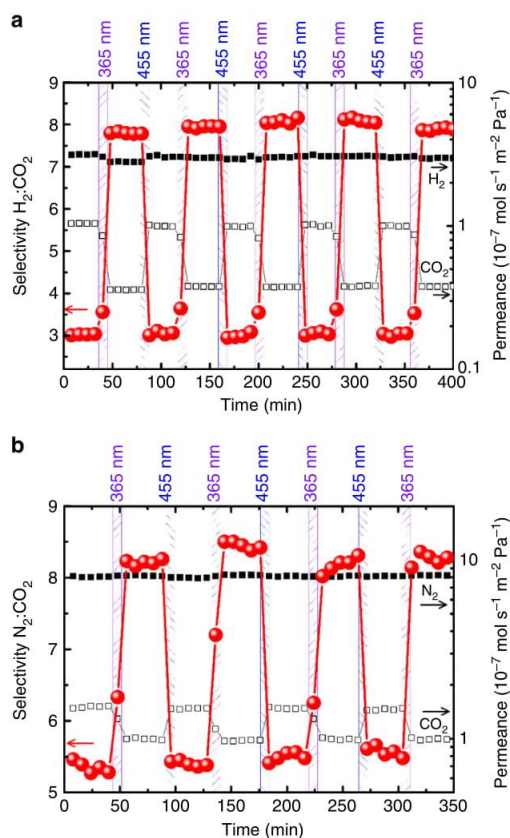
Figure 5 | Photoswitchable membrane separation. The separation of $H_2:CO_2$ and $N_2:CO_2$ mixtures is shown in (**a,b**), respectively. The membrane is irradiated by light of 365 and 455 nm for 5 min each. The permeances of H_2 and CO_2 (**a**), as well as N_2 and CO_2 (**b**) are shown as black solid squares and black open squares, respectively, with the logarithmic scale on the right-hand side. The molecular selectivities (or separation factors) are shown as red spheres with the scale on the left-hand side.

*trans* isomers can be adjusted by controlling the illumination time of the LED light with either 365 or 455 nm wavelength, see Fig. 3a,b. Moreover, a given *cis:trans* azobenzene ratio can also be achieved by simultaneously irradiating the SURMOF film with light of 365 and 455 nm, resulting in a steady state with equal rates of simultaneous *trans*-to-*cis* and *cis*-to-*trans* isomerizations. By adjusting the intensities of the respective LEDs with 365 or 455 nm wavelengths, a well-defined *cis:trans* ratio can be adjusted, see Fig. 3c. It should be noted that *cis* azobenzene can undergo thermal relaxation back to *trans* azobenzene with a thermal relaxation time of about 20 days at room temperature[42]. Therefore, the isomerization state of the photoswitchable SURMOF can be considered as stable in the dark, this means, without light irradiation, for the duration of the experiment (approximately a few hours).

Tunable and remote-controllable membrane permeation. The investigation of the photoswitchable membrane permeation was executed by growing $Cu_2(AzoBPDC)_2(AzoBiPyB)$ SURMOFs on mesoporous aluminium oxide supports. As shown by the SEM image in Fig. 4b, a continuous, dense and pinhole-free SURMOF film with a thickness of about 2 μm was formed on the mesoporous support. The X-ray diffractograms (Supplementary Fig. 5) verify the crystalline structure of the $Cu_2(AzoBPDC)_2$ (AzoBiPyB) SURMOF on the mesoporous support. For performing the membrane separation measurements, a Wicke–Kallenbach setup[45] with an optical fibre enabling the *in situ* irradiation of the MOF membrane was designed and built (Fig. 4a). This set-up allows to photoswitch the $Cu_2(AzoBPDC)_2(AzoBiPyB)$ SURMOF membrane, and to adjust the *cis:trans* azobenzene ratio during the membrane separation experiments. Here, the molecular separations of two different binary mixtures, $H_2:CO_2$ (pre-combustion mixtures) and $N_2:CO_2$ (post-combustion mixtures), were studied.

The membrane permeances and separation factors of hydrogen and carbon dioxide from the 50%:50% feed mixture are shown in Fig. 5a. The high separation factor indicates the absence of defects and pinholes in the membrane. While the permeation of hydrogen decreases only slightly, the permeation of carbon dioxide significantly decreases on switching the azobenzene-containing MOF membrane from *trans* to *cis*. The CO_2 permeance can be switched between ∼ 4 and 10×10^{-8} mol s^{-1} m^{-2} Pa^{-1}. The molecular $H_2:CO_2$ separation factor increases

ARTICLE
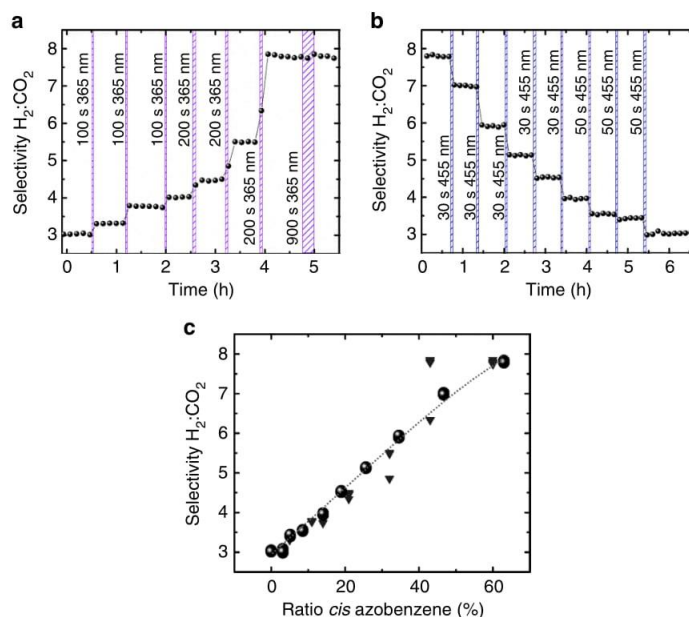
Figure 6 | Tuning the H$_2$:CO$_2$ separation factor by adjusting the *cis*:*trans* azobenzene ratio. (**a**) The Cu$_2$(AzoBPDC)$_2$(AzoBiPyB) membrane, which is initially in the *trans* state, is irradiated with ultraviolet-light for time intervals of 100 and 200 s, resulting in an increase of the H$_2$:CO$_2$ selectivity. (**b**) The membrane is initially in the *cis* state and is irradiated with 455 nm for time intervals of 30 and 50 s. (**c**) Correlation of the H$_2$:CO$_2$ separation factor with the ratio of *cis* azobenzene. The grey triangle and black spheres represent the data from figure (**a**,**b**), respectively; the correlation to the *cis* azobenzene ratio results from the comparison with the IRRAS data, see Supplementary Fig. 6.

from 3.0 in the *trans* state (100% trans, 0% *cis*) to about 8.0 in the *cis* state (37% *trans*, 63% *cis*). After irradiation with 455 nm, this means, the azobenzene-side-groups are switched back to the basic *trans* state, the initial permeances and the separation factor of 3 are attained. Five consecutive cycles of irradiation with 365 and 455 nm, this means, switching between the *trans* and the *cis* state, were performed. It was found that the switching of the membrane permeance and separation factor are fully reversible and, in addition, shows no sign of bleaching.

In a previous study with alkanes, alcohols and diols as guest molecules, it could be shown that the difference of the uptake by the azobenzene-containing MOF in the *cis* and in the *trans* state is caused by the switching of the azobenzene dipole moment, which amounts to 0 Debye in *trans* and 3 Debye in *cis*, and the dipole–dipole interaction with the guest molecules[39]. Thus, we may assume that the molecular mechanism resulting in the switching of the molecular separation is related to the different interaction of the hydrogen and carbon dioxide multipole moments with the *cis*- or *trans*-MOF, rather than a pore size effect or steric hindrance. Indeed, the dipole moment of the *cis* azobenzene is expected to result in a higher attractive interaction with the fairly strong quadrupole-moment of carbon dioxide, thus slowing down the carbon dioxide diffusion, while the interaction with hydrogen is not affected by the *trans-cis* switching. As a result, the different impact of the *trans-cis* switching leads to the switching of the H$_2$:CO$_2$ separation factor.

A reversible switching of the molecular selectivity is also observed for the separation of the N$_2$:CO$_2$ mixture, where the selectivity increases from 5.5 to 8.5 when switching from *trans* to *cis*, see Fig. 5b. While the carbon dioxide permeation significantly decreases on *trans*-to-*cis* isomerization, the nitrogen permeation is hardly affected. The observed permeation selectivity of nitrogen over carbon dioxide is characteristic for wide-pore

MOF/zeolite membranes with an adsorption controlled separation mechanism[46–48], whereas narrow-pore MOF/zeolite membranes show a preferred carbon dioxide (critical diameter 3.3 Å) permeation in comparison with nitrogen (3.6 Å) because of a diffusion-controlled molecular sieve mechanism[45,49,50].

A profound feature of the photoswitchable membrane is that the impressive (On–Off) switching of the separation factors (between membranes with minimum and maximum *cis* ratios) can be combined with the option of fine-tuning the *cis* azobenzene ratios. The H$_2$:CO$_2$ separation factor of the membrane in the *trans* state can be increased in arbitrary steps until the maximum separation factor is reached by irradiation with ultraviolet-light for certain times, Fig. 6a. On the other hand, the separation factor of the *cis* membrane can be decreased in arbitrary steps by irradiation with 455 nm, Fig. 6b. Thus, the separation factor can not only be switched between the minimum and maximum values, that is, 3.0 for 0% *cis* azobenzene and 8.0 for 63% *cis* azobenzene, but also each value in between can be realized by choosing appropriate irradiation times, that is, by adjusting the *cis* azobenzene ratio. The continuous tuning of the *cis* azobenzene ratio by controlled irradiation times with ultraviolet or visible light (Fig. 3) thus allows for a continuous tuning of the separation factor (Fig. 6). A correlation of the membrane selectivity with the *cis*-azobenzene ratio from the IRRAS data are shown in Fig. 6c. Because of the slow thermal isomerization of the azobenzene groups, the separation factor belonging to a mixed *cis:trans* state, once adjusted, is stable in the dark for the duration of the experiments.

Discussion

The ratio of the azobenzene isomers can also be controlled by adjusting the relative intensities of the multi-component light

irradiation with ultraviolet and visible light (Fig. 3c). For instance, a $H_2:CO_2$ selectivity of 4.5 is reached for a *cis* ratio of about 20%. This ratio can be adjusted by irradiating the (100%) *trans* membrane with 365 nm for about 500 s (Fig. 6a), by irradiating the (63%) *cis* membrane with 455 nm for about 120 s (Fig. 6b) or by simultaneously irradiating the sample with 365 and 455 nm with an intensity ratio of about 20%:80% (Fig. 3c).

By increasing the *cis* ratio, that is, by increasing the irradiation time with ultraviolet-light or by increasing the relative ultraviolet intensity, the separation factor is increased. Here, the maximum ratio of *cis* azobenzene is about 63%, resulting in the highest separation factor of about 8.0. It can be assumed that even higher *cis:trans* isomerization ratios, for example, enabled by functionalized azobenzene moieties[51], would result in higher switching yields and would enlarge the tunable separation factor range.

The potential of the tunable membrane is demonstrated by controlling the molecular composition of the $H_2:CO_2$ permeate flux and, therewith, controlling the flammability and the safety of this pre-combustion mixture when mixed with air or oxygen. When the permeate flux is mixed with air in a ratio 1:20, the resulting gas flow through the membrane in the *trans* state has a hydrogen content of 3.7%, while the flux through the *cis* membrane has a hydrogen content of 4.4%. Since the flammability limit of hydrogen in air is 4.0% (ref. 52), the photoswitchable membrane in the *cis* state results in a flammable gas mixture and the *trans* membrane in a non-flammable gas mixture. When the permeate flux is mixed with air in a ratio 1:6, the flux through the *cis* membrane (with an H_2 content of 12.7%) may be detonable, while the flux through the *trans* membrane (with an H_2 content of 10.7%) is not detonable[52]. As demonstrated above, each composition in between can be tuned, enabling a remote-controlled adjusting of hazardous or non-hazardous conditions.

In conclusion, we have fabricated a novel MOF membrane, for which permeation, as well as selectivity can be remotely controlled by photoswitching the azobenzene-side-groups decorating the MOF pores. The separation factor of a $H_2:CO_2$ mixture was switched between 3 and 8. Moreover, the separation factor, and accordingly the molecular composition of the permeate flux, can be precisely adjusted within this range. This means for this pre-combustion gas mixture, the combustibility and ignition point (when mixed with air) can be continuously tuned by light irradiation of this smart membrane. The concept of switching and continuously tuning the membrane selectivities can be extended to the separation of other gas mixtures, for example, $N_2:CO_2$. Further innovative application might be the control of the accessibility to a catalyst or sensor surface and the controlled (selective) release of encapsulated fragrances or drugs. In addition, it could also be profoundly extended to other kinds of membranes like polymeric membranes[2] or mixed-matrix MOF membranes[9] by functionalizing these materials with photosensitive moieties.

Methods

X-ray diffraction. X-ray diffraction measurements in out-of-plane geometry (also reffered to as co-planar orientation) were carried out using a Bruker D8-Advance diffractometer equipped with a position sensitive detector Lynxeye in θ–θ geometry. Variable divergence slit and 2.3° Soller-slit were used on the secondary side. A Cu-anode with Cu $K_{\alpha1}$ radiation ($\lambda = 0.154$ nm) was used. The measurements were carried out with a scan step of 0.02° at 40 kV and 40 mA.

Infrared reflection-absorption spectroscopy. IRRAS of the samples were performed with a resolution of 2 cm^{-1} using a FTIR spectrometer of type Bruker VERTEX 80. All the IRRAS results were recorded in grazing incidence reflection mode at an angle of incidence of 80° relative to the surface normal using liquid-

nitrogen-cooled mercury–cadmium–telluride mid band detectors. Perdeuterated hexadecanethiol-SAMs on Au/Si were used for reference measurements.

Ultraviolet–vis spectroscopy. The ultraviolet–vis spectra were recorded by means of a Cary5000 spectrometer with a UMA unit from Agilent. Ultraviolet irradiation was performed with a 365 nm LED light from PrizMatix with a power or 112 mW. The visible light irradiation was performed with a 455 nm LED light with 135 mW. The distance between the sample and the LED was about 5 cm.

Scanning electron microscopy. SEM cross-section pictures were taken with a field-emission electron microscope JEOL-JSM-6700 F at 10 kV accelerating voltage and 10 μA emission current. To prevent the sample from charging, carbon was evaporated on the surface to provide a conductive surface coating using a Leica EMSCD500. The working distance was 15 mm.

SAM-preparation. For SAM formation, a clean gold substrate (that is, gold coated siliconwafer) was rinsed with pure ethanol and then immersed in a solution of MUD with a concentration of 1 mM in ethanol for 18 h. Afterwards the substrate was rinsed thoroughly with ethanol and dried under nitrogen stream.

Plasma treatment. The quartz glass and porous aluminium oxide substrates were treated by oxygen plasma (Diener Plasma; 50 sccm, pure O_2) for 10 min to remove impurities, as well as increase the number of OH functional groups and the hydrophilicy.

SURMOF synthesis. The experimental procedure used to grow SURMOF films on functional surfaces has been discussed in detail previously[35,37]. In summary, the layer-by-layer growth process consists of alternately immersing the substrate in the ethanolic solutions of the building units, that is, the metal knots (here: 1 mM copper acetate) and the organic linkers (here: 0.1 mM AzoBPDC and 0.1 mM AzoBiPyB; the synthesis of the linkers is explained in refs 26,30). Between each immersion step, the substrates were rinsed thoroughly with ethanol. In the present work, the substrates were immersed into copper acetate solution for 15 min, subsequently rinsed with pure ethanol solution for 2 min, and then immersed into the linker solution for 30 min. All solutions were kept at 60 °C during MOF film preparation. The SURMOF films on porous aluminium oxide supports (asymmetric mesoporous aluminium oxide supports from IKTS Hermsdorf, Germany) were prepared in 90 synthesis cycles. The SURMOF samples for infrared and ultraviolet–vis spectroscopy were prepared in 60 synthesis cycles on MUD-functionalized gold surfaces and on quartz glass, respectively. Since the sample is protected from light irradiation during the synthesis, all azobenzene-side-groups in the pristine SURMOF film are in the thermodynamically most stable state, the *trans* ground state.

Gas permeation. Gas permeation was carried out using an online gas chromatograph Agilent Technologies 7890A. Evaluation of the membrane was performed by mixed-gas permeation. Viton O-Rings (FKM 70 Vi 370) were used to seal the membrane gas-tight in its housing. *In-situ* irradiation of the membrane layer was achieved by a fibre-coupled, monochromatic high power Prizmatix FC-5 LED. Before the permeation data were recorded, the membrane was activated at 50 °C in a pure nitrogen flow for 24 h. For pre-combustion hydrogen separation at 25 °C, a 50:50 mixture of $H_2:CO_2$ was used at flow-rates of 25 ml min^{-1} each. The feed-gas was N_2 at a 50 ml min^{-1} flow rate. For post-combustion separation at 35 °C, a 90:10 $N_2:CO_2$ mixture was used at volumetric flow rates of 45 ml min^{-1} for N_2 and 5 ml min^{-1} for CO_2. There, CH_4 was applied on the sweep side at a flow rate of 50 ml min^{-1}. The experiments were performed at ambient pressure, that is, no overpressure was applied.

Data availability. The data sets generated during and/or analysed during the current study are available from the corresponding author on reasonable request.

References

1. Sholl, D. S. & Lively, R. P. Seven chemical separations to change the world. *Nature* **533,** 316–316 (2016).
2. Karan, S., Jiang, Z. W. & Livingston, A. G. Sub-10 nm polyamide nanofilms with ultrafast solvent transport for molecular separation. *Science* **348,** 1347–1351 (2015).
3. Turchanin, A. *et al.* One nanometer thin carbon nanosheets with tunable conductivity and stiffness. *Adv. Mater.* **21,** 1233 (2009).
4. Celebi, K. *et al.* Ultimate permeation across atomically thin porous graphene. *Science* **344,** 289–292 (2014).
5. Kim, H. W. *et al.* Selective gas transport through few-layered graphene and graphene oxide membranes. *Science* **342,** 91–95 (2013).
6. Furukawa, H., Cordova, K. E., O'Keeffe, M. & Yaghi, O. M. The chemistry and applications of metal-organic frameworks. *Science* **341,** 1230444 (2013).

ARTICLE

7. Cadiau, A., Adil, K., Bhatt, P. M., Belmabkhout, Y. & Eddaoudi, M. A metal-organic framework-based splitter for separating propylene from propane. *Science* **353,** 137–140 (2016).

8. Cui, X. L. *et al.* Pore chemistry and size control in hybrid porous materials for acetylene capture from ethylene. *Science* **353,** 141–144 (2016).

9. Rodenas, T. *et al.* Metal–organic framework nanosheets in polymer composite materials for gas separation. *Nat. Mater.* **14,** 48–55 (2015).

10. Ameloot, R. *et al.* Interfacial synthesis of hollow metal-organic framework capsules demonstrating selective permeability. *Nat. Chem.* **3,** 382–387 (2011).

11. Brown, A. J. *et al.* Interfacial microfluidic processing of metal-organic framework hollow fiber membranes. *Science* **345,** 72–75 (2014).

12. Li, Y. S. *et al.* Molecular sieve membrane: supported metal-organic framework with high hydrogen selectivity. *Angew. Chem. Int. Ed.* **49,** 548–551 (2010).

13. Wang, Z. Q. & Cohen, S. M. Postsynthetic modification of metal-organic frameworks. *Chem. Soc. Rev.* **38,** 1315–1329 (2009).

14. Zhang, J., Zou, Q. & Tian, H. Photochromic materials: more than meets the eye. *Adv. Mater.* **25,** 378–399 (2013).

15. Bandara, H. M. D. & Burdette, S. C. Photoisomerization in different classes of azobenzene. *Chem. Soc. Rev.* **41,** 1809–1825 (2012).

16. Russew, M.-M. & Hecht, S. Photoswitches: from molecules to materials. *Adv. Mater.* **22,** 3348–3360 (2010).

17. Iamsaard, S. *et al.* Conversion of light into macroscopic helical motion. *Nat. Chem.* **6,** 229–235 (2014).

18. van Oosten, C. L., Bastiaansen, C. W. M. & Broer, D. J. Printed artificial cilia from liquid-crystal network actuators modularly driven by light. *Nat. Mater.* **8,** 677–682 (2009).

19. Yamada, M. *et al.* Photomobile polymer materials: Towards light-driven plastic motors. *Angew. Chem. Int. Ed.* **47,** 4986–4988 (2008).

20. Baroncini, M. *et al.* Photoinduced reversible switching of porosity in molecular crystals based on star-shaped azobenzene tetramers. *Nat. Chem.* **7,** 634–640 (2015).

21. Yamaguchi, H. *et al.* Photoswitchable gel assembly based on molecular recognition. *Nat. Commun.* **3,** 603 (2012).

22. Modrow, A., Zargarani, D., Herges, R. & Stock, N. The first porous MOF with photoswitchable linker molecules. *Dalton Trans.* **40,** 4217–4222 (2011).

23. Mukhopadhyay, R. D., Praveen, V. K. & Ajayaghosh, A. Photoresponsive metal-organic materials: exploiting the azobenzene switch. *Mater. Horiz.* **1,** 572–576 (2014).

24. Castellanos, S., Kapteijn, F. & Gascon, J. Photoswitchable metal organic frameworks: turn on the lights and close the windows. *Crystengcomm* **18,** 4006–4012 (2016).

25. Walton, I. M. *et al.* Photo-responsive MOFs: light-induced switching of porous single crystals containing a photochromic diarylethene. *Chem. Commun.* **49,** 8012–8014 (2013).

26. Heinke, L. *et al.* Photoswitching in two-component surface-mounted metal-organic frameworks: optically triggered release from a molecular container. *Acs Nano* **8,** 1463–1467 (2014).

27. Brown, J. *et al.* Photophysical pore control in an azobenzene-containing metal-organic framework. *Chem. Sci.* **4,** 2858–2864 (2013).

28. Meng, X., Gui, B., Yuan, D., Zeller, M. & Wang, C. Mechanized azobenzene-functionalized zirconium metal-organic framework for on-command cargo release. *Sci. Adv.* **2,** e1600480 (2016).

29. Modrow, A., Zargarani, D., Herges, R. & Stock, N. Introducing a photo-switchable azo-functionality inside Cr-MIL-101-NH$_2$ by covalent post-synthetic modification. *Dalton Trans.* **41,** 8690–8696 (2012).

30. Wang, Z. *et al.* Photoswitching in nanoporous, crystalline solids: an experimental and theoretical study for azobenzene linkers incorporated in metal-organic frameworks. *Phys. Chem. Chem. Phys.* **17,** 14582–14587 (2015).

31. Yanai, N. *et al.* Guest-to-host transmission of structural changes for stimuli-responsive adsorption property. *J. Am. Chem. Soc.* **134,** 4501–4504 (2012).

32. Park, J. *et al.* Reversible alteration of CO$_2$ adsorption upon photochemical or thermal treatment in a metal-organic framework. *J. Am. Chem. Soc.* **134,** 99–102 (2012).

33. Zhu, Y. & Zhang, W. Reversible tuning of pore size and CO$_2$ adsorption in azobenzene functionalized porous organic polymers. *Chem. Sci.* **5,** 4957–4961 (2014).

34. Castellanos, S. *et al.* Structural effects in visible-light-responsive metal-organic frameworks incorporating ortho-fluoroazobenzenes. *Chem. Eur. J.* **22,** 746–752 (2016).

35. Shekhah, O. *et al.* Step-by-step route for the synthesis of metal-organic frameworks. *J. Am. Chem. Soc.* **129,** 15118–15119 (2007).

36. Shekhah, O., Liu, J., Fischer, R. A. & Wöll, C. MOF thin films: existing and future applications. *Chem. Soc. Rev.* **40,** 1081–1106 (2011).

37. Heinke, L., Tu, M., Wannapaiboon, S., Fischer, R. A. & Wöll, C. Surface-mounted metal-organic frameworks for applications in sensing and separation. *Microporous Mesoporous Mater.* **216,** 200–215 (2015).

38. Heinke, L., Gu, Z. & Wöll, C. The surface barrier phenomenon at the loading of metal-organic frameworks. *Nat. Commun.* **5,** 4562 (2014).

39. Wang, Z., Grosjean, S., Braese, S. & Heinke, L. Photoswitchable adsorption in metal-organic frameworks based on polar guest-host interactions. *ChemPhysChem* **16,** 3779–3783 (2015).

40. Heinke, L. & Wöll, C. Adsorption and diffusion in thin films of nanoporous metal-organic frameworks: ferrocene in SURMOF Cu$_2$(ndc)$_2$(dabco). *Phys. Chem. Chem. Phys.* **15,** 9295–9299 (2013).

41. Gu, Z.-G. *et al.* Transparent films of metal-organic frameworks for optical applications. *Microporous Mesoporous Mater.* **211,** 82–87 (2015).

42. Yu, X. *et al.* cis-to-trans isomerization of azobenzene investigated by using thin films of metal-organic frameworks. *Phys. Chem. Chem. Phys.* **17,** 22721–22725 (2015).

43. Duarte, L., Fausto, R. & Reva, I. Structural and spectroscopic characterization of E- and Z-isomers of azobenzene. *Phys. Chem. Chem. Phys.* **16,** 16919–16930 (2014).

44. Hermann, D., Emerich, H., Lepski, R., Schaniel, D. & Ruschewitz, U. Metal-Organic Frameworks as Hosts for Photochromic Guest Molecules. *Inorg. Chem.* **52,** 2744–2749 (2013).

45. Bux, H. *et al.* Zeolitic imidazolate framework membrane with molecular sieving properties by microwave-assisted solvothermal synthesis. *J. Am. Chem. Soc.* **131,** 16000 (2009).

46. Huang, A., Wang, N. & Caro, J. Seeding-free synthesis of dense zeolite FAU membranes on 3-aminopropyltriethoxysilane-functionalized alumina supports. *J. Membr. Sci.* **389,** 272–279 (2012).

47. Guo, Y., Mao, Y., Hu, P., Ying, Y. & Peng, X. Self-confined synthesis of HKUST-1 membranes from CuO nanosheets at room temperature. *Chem. Select* **1,** 108–113 (2016).

48. Wang, N., Mundstock, A., Liu, Y., Huang, A. & Caro, J. Amine-modified Mg-MOF-74/CPO-27-Mg membrane with enhanced H-2/CO$_2$ separation. *Chem. Eng. Sci.* **124,** 27–36 (2015).

49. Huang, A., Dou, W. & Caro, J. Steam-stable zeolitic imidazolate framework ZIF-90 membrane with hydrogen selectivity through covalent functionalization. *J. Am. Chem. Soc.* **132,** 15562–15564 (2010).

50. Liu, Q., Wang, N. Y., Caro, J. & Huang, A. S. Bio-inspired polydopamine: a versatile and powerful platform for covalent synthesis of molecular sieve membranes. *J. Am. Chem. Soc.* **135,** 17679–17682 (2013).

51. Bleger, D., Schwarz, J., Brouwer, A. M. & Hecht, S. o-Fluoroazobenzenes as readily synthesized photoswitches offering nearly quantitative two-way isomerization with visible light. *J. Am. Chem. Soc.* **134,** 20597–20600 (2012).

52. Alcock, J. L., Shirvill, L. C. & Cracknell, R. F. in *Report EIHP 2, 5th Framework Programme (1998–2002)*, (*Shell Global Solutions.*, 2001).

Acknowledgements

Author contributions

All authors contributed to writing the manuscript and have approved the final version of the manuscript. Z.W. synthesized the samples and performed the thin film switching experiments (X-ray diffraction, ultraviolet–vis, IRRAS). A.K. performed the membrane switching experiments and the SEM measurements. S.G., D.W. and S.B. synthesized the photoswitchable molecules. C.W. and J.C. were involved in planning and supervising the experiments. L.H. planned and supervised the experiments and wrote the manuscript.

Additional information

- 76 -

4.3. Switching Thin Films of Azobenzene-Containing Metal–Organic Frameworks with Visible Light

K. Müller, A. Knebel, F. Zhao, D. Bléger, J. Caro, L. Heinke

- 78 -

▌**Photochemistry**

Switching Thin Films of Azobenzene-Containing Metal–Organic Frameworks with Visible Light

Kai Müller[+],[a] Alexander Knebel[+],*[b] Fangli Zhao,[c] David Bléger,*[c] Jürgen Caro,[b] and Lars Heinke*[a]

Abstract: Stimuli-responsive molecules change their properties when exposed to external signals, such as light, and enable the preparation of smart materials. UV light, which often destroys organic materials, is typically required for activating the desired response of photoswitchable compounds, significantly limiting the potential applications of light-operated smart materials. Herein, we present the first metal–organic framework (MOF), which enables reversible modulation of key properties upon irradiation with visible light only. The fluorinated azobenzene side groups in the MOF structure can be reversibly switched between the *trans* and *cis* state by green and violet light, avoiding UV light. It was demonstrated that the uptake of guest molecules by these MOF films can be switched in a fully remote-controlled way. The membrane separation of hydrogen/hydrocarbon mixtures was investigated. The light-induced changes of the MOF pore size result in the switching of the permeation and of the selection factor.

Stimuli-responsive molecules change their structures and properties as a response to an external signal like light, temperature, electric fields, or chemicals. These compounds, either in solution, on surfaces, or incorporated in adequate matrixes,[1] may be used for various purposes at all scales down to molecular nanomachines and even nanocars.[2] One particular aim is to use stimuli-responsive molecules to prepare (macroscopic) smart materials, which change their properties in a remote-controlled way. Light is a particularly simple and practical signal, which enables very fast responses. In addition, true remote control over large distances, without direct contact to the material is possible. Therefore, photoswitchable materials, which incorporate photochromic molecules,[3] attract a lot of attention.[4] For example, polymers and liquid crystals containing azobenzene moieties have been used as light-driven actuators[5] and motors.[6] Another relevant class of materials for the incorporation of smart moieties are metal–organic frameworks (MOFs).[7] MOFs are crystalline solids composed of metal nodes connected by organic linker molecules. This material class possesses a plethora of exclusive properties, such as well-defined, nanoporous structures, large specific surface areas, and large structural and chemical variety.[7] The structure of MOFs is particularly suitable for the introduction of azobenzene side groups, which require sufficient free volume to isomerize. In this way, color change,[8] remote-controlled adsorption[9] and release[10] of guest molecules as well as continuously tunable molecular membrane separation[11] have been demonstrated. UV light, which is required to induce the *trans*-to-*cis* photoisomerization of (plain) azobenzene groups, may destroy and decrease the lifespan of biological or organic material and hinders, for example, biological applications. Therefore, advanced azobenzene derivatives, which can be reversibly switched without UV irradiation, were developed.[12] The first MOF materials with such an advanced photochromic moiety were recently reported;[13] however, the photoisomerization in the MOF was sterically hindered (F-azo-MIL-53(Al)[13]) or showed no modulation of their macroscopic properties, such as the CO_2 adsorption isotherm (F-azo-UiO-66(Zr)[13]).

Herein, we describe the design of a nanoporous, photoswitchable MOF thin film functionalized with *o*-fluoroazobenzene moieties (Figure 1), which can reversibly isomerize between the *trans* and the *cis* configuration with visible light only. Apart from avoiding the damaging character of UV light, ligand-to-metal-charge transfer, which is excited by UV light in the Cu-paddle-wheel MOF structures,[14] is not stimulated when switching the photochromic moieties with visible light. As a result, very high isomerization yields of the azobenzene moieties, unprecedented in MOFs, were realized. By controlling the isomerization state of the photosensitive groups with green and violet light, the uptake amount of guest molecules by the MOF film was controlled. Furthermore, visible-light-switchable MOF membranes were prepared and the separation factors of H_2:C_2H_4 and H_2:C_3H_6 mixtures permeating the membrane were remote-controlled.

[a] K. Müller,[+] Dr. L. Heinke
Chemistry of Oxydic and Organic Interfaces
Institute of Functional Interfaces, Karlsruhe Institute of Technology (KIT)
Hermann-von-Helmholtz-Platz 1
76344 Eggenstein-Leopoldshafen (Germany)
E-mail: lars.heinke@kit.edu

[b] A. Knebel,[+] Prof. Dr. J. Caro
Institute for Physical Chemistry and Electrochemistry
Leibniz University Hanover, Callinstrasse 3a, 30167 Hannover (Germany)

[c] F. Zhao, Dr. D. Bléger
Department of Chemistry, Humboldt-Universität zu Berlin
Brook-Taylor-Strasse 2, 12489 Berlin (Germany)
E-mail: david.bleger@chemie.hu-berlin.de

[+] These authors contributed equally to this work.

🖳 Supporting information and the ORCID identification number(s) for the author(s) of this article can be found under:
http://dx.doi.org/10.1002/chem.201700989.
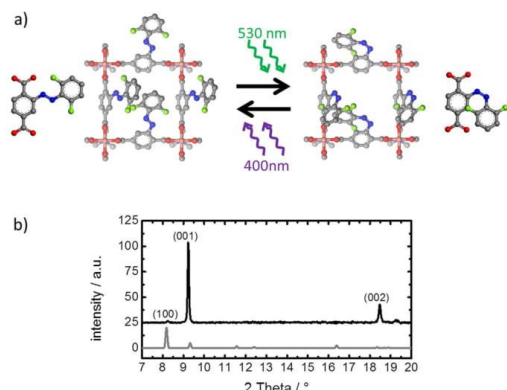
Figure 1. a) Structure of Cu$_2$(F$_2$AzoBDC)$_2$(dabco), in which the fluorinated azobenzene side can be reversibly switched from *trans* (left-hand side) to *cis* (right-hand side) by irradiation with green light (530 nm) and from *cis* to *trans* be irradiation with violet light (400 nm). The view along the (001) direction is shown, a different point of view is shown in Figure S1 (see the Supporting Information). The photoswitchable linker F$_2$AzoBDC is shown next to the MOF structure. Carbon atoms are grey, oxygen red, copper orange, fluorine green, and nitrogen blue. For clarity, the hydrogen atoms are not shown. b) X-ray diffractogram of the Cu$_2$(F$_2$AzoBDC)$_2$(dabco) SURMOF grown on a functionalized gold surface. The grey line shows the calculated powder diffractogram of the structure.

The thin MOF films were prepared in a layer-by-layer fashion, resulting in surface-mounted MOFs (SURMOFs).[15] There, the substrate was alternatively immersed in the solution of the metal nodes (herein: copper(II) acetate) and the organic linker molecules (1,4-diazabicyclo[2.2.2]octane (dabco) and F$_2$AzoBDC linker). The prepared Cu$_2$(F$_2$AzoBDC)$_2$(dabco) SURMOF has a pillared-layer structure. The X-ray diffractogram shows the crystalline, oriented growth of the Cu$_2$(F$_2$AzoBDC)$_2$(dabco) SURMOF with a preferred (001) orientation (Figure 1).

The photoisomerization of the thin MOF film was investigated by using UV/Vis and infrared-reflection absorption spectroscopy (IRRAS; Figure 2). UV/Vis spectroscopy of the SURMOF (Figure 2b) showed that the irradiation with violet (400 nm) light resulted in an increase of the π→π* band at 320 nm, whereas the irradiation with green (530 nm) light resulted in a decrease of the π→π* band. In addition, the n→π* band (or shoulder) at 450 nm was shifted to larger wavelengths when irradiated with violet light and to smaller wavelengths when irradiated with green light, respectively. This is a clear indication for the *trans*/*cis* isomerization of the fluorinated azobenzene moiety, as observed for the linker molecule in ethanol (Figure 2a), in which violet and green light induce *cis*-to-*trans* and *trans*-to-*cis* isomerization, respectively. The reversibility of the photoisomerization in the SURMOF was demonstrated by performing five irradiation cycles, in which no sign of photobleaching was found (see inset of Figure 2b).

The IRRA spectra of the SURMOF in the *trans* and in the *cis* states are shown in Figure 2c. While the vibration bands of the MOF scaffold remained unchanged upon light irradiation and *trans*/*cis* isomerization, the bands of the fluorinated azoben-
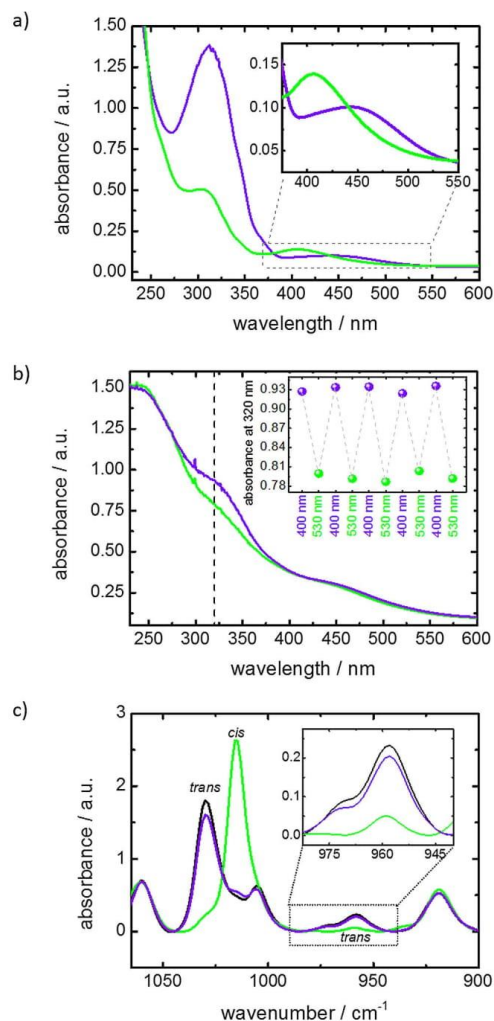
Figure 2. UV/Vis absorbance spectra of the F$_2$AzoBDC linker in ethanol (a) and of the Cu$_2$(F$_2$AzoBDC)$_2$(dabco) SURMOF on quartz (b). The samples after irradiation with violet light (*trans*-rich state) and green light (*cis*-rich state) are shown in violet and green, respectively. The change of the n→π* band (at 450 nm) is highlighted in the zoom-in a). The inset in b) shows the absorbance at 320 nm measured during five switching cycles. The large SURMOF band at approximately 250 nm can be assigned to the Cu knot in the framework.[14] c) IRRA spectra of the Cu$_2$(F$_2$AzoBDC)$_2$(dabco) SURMOF on a gold substrate after irradiation with violet light (violet line), after irradiation with green light (green line) and after thermal relaxation at 70 °C for three days (black line). A larger range IRRA spectrum is shown in Figure SI2 in the Supporting Information.

zene side group changed. Upon violet-light irradiation, the intensities of the vibration bands at 1030 and 960 cm^{-1} increase, whereas the band at 1015 cm^{-1} decreases. Conversely, upon green-light irradiation, the bands at 1030 and 960 cm^{-1} de-

crease, whereas the band at 1015 cm^{-1} increases. Therefore, we conclude that the vibration bands at 1030 and 960 cm^{-1} can be assigned to the *trans* state and the vibration band at 1015 cm^{-1} can be assigned to the *cis* state. While the bands at 1015 and 1030 cm^{-1} partially overlap, the *trans* band at 960 cm^{-1} enable a precise analysis. The area of the 960 cm^{-1} band is 0.57 after irradiation with green light for 30 minutes, 3.54 after irradiation with violet light for 30 minutes, and 4.08 after thermal relaxation. Thus, assuming that no other band overlaps at 960 cm^{-1}, the amount of *trans* azobenzene can be switched between 14 and 87 % by irradiation with green and violet light, respectively. Remarkably, the switching yield of the fluorinated azobenzene side groups in the MOF is in very good agreement with the switching yield, which was determined for the linker molecules in DMSO solution.[13] It should be stressed that this switching yield is high compared to plain azobenzene moieties in other SURMOFs, which was determined to be about 63 %,[11] hence demonstrating the benefits of the fluoro-azobenzene moiety combined with green-light irradiation.

To investigate the possibility to photomodulate the uptake of small molecules, thin films of Cu$_2$(F$_2$AzoBDC)$_2$(dabco) SURMOF were prepared on gold-coated quartz crystal microbalance (QCM) sensors. The initially activated, that is, empty, SURMOF in the *trans* state was exposed to the vapor of the guest molecules, 1,4-butanediol. This compound was chosen for its suitable size, as well as its polar character, to take advantage of the polarity difference between *trans* and *cis* azobenzenes.[16] DFT calculations (see the Supporting Information, Table SI1) showed that dipole moment change of fluoroazobenzene during the *trans/cis* isomerization is similar to that of plain azobenzene. After approximately 10 hours of butanediol uptake by the SURMOF, the equilibrium loading in the *trans* state was obtained and the sample was irradiated with green light to switch the linker to the *cis* state. A significant increase of the uptake was observed (Figure 3). By repeating this experiment three times with the same sample, it was found that the *trans*-to-*cis* isomerization resulted in an increase of the butanediol loading by about 47 ± 20 %. This is significantly more than what was observed in other azobenzene-containing SURMOFs.[9b, 10a, 16] It can be assumed that the larger impact of the *trans*-to-*cis* switching is a result of the larger photoisomerization yield and of the large amount of photoswitchable moieties per small pore volume of the Cu$_2$(F$_2$AzoBDC)$_2$(dabco) SURMOF in comparison to previously investigated, structurally different SURMOFs.

To further explore the potential of the visible-light-switchable SURMOF, we performed hydrogen-separation experiments on a membrane consisting of a thin SURMOF film grown on a mesoporous Al$_2$O$_3$ substrate[11] (Figure 4a). The SEM and EDX images showed a homogeneous MOF membrane of approximately 800 nm thickness on top of the mesoporous Al$_2$O$_3$ support. The X-ray diffractogram of the SURMOF on the mesoporous support is shown in Figure SI3b in the Supporting Information. Mixtures of hydrogen with either ethylene or propene flowing from the feed side were separated by the MOF membrane (Figure 4), and the process was monitored in situ by using a Wicke–Kallenbach setup (see Figure SI3 in the Support-
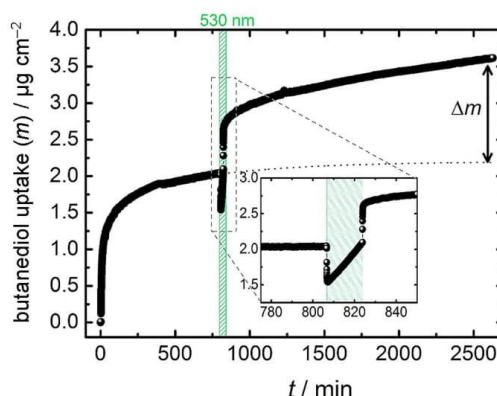

Figure 3. 1,4-Butanediol uptake by Cu$_2$(F$_2$AzoBDC)$_2$(dabco) SURMOF measured by QCM. The 1,4-butanediol uptake by the SURMOF in the *trans* state began at *t* = 0 min. At about 800 min, the sample was irradiated with green light for 15 min. The *trans*-to-*cis* photoisomerization of the SURMOF results in a butanediol uptake increase by Δ*m* ≈ 1.4 μg cm^{-2}. The inset shows a zoom-in of the uptake during illumination. The instantaneous decrease and increase of the determined mass when switching the light on and off, respectively, are most likely caused by a small (local) temperature increase during light irradiation.

ing Information). These particular mixtures, which we investigated for the first time in the context of photoswitchabe membranes, were selected, because dehydrogenation of hydrocarbons is a relevant industrial example of catalytic partial oxidation processes.[17] Moreover, it has been shown that mixtures of hydrocarbons with hydrogen are good experimental systems to investigate the separation performances of membranes.[18] Although the permeance of hydrogen was barely affected by the *trans/cis* switching, the permeances of ethylene and of propene increased by about 25 and 30 %, respectively, when irradiating the membrane with green light. The initial permeance is recovered upon irradiation with violet light. Thus, the remote-controlled switching of the membrane selectivity is reversible, and the separation factor can be switched between 6.6 and 8.2 for the mixture with ethylene, and between approximately 8.8 and 12.6 for the mixture with propene. Continuous tuning within these ranges is possible by adjusting the irradiation times or by mixing the green and the violet light.[11]

On the other hand, no significant impact of the *trans/cis* switching was found for the separation of hydrogen and carbon dioxide (Figure SI4 in the Supporting Information). This is in contrast to azobenzene-containing SURMOF membrane of type Cu$_2$(AzoBPDC)$_2$(AzoBiPyB) with a much larger pore size, in which a strong effect of the *trans/cis* isomerization was observed for hydrogen-carbon dioxide.[11]

Due to this fact and because the difference of polarity between *cis* and *trans* azobenzene cannot influence the adsorption of the apolar hydrocarbons, we conclude that the observed photomodulation of the separation by Cu$_2$(F$_2$AzoBDC)$_2$(dabco) membranes was caused by steric effects rather than by changes of the dipole moment. The small-
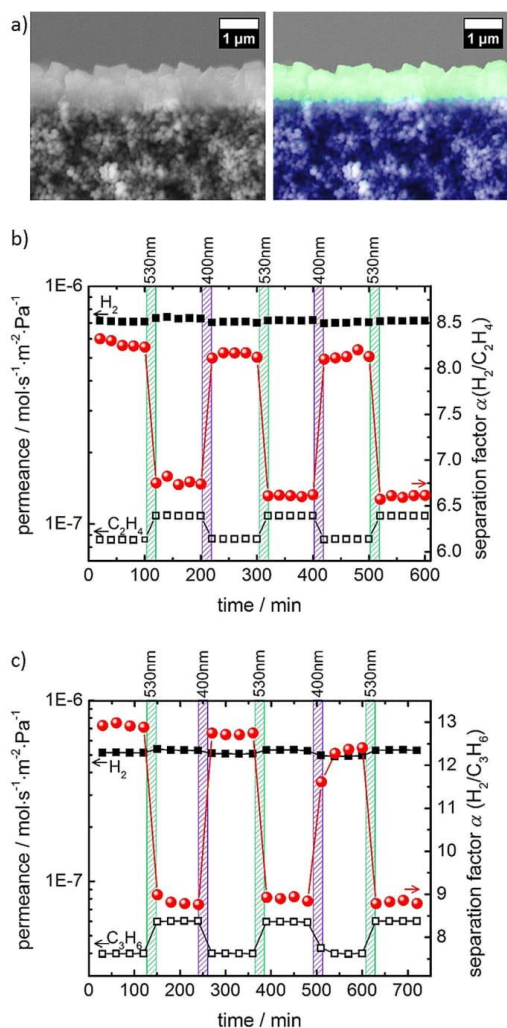
Figure 4. a) Scanning electron microscopy (SEM, left) and energy-dispersive X-ray mapping (EDX, green–Cu–$L_{\alpha 1,2}$ and blue–Al–$K_{\alpha 1}$, right) images of the photoswitchable membrane on the porous support. Membrane selectivity values of (b) H_2:C_2H_4 and (c) H_2:C_3H_6 gas mixtures, switched in situ by illumination by 400 and 530 nm light for three cycles. Each illumination time was 20 min. The permeances of H_2 (solid square) and C_2H_4 or C_3H_6 (open squares) are shown on the left-hand side of the graphs, whereas the resulting separation factors (red spheres) are shown on the right-hand side.

er pore diameter of the SURMOF in the *trans* state results in a smaller permeation of the hydrocarbons, compared to the *cis* state with a larger pore diameter. This is also in agreement with the fact that a larger switching impact was observed for the larger hydrocarbon molecule and that the permeation of the small hydrogen molecules is not affected. Hence, contrary to precedent design,[11] the permeation was controlled by

switching the pore size (i.e., by pore opening and closing) rather than by modulating the polarity of the MOF. We believe that steric effects in the small-pore $Cu_2(F_2AzoBDC)_2(dabco)$ MOF superimpose the effect of the azobenzene polarity switching, and therefore no switching effect was observed for the H_2:CO_2 separation.

In conclusion, thin films of metal–organic frameworks with fluorinated azobenzene side groups have been prepared, which can be reversibly switched with visible light only. On one hand, the guest molecule uptake by the thin film could be switched in a remote-controlled way. On the other hand, the membrane separation factors of hydrogen-hydrocarbons mixtures were reversibly modulated due to dynamic, remote-controlled pore opening/closing. It was demonstrated that visible light leads to high performances at several levels by avoiding the excitation of ligand-to-metal-charge transfer in the MOF by UV light and by obtaining high switching yields leading, for example, to a large difference in the guest molecule uptake. Generally, switching the properties of nanoporous materials by visible light instead of UV light significantly extends the potential areas of uses. Applications in life sciences and biomaterials, which are typically incompatible with UV irradiation, can now be explored. Furthermore, higher light intensities can be used without destroying the MOF material. Future aims are the optimization of the pore structure, which will result in an increase of the switching effect due to complete photo-induced opening/closing of the pores.

Experimental Section

The MOF films were prepared in a step-by-step fashion on a modified substrate surface, as was previously described in detail.[15] In this procedure, the substrate was alternatively immersed in an ethanol solution of the metal node (1 mM $Cu(OAc)_2$) and of the organic linker (0.1 mM dabco = 1,4-diazabicyclo[2.2.2]octane and $F_2AzoBDC$ = (E)-2-((2,6-difluorophenyl)diazenyl)terephthalic acid, synthesis of which was reported elsewhere[13]). The immersion times were 15 min for the metal node and 30 min for the organic linker solutions. Between each immersion step, the substrate was rinsed with pure ethanol for 2 min. The temperature during the synthesis was 60 °C. The samples were prepared in 30 cycles for IRRAS experiments, 50 cycles for the UV/Vis experiments and in 100 cycles for the QCM and membrane experiments. The gold substrates were functionalized by a self-assembled monolayer (SAM) of 11-mercapto-1-undecanol (MUD). The SAM formation was performed by immersing the substrate in a 1 mM MUD solution for one day. The mesoporous Al_2O_3 membranes and the quartz substrates were treated by an oxygen plasma (Diener Plasma, airflow: 50 sccm, pure oxygen) for 15 min prior to the SURMOF synthesis.[19]

X-ray diffraction (XRD) measurements were performed using a Bruker D8 Advance equipped with a Lynxeye detector in θ–θ geometry and using Cu$_{K\alpha}$ radiation ($\lambda = 0.154$ nm).

IRRAS was performed by using a Bruker Vertex 80 spectrometer with a grazing incident reflection angle of 80° relative to the normal. Reference measurements were done with a perdeuterated hexadecanethiol-SAM on a gold surface. The UV/Vis spectra were recorded by using a Cary5000 spectrometer from Agilent equipped with an UMA unit. Uptake experiments were performed using a Q-

Sense E4 Quartz crystal microbalance (QCM), the experimental setup was previously described.[20] The sample temperature was set to 25 °C. The irradiations were performed with 400 and 530 nm LEDs from PrizMatix with a power or 65 and 55 mW, respectively. The distance between the samples and the LEDs was approximately 5 cm.

The membrane permeation experiments were carried out using a Wicke–Kallenbach setup, which allows the in situ illumination of the membrane by LEDs of various wavelengths. A detailed description of the setup can be found in Reference [11]. Before the experiments, the membrane was activated in a N_2 flow at 80 °C for 24 h. The flow rate for each gas of the binary mixtures (H_2:C_2H_4 or H_2:C_3H_6) on the feed side was set to 25 mL min^{-1}, whereas the sweep gas N_2 had a flow rate of 50 mL min^{-1}. The gas-permeation experiments were performed at room temperature and under ambient conditions without overpressure. SEM analysis was performed with a JEOL JSM-6700F field emission scanning electron microscope. Images and EDX mapping were taken at 10 kV accelerating voltage and with 10 μA emission current and at 15 mm working distance. To avoid overcharging, samples were evaporated with carbon in a LEICA EMSCD500.

Conflict of interest

The authors declare no conflict of interest.

[1] M.-M. Russew, S. Hecht, Adv. Mater. 2010, 22, 3348–3360.
[2] a) W. R. Browne, B. L. Feringa, Nat. Nanotechnol. 2006, 1, 25–35; b) P.-T. Chiang, J. Mielke, J. Godoy, J. M. Guerrero, L. B. Alemany, C. J. Villagomez, A. Saywell, L. Grill, J. M. Tour, ACS Nano 2012, 6, 592–597.
[3] H. Dürr, Photochromism: Molecules and Systems, Elsevier, Amsterdam, 2003, ISBN: 9780444513229.
[4] a) J. Zhang, Q. Zou, H. Tian, Adv. Mater. 2013, 25, 378–399; b) R. Göstl, A. Senf, S. Hecht, Chem. Soc. Rev. 2014, 43, 1982–1996; c) H. M. D. Bandara, S. C. Burdette, Chem. Soc. Rev. 2012, 41, 1809–1825.
[5] a) S. Iamsaard, S. J. Asshoff, B. Matt, T. Kudernac, J. J. L. M. Cornelissen, S. P. Fletcher, N. Katsonis, Nat. Chem. 2014, 6, 229–235; b) C. L. van Oosten, C. W. M. Bastiaansen, D. J. Broer, Nat. Mater. 2009, 8, 677–682.
[6] M. Yamada, M. Kondo, J.-i. Mamiya, Y. Yu, M. Kinoshita, C. J. Barrett, T. Ikeda, Angew. Chem. Int. Ed. 2008, 47, 4986–4988; Angew. Chem. 2008, 120, 5064–5066.
[7] H. Furukawa, K. E. Cordova, M. O'Keeffe, O. M. Yaghi, Science 2013, 341, 1230444.
[8] I. M. Walton, J. M. Cox, J. A. Coppin, C. M. Linderman, D. G. Patel, J. B. Benedict, Chem. Commun. 2013, 49, 8012–8014.
[9] a) A. Modrow, D. Zargarani, R. Herges, N. Stock, Dalton Trans. 2012, 41, 8690–8696; b) Z. Wang, L. Heinke, J. Jelic, M. Cakici, M. Dommaschk, R. J. Maurer, H. Oberhofer, S. Grosjean, R. Herges, S. Bräse, K. Reuter, C. Wöll, Phys. Chem. Chem. Phys. 2015, 17, 14582–14587; c) N. Yanai, T. Uemura, M. Inoue, R. Matsuda, T. Fukushima, M. Tsujimoto, S. Isoda, S. Kitagawa, J. Am. Chem. Soc. 2012, 134, 4501–4504; d) J. Park, D. Q. Yuan, K. T. Pham, J. R. Li, A. Yakovenko, H. C. Zhou, J. Am. Chem. Soc. 2012, 134, 99–102.
[10] a) L. Heinke, M. Cakici, M. Dommaschk, S. Grosjean, R. Herges, S. Bräse, C. Wöll, ACS Nano 2014, 8, 1463–1467; b) J. Brown, B. L. Henderson, M. D. Kiesz, A. C. Whalley, W. Morris, S. Grunder, H. Deng, H. Furukawa, J. I. Zink, J. F. Stoddart, O. M. Yaghi, Chem. Sci. 2013, 4, 2858–2864; c) X. Meng, B. Gui, D. Yuan, M. Zeller, C. Wang, Sci. Adv. 2016, 2, e1600480.
[11] Z. Wang, A. Knebel, S. Grosjean, D. Wagner, S. Bräse, C. Wöll, J. Caro, L. Heinke, Nat. Commun. 2016, 7, 13872.
[12] a) D. Bléger, S. Hecht, Angew. Chem. Int. Ed. 2015, 54, 11338–11349; Angew. Chem. 2015, 127, 11494–11506; b) D. Bléger, J. Schwarz, A. M. Brouwer, S. Hecht, J. Am. Chem. Soc. 2012, 134, 20597–20600; c) C. Knie, M. Utecht, F. L. Zhao, H. Kulla, S. Kovalenko, A. M. Brouwer, P. Saalfrank, S. Hecht, D. Bleger, Chem. Eur. J. 2014, 20, 16492–16501.
[13] S. Castellanos, A. Goulet-Hanssens, F. Zhao, A. Dikhtiarenko, A. Pustovarenko, S. Hecht, J. Gascon, F. Kapteijn, D. Bleger, Chem. Eur. J. 2016, 22, 746–752.
[14] Z. Gu, L. Heinke, C. Wöll, T. Neumann, W. Wenzel, Q. Li, K. Fink, O. D. Gordan, D. R. T. Zahn, Appl. Phys. Lett. 2015, 107, 183301.
[15] a) O. Shekhah, H. Wang, S. Kowarik, F. Schreiber, M. Paulus, M. Tolan, C. Sternemann, F. Evers, D. Zacher, R. A. Fischer, C. Wöll, J. Am. Chem. Soc. 2007, 129, 15118–15119; b) L. Heinke, M. Tu, S. Wannapaiboon, R. A. Fischer, C. Wöll, Microporous Mesoporous Mater. 2015, 216, 200–215.
[16] Z. Wang, S. Grosjean, S. Braese, L. Heinke, ChemPhysChem 2015, 16, 3779–3783.
[17] O. Czuprat, J. Caro, V. A. Kondratenko, E. V. Kondratenko, Catal. Commun. 2010, 11, 1211–1214.
[18] S. Friebe, B. Geppert, J. Caro, Angew. Chem. Int. Ed. 2015, 54, 7790–7794; Angew. Chem. 2015, 127, 7900–7904.
[19] S. Hurrle, S. Friebe, J. Wohlgemuth, C. Wöll, J. Caro, L. Heinke, Chem. Eur. J. 2017, 23, 2294–2298.
[20] a) W. Zhou, C. Wöll, L. Heinke, Materials 2015, 8, 3767; b) L. Heinke, C. Wöll, Phys. Chem. Chem. Phys. 2013, 15, 9295–9299.

- 84 -

4.4. Azobenzene Guest Molecules as Light-Switchable CO₂-Valves in an Ultrathin UiO-67 Membrane

Azobenzene Guest Molecules as Light-Switchable CO$_2$ Valves in an Ultrathin UiO-67 Membrane

Alexander Knebel,*[†] Lion Sundermann,[†] Alexander Mohmeyer,[‡] Ina Strauß,[†,§] Sebastian Friebe,[†] Peter Behrens,[‡,§] and Jürgen Caro*[†]

[†]Institute for Physical Chemistry and Electrochemistry, Leibniz University Hannover, Callinstraße 3A, 30167 Hannover, Germany

[‡]Institute for Inorganic Chemistry, Leibniz University Hannover, Callinstraße 9, 30167 Hannover, Germany

[§]Laboratory of Nano and Quantum Engineering (LNQE), Leibniz University Hannover, Schneiderberg 39, 30167 Hannover, Germany

ⓢ Supporting Information

ABSTRACT: Metal−organic frameworks (MOFs) with an exceptionally large pore volume and inner surface area are perfect materials for loading with intelligent guest molecules. First, an ultrathin 200 nm high-flux UiO-67 layer deposited on a porous α-Al$_2$O$_3$ support by solvothermal growth has been developed. This neat UiO-67 membrane is then used as a host material for light-responsive guest molecules. Azobenzene (AZB) is loaded in the pores of the UiO-67 membrane. From adsorption measurements, we determined that the pores of UiO-67 are completely filled with AZB and, thereby, steric hindrance inhibits any optical switching. After *in situ* thermally controlled desorption of AZB from the membrane, AZB can be switched and gas permeation changes are observed, yielding an uncomplicated and effective smart material with remote controllable gas permeation. The switching of AZB in solution and inside the host could be demonstrated by ultraviolet−visible spectroscopy. Tracking the completely reversible control over the permeance of CO$_2$ and the H$_2$/CO$_2$ separation through the AZB-loaded UiO-67 layer is possible by *in situ* irradiation and permeation. Mechanistic investigations show that a light-induced gate opening and closing takes place. A remote controllable host−guest, ultrathin smart MOF membrane is developed, characterized, and applied to switch the gas composition by external stimuli.
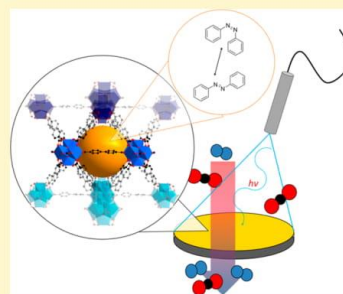
1. INTRODUCTION

Metal−organic frameworks (MOFs), consisting of metal or metal oxide nodes interconnected by organic linker molecules, exhibit extraordinary properties as porous materials for gas separation and purification and can also be utilized as smart and intelligent materials. With molecularly designed linker molecules or linkers with side-chain functionalities that react as a result of external stimuli, several highly special properties could be introduced into the frameworks.[1−3] Complicated synthesis and noncommercial organic ligands are often used, mostly tailor-made on the lab scale at very low yields, to show certain smart (photoresponsive) functions, for example, photochromism[4,5] or photoinduced drug release.[6] Accompanied by the synthetically difficult approach to molecularly engineered linkers, deposition of the MOF as a thin layer on functional surfaces is rather complicated, but necessary to achieve the custom-made function. The first developed porous and light-switchable MOF was reported in 2011 by Modrow et al.[7] For functional membranes, usually a layer-by-layer deposition, including several washing steps, is employed to form a surface-anchored metal−organic framework (SURMOF) with tailored functionality and a state-of-the-art thickness and flux.[8,9] A synthetically much easier and cheaper approach,[4] but rarely

reported in the literature,[10−12] is the combination of solvothermally grown MOFs as host materials for smart guest molecules in the preparation of intelligent host−guest materials. Smart membrane systems in general have been investigated rarely, but there are examples like that of Liu et al.,[13] in which K$^+$ ion-cognitive gates were introduced into polymeric nylon composite membranes.

However, again with respect to the MOF topic, it has been shown several times, with photoswitchable tailor-made linkers, that photophysical pore control in MOFs is possible.[5,11,14,15] Just recently, we published a cooperation project in which a SURMOF membrane layer with azobenzene (AZB) side-chain functionality was prepared and successfully used for gas separation.[16]

We herein report, for the first time, a submicrometer sized, 200 nm thin UiO-67 membrane that has been synthesized solvothermally. Other thin layer UiO membranes for different purposes have been published recently. For instance, thin layer UiO-66 membranes are used for organoselective pervapora-

tion,[17] UiO-66 hollowfiber membranes for use in organic dehydration[18] and desalination,[19] and metal-supported UiO-66 membranes for gas separation of moist gases.[20] Until now, most state-of-the-art membranes, for example, ZIF-8 membranes, were produced by *in situ* or counter diffusion methods and reached a minimal thickness of 1 μm.[21]

However, the thin layer UiO-67 membrane allows light switching of AZB as a guest molecule, and the neat membrane also itself shows good gas separation properties. In addition, the AZB molecules alter the separation properties through gating effects in the UiO-67 framework. This was shown using *in situ* gas permeation measurements in a specifically designed Wicke−Kallenbach permeation cell. In the end, a mechanistic explanation is given, from spectroscopic measurements, showing that AZB guest molecules form π-stacking complexes with the MOF linkers. Thus, it was shown that AZB influences the gates of UiO-67 by light irradiation.

2. MATERIALS AND METHODS

2.1. Reagents and Chemicals. All chemicals were used as received from commercial vendors. The asymmetric α-Al$_2$O$_3$ porous support discs with a diameter of 18 mm (1.8 μm grains as the basis layer, 70 nm grains as the top layer) were purchased from Fraunhofer Institute for Ceramic Technologies and Systems IKTS (Hermsdorf, Germany). The chemicals used for this work were glacial acetic acid (≥99.7%, HPLC grade, Fisher Scientific), acetone (≥99.9%, Sigma-Aldrich), azobenzene (AZB, for elemental analysis, Merck), biphenyl-4,4′-dicarboxylic acid (BPDC, 98%, Acros Organics), methanol (MeOH, ≥99.8%, Sigma-Aldrich), *N,N*-dimethylformamide (DMF, 99.8% anhydrous, Sigma-Aldrich), and ZrCl$_4$ (anhydrous, 98%, Alfa Aesar).

2.2. UiO-67 Membrane Synthesis. The UiO-67 membrane was synthesized by a solvothermal procedure. First, the α-Al$_2$O$_3$ support (IKTS) was placed face down in a PTFE holder that fits into the autoclave. The autoclave was preheated to 150 °C. At the same time, two solutions were preheated to 150 °C. The first solution consisted of 0.28 g of ZrCl$_4$ and 4.5 mL of DMF, and the second solution consisted of 0.612 g of BPDC with 10 mL of DMF. The solutions were mixed in the preheated autoclave. After that, 2 mL of DMF and 0.36 mL of acetic acid (99.7%) were added. The autoclave was sealed, and the reaction mixture was held at 220 °C for 24 h. The membrane layer was washed afterward by solvent exchange first in DMF (2 h), then in MeOH (2 h), and finally in acetone (2 h). The membrane was dried at 60 °C for 12 h.

2.3. UiO-67 Powder Synthesis. The UiO-67 powder was synthesized solvothermally by mixing two preheated solutions at 150 °C. The first solution consisted of 0.28 g of ZrCl$_4$ and 4.5 mL of DMF, and the second solution consisted of 0.612 g of BPDC, 10 mL of DMF, and 100 μL of acetic acid (99.7%). The solutions were mixed in a preheated PTFE-lined autoclave at 150 °C. The autoclave was sealed and heated to 180 °C for 24 h. The particles were washed in the centrifuge at 10000 rpm twice with DMF, once with MeOH, and finally once with acetone. The powder was then dried for 12 h at 60 °C.

2.4. Azobenzene Loading. The powder was loaded via the gas phase at 120 °C in a sealed vacuum flask under an autogenous pressure of AZB for 12 h. Loading the membrane over the gas phase was not possible without cracking the membrane layer. Therefore, the membrane was loaded in a 0.01 M AZB solution in acetone for 5 min. Then, the membrane surface was washed of residual surface AZB by dipping the supported layer in a fresh acetone solution for 5 s. The membrane was dried in air for 12 h.

2.5. Single-Gas Permeation. For the characterization of the UiO-67 membrane, single-gas permeation was used. The gas flux was regulated by remote-controlled mass flow controllers. Single-gas permeation was performed using a 50 mL/min gas flux on the feed side. As the feed gas, H$_2$, CO$_2$, N$_2$, CH$_4$, ethane (C$_2$H$_6$), and propane (C$_3$H$_8$) were used. On the sweep side, N$_2$ was used in all cases, except

for N$_2$ single-gas permeation, where CH$_4$ was used on the sweep side. The sweep-gas flux was 50 mL/min; thus, the system operated without pressure differences. The single-gas permeation experiments were performed at room temperature (RT) and under ambient conditions. Each data point is an average value from five measurement data points and was collected after equilibration times of around 24 h.

2.6. Mixed-Gas Permeation. Mixed-gas permeation experiments were performed using binary mixtures of H$_2$ with CO$_2$, N$_2$, CH$_4$, C$_2$H$_6$, and C$_3$H$_8$ in a 1:1 ratio. The flux of each gas was 25 mL/min, resulting in an overall feed-gas flux for the binary mixture of 50 mL/min. On the sweep side, N$_2$ was applied (or in case of the H$_2$/N$_2$ binary mixture, CH$_4$) at a flow rate of 50 mL/min. The membrane was kept under ambient conditions.

2.7. *In Situ* Mixed-Gas Permeation and Irradiation. For *in situ* gas permeation, a H$_2$/CO$_2$ mixed gas with a flow rate of 25 mL/min each was applied on the feed side of the membrane. On the sweep side, a 50 mL/min flow rate of N$_2$ was applied. The membrane was kept under ambient conditions. To irradiate the sample with ultraviolet−visible (UV−vis) light, a Prizmatix FC5-LED high-power, fiber-coupled LED system was used. For the controlled desorption of AZB in the gas flow, the temperature of the membrane was adjusted to 80 °C and the increase in the level of CO$_2$ permeation with time was monitored. While the desorption of AZB took place, the membrane was constantly irradiated at λ = 365 nm. After a certain amount of desorbed AZB after some time, the increase in CO$_2$ permeance increased rather quickly compared to that for the desorption process. This was an indicator of the achievement of AZB switchability.

To obtain a curve in a plot of permeance versus time, the membrane was then cooled to RT. Gas permeation was performed under *in situ* irradiation alternating with λ = 365 nm and λ = 465 nm at RT. When a saturation level of the permeance change was reached, the wavelength was changed, yielding a quasi-sinusoidal switching plot for the selectivity of the H$_2$/CO$_2$ mixture.

2.8. N$_2$ Sorption. Nitrogen sorption isotherms were measured at 77 K on a Quantachrome Autosorb-3 instrument. Samples were outgassed in vacuum at room temperature for 24 h prior to the sorption measurement. Surface areas were estimated by applying the Brunauer−Emmett−Teller (BET) equation. To determine the BET surface area, the "Micropore BET Assistant" implemented in ASiQwin version 2.0 from Quantachrome was used. The pore size distributions were calculated using nonlinear density functional theory (NLDFT) fitting of the Quantachrome Kernel "N$_2$ at 77 K zeolites/silica" to the experimental data. The total pore volumes were estimated by the single-point method at p/p^0 = 0.95.

2.9. Thermogravimetric Analysis, Differential Scanning Calorimetry, and Differential Thermal Analysis. Thermogravimetric analysis (TG), differential scanning calorimetry (DSC), and differential thermal analysis (DTA) were performed using a Netzsch Sta 409PC/PG instrument under an Ar atmosphere, starting at 40 °C and ending at 800 °C with a heating rate of 5 K/min.

2.10. SEM and EDXM. Scanning electron microscopy (SEM) was performed with a field emission scanning electron microscope (JEOL JSM-6700F). Pictures of particles deposited on graphite were taken at an acceleration voltage of 2 kV and an acceleration current of 10 μA. Energy dispersive X-ray mapping (EDXM) and the corresponding images of the membrane cross section were taken at an acceleration voltage of 10 kV and an acceleration current of 10 μA. To prevent overcharging, the membrane was coated with carbon using the Leica EMSCD500 instrument.

2.11. UV−Vis Spectroscopy. UV−vis spectroscopy was performed using a Cary 5000 UV−vis spectrophotometer from Agilent Technologies. The samples were measured in quartz glass cuvettes with a 1 mm thickness. UiO-67 and AZB@UiO-67 powder was deposited on the glass faces. All samples were measured in an integrated sphere to take reflection and transmission into account. The spectra are not normalized. Calculation results for the approximately switchable amounts (in percent *cis*) have been obtained using AZB in ethanol changes as a comparison.[11,23−26]

2.12. Infrared Spectroscopy. Fourier transform infrared (FTIR) spectra were recorded using an Agilent Cary 630 FTIR spectrometer
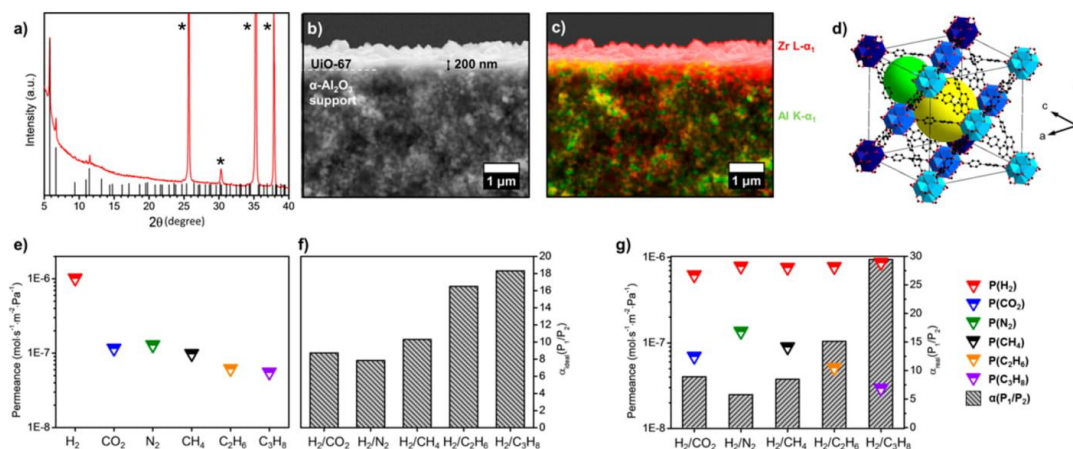
Figure 1. UiO-67 layer investigated by (a) XRD, (b) SEM, and (c) EDX mapping. The crystal structure of UiO-67 is shown in panel (d). The UiO-67 layer is very thin (200 nm), as shown in panel (c), so that XRD gives only low reflex intensities. XRD shows strong support reflexes that are denoted with asterisks in panel (a). However, the reflexes could be identified as UiO-67.[22] Permeances for the neat UiO-67 layer without AZB loading are given as follows. The single-gas permeances and ideal permselectivities (in a hypothetical mixture with H_2) are shown in panels (e) and (f), respectively. The mixed-gas permeances and real permselectivities for H_2-containing mixtures are given in panel (g). Permeation data are provided in Tables S1 and S2. Details of the experimental setup are given in Figure S1.

with a diamond attenuated total reflectance unit. The spectra were recorded over the full spectral range from 4000 to 650 cm^{-1} with a resolution of 2 cm^{-1} at 64 scans and are not normalized.

2.13. X-ray Diffraction. For X-ray diffraction (XRD), a Bruker D8-Advance diffractometer with LYNXEYE detection technology was used. For the measurement, the sample was mounted on a polymer holder. Bragg–Brentano θ–θ geometry and Cu Kα radiation (λ = 0.154 nm) were used. For the recording of the XRD pattern, a 2θ range of 4–60° was applied, at 0.0341° and 1 s per step for a total of 1639 steps. The samples were not rotated during the measurement.

3. RESULTS AND DISCUSSION

3.1. UiO-67 Membrane Syntheses and Characterization. The UiO-67 membrane layer has been characterized by XRD (cf. Figure 1), scanning electron microscopy (SEM), and energy dispersive X-ray mapping (EDX mapping) (cf Figure 1b,c), and gas permeation data were collected for the neat membrane (Figure 1e–g). The SEM images show a cross section of the supported UiO-67 membrane. The UiO-67 structure, shown in Figure 1d, consists of $[Zr_6O_4(OH)_4]^{12+}$ clusters, forming the secondary building units, which are interconnected by biphenyl-4,4′-dicarboxylic acid (BPDC). The network forms cages with two sizes. The large cage (yellow) has a diameter of 18 Å, and the smaller cage (green) has a diameter of 12 Å.[27] XRD of the membrane layer in Figure 1a, with our awareness of the membrane thickness pictured by SEM and EDX mapping (Figure 1b,c), shows good crystallinity and a good signal-to-noise ratio. Thus, it could be identified as an ultrathin UiO-67 MOF layer.[22] However, the reflexes obtained are of low intensity because of the very thin layer. It must be highlighted that this membrane layer was solvothermally synthesized. To obtain such an ultrathin membrane, knowledge of the crystallization process was significantly important.[28] Determined by the SEM imaging and the corresponding EDX mapping of the layer [analyzing the elemental maps of Zr-L-α_1 and Al–K-α_1 (cf. Figure 1)], the UiO-67 layer is around 200 nm thick. From the EDX mapping

of the SEM image in Figure 1c, it is clear that the Zr-MOF layer is anchored well on the Al_2O_3 support and shows a homogeneous layer thickness.

The permeation data of the neat UiO-67 membrane show that the membrane is dense and has a high flux (Figure 1e–g). As UiO-67 is a MOF with large pores (cavities of ~12 and ~18 Å with pore windows of 8 Å),[29] and the MOF layer, 200 nm, is rather thin, high-flux permeances were expected. The permeance of a gas through a membrane is given in units of moles per membrane area, time, and partial pressure difference over the membrane. Figure 1e shows that the single-gas permeances are slightly higher than the mixed-gas permeances in Figure 1g. In both single- and mixed-gas permeation, the different gas permeances decrease with an increasing critical diameter of the molecules from H_2 to C_3H_8. Interesting is the ideal permselectivity of hydrogen to other gases calculated as the ratio of the single-gas permeances in Figure 1f and compared to the real permselectivities of H_2 against other gases in the mixed-gas separation in Figure 1g. First, the trend is the same for ideal- and mixed-gas selectivities. However, the real H_2/propane selectivity of 29.4 in the mixture is a factor of 1.6 larger than the predicted ideal selectivity of 18.3. Because the separation in the real mixture is better than expected from the ideal separation predictions, we can conclude that the membrane separation relies on an interplay of mixed-gas competitive adsorption and diffusion.[30] The high flux and decent hydrogen selectivity make the membrane suitable for hydrogen purification applications.

3.2. Determining the AZB Loading of UiO-67. Because the UiO-67 layer was grown as a dense membrane with clear gas separating properties, the large pore size of UiO-67 allows adsorption of hydrocarbons and thus the modification of the membrane layer with AZB via liquid phase adsorption. AZB as an UV−vis light-switchable compound has been loaded as a guest molecule into the MOF network via adsorption from an acetone solution, without further postsynthetic functionalization. Powder samples were also loaded, and the AZB loading

Article

and space occupation were evaluated by N_2 sorption. The isotherms are shown in Figure 2. The pristine, AZB-free UiO-
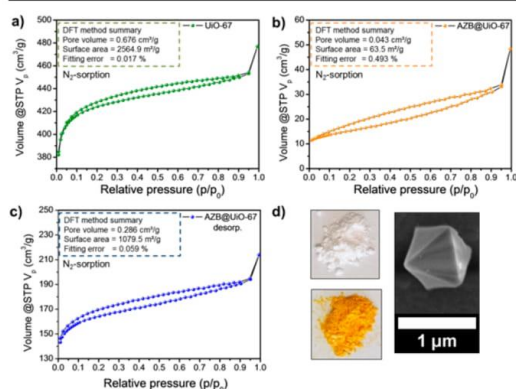

Figure 2. N_2 adsorption isotherms of (a) the pristine, AZB-free UiO-67 powder, (b) the AZB@UiO-67 host−guest composite, and (c) partly AZB-desorbed AZB@UiO-67 powder. Photographs of the empty and AZB-loaded powders and a SEM image of a single particle of the powder are shown in panel (d). For the pristine powder in panel (a), an inner surface area of 2565 m^2/g was calculated with the DFT method. Eventually, for the loaded AZB@UiO-67 powder (b), an inner surface area of 63 m^2/g was calculated, and AZB desorption of the sample (c) yielded 1080 m^2/g. The powder XRD data are shown in Figure S2.

67 is shown in Figure 2a, fully loaded UiO-67 in Figure 2b, and partial AZB desorption in Figure 2c. From these data, it is clear that UiO-67 can be completely loaded with the AZB molecules and leaves no free space inside the MOF, which inhibits any optical switching of the densely packed AZB, as it is similarly found for solid AZB, as well as for structural isoreticular UiO Zr-MOFs with AZB linkers.[31]

The N_2 isotherm (Figure 2b) clearly shows for AZB-loaded UiO-67 a very small inner microporous surface area of 63 m^2/g compared to a surface area of 2565 m^2/g (Figure 2). From these results, we can assume that the adsorption in the pore of the fully AZB-loaded UiO-67 is negligible, and the low N_2 adsorption can be attributed to the interparticle space.

3.3. Activation and Remote Control of the AZB@UiO-67 Membrane. Therefore, it is not surprising that for a fully AZB-loaded UiO-67 membrane no gas flux through the membrane layer could be observed (Figure 3), which originally has been very high for the neat, AZB-free UiO-67 membrane (cf. Figure 1e−g). As shown in Figure 3a, some AZB had to be desorbed first, because the fully AZB-loaded UiO-67 membrane did not allow (i) any gas transport of probe molecules or (ii) *trans*−*cis* switching of AZB. Gas transport and switchability have been realized by a trick: thermally controlled desorption, which was indirectly traced over the CO_2 permeance at 353 K under *in situ* irradiation at 365 nm. The time dependencies of AZB desorption, the amount of AZB desorbed from a fully AZB-loaded UiO-67 membrane, could be reproduced for the powder sample under a H_2/CO_2 mixed-gas flow at 353 K. AZB switching has also been proven by spectroscopic techniques for AZB in ethanol and is compared with switching of AZB in a UiO-67 powder sample in UV−vis experiments, shown in panels b and c of Figure 4, respectively. The sample was additionally investigated by N_2 sorption afterward, yielding an
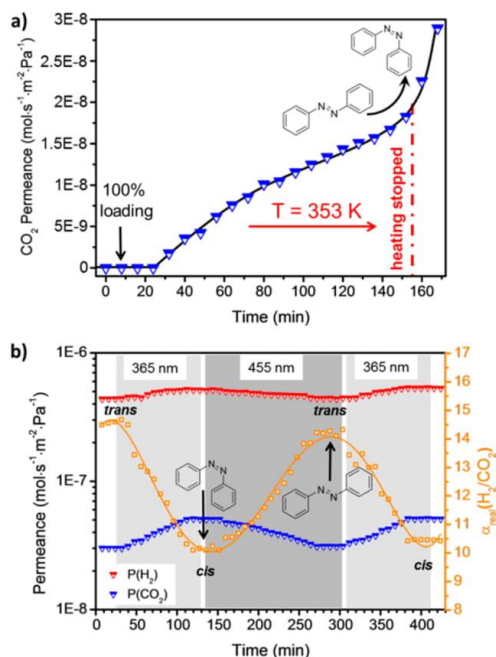
Figure 3. (a) Controlled thermal desorption of AZB from the supported UiO-67 layer. The desorption of AZB (starting with a fully loaded membrane with no permeance at all) was indirectly traced over the increasing CO_2 permeance. During the *in situ* desorption of AZB, the LED was constantly irradiating the top layer of the AZB@UiO-67 membrane at 365 nm, thus switching the AZB from *trans* to *cis*. The indicator of the maximal switchable amount of AZB inside the MOF was the rapid increase in CO_2 permeance after a certain AZB desorption, where the heating was stopped. (b) Reversible gas permeation of the equimolar H_2/CO_2 mixture upon *in situ* reversible switching of AZB in UiO-67 at a constant and reduced AZB loading. A sinusoidal change in mixed-gas separation factor α (H_2/CO_2) is observed. The *in situ* permeation data are listed in Table S3, and the experimental setup is given in Figure S1.

inner surface area of 1080 m^2/g (cf. Figure 2c). From gas permeation, spectroscopy, and sorption measurements, showing that switching is possible with a particular amount of AZB, in combination with thermogravimetric analysis (see Figure S3−S5), a quite accurate optimum AZB loading was determined that allows (i) gas transport and (ii) AZB photoisomerization. The fully loaded UiO-67 has 36.6 wt % AZB adsorbed inside the structure. After desorption, the optimal switchable amount is found to be 19 wt % AZB. The switching of gas transport through the AZB-loaded UiO-67 membrane could be achieved reversibly at room temperature (cf. Figure 3b).

Upon irradiation of the membrane at 293 K with λ = 365 nm light, an increase in CO_2 permeance is observed. The switching of the AZB into the *cis* form is responsible for this increase in the CO_2 permeation. By using light in the visible part of the spectrum (λ = 455 nm), it was possible to switch the AZB back into the *trans* form.

Switching the AZB into dynamic equilibrium *trans* or *cis* configuration needs continuous irradiation and a relatively long
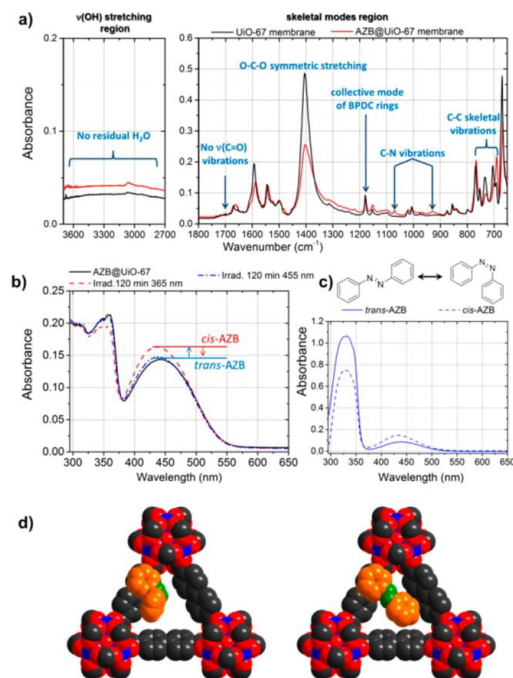
Figure 4. ATR-IR (attenuated total reflection infrared) spectra. (a) UiO-67 ATR-IR spectra for the skeletal modes and the ν(OH) region. No residual guest molecules, H_2O, DMF, or acetone is visible at ≈ 1700 cm^{-1} in the ν(C=O) region or in the ν(OH) region. In the IR spectra, via comparison of the AZB@UiO-67 membrane and neat-UiO-67, the AZB adds C−N vibrational bands to the spectrum. Interpretations of the mechanism of switching have been made. Overall skeletal vibration suppression/alteration through AZB is assigned to π-stacking complexes of the benzene rings of AZB and BPDC. (b) UV–vis spectra of AZB@UiO-67 powder samples after controlled desorption. To compare the results and calculate a switching yield, AZB isomerism through irradiation is given for AZB in ethanol in panel (c). (d) Sketch of the gate switching mechanism with a space-filling model of a pore window of UiO-67 and AZB in the *cis* conformation on the left and the *trans* conformation on the right. Oxygens are colored red, nitrogens green, carbons of the MOF gray, carbons of the AZB orange, and zirconiums blue. Hydrogen atoms are hidden.

irradiation time. Once in the equilibrium state, the respective isomers remain stable for at least 24 h. Switching the AZB@UiO-67 at room temperature into the *trans* isomer takes 106 min at 455 nm, and maximal *cis* isomerization is reached after irradiation with UV light at 365 nm for 120 min. In the case of the *trans* configuration of AZB, the H_2/CO_2 separation factor is 14.7, which can be explained as a gating process rather than an electrostatic effect.[32] Through a change in conformation to *cis*, the CO_2 gate is open, yielding a H_2/CO_2 permselectivity of 10.1 and a higher CO_2 permeance. In fact, the H_2 permeance also slightly increases when switching to *cis* and decreases when switching to *trans*, which indicates gating effects. The size of guest molecule AZB (C4−C4′ distance) changes from 9 to 5.5 Å,[11] and this leads to the assumption that, besides the fact that the dipole moments of the AZB

change, a switching of the pore channel sizes would contribute even more.

3.4. Understanding the Mechanism of AZB@UiO-67 Switching. To understand the mechanism of switching, it is important to know how many AZB molecules per elemental cell (EC) can switch. As mentioned above, the large cage has a diameter of 18 Å and the small cage a diameter of 12 Å. Per EC, four superoctahedral and eight supertetrahedral cavities exist. A hypothetical maximal loading of 62 wt % AZB should be possible, when assuming it is loaded with solid AZB (density of 1.09 g/cm^3) and using the DFT pore volume of 0.676 cm^3/g (cf. Figure 2). Calculating the volume of the free space in UiO-67, by assuming spherical cavities, and dividing it by 270 Å^3 for one molecule of *trans*-AZB[33] (thermodynamically stable form) results in an overall maximal loading of 249 AZB molecules per EC. However, from the experimental thermogravimetric analysis (see the Supporting Information), a maximal loading of 36.6 wt % results in a completely filled UiO-67, which is thereby equivalent to 147 AZB molecules per EC. The amount of AZB is decreased because it behaves like a solution inside the MOF structure and, thus, occupies more space, and steric hindrance occurs inside the cavities. When thermally activated, UiO-67 is filled with only 19 wt %, i.e., 74 AZB molecules per EC. From that amount, there is ∼12% AZB that can be addressed by irradiation, which means that nine AZB molecules can be switched per EC. Via comparison of our recent research with a 40% switchable Azo-SURMOF membrane, five moieties could be switched per EC.[16] Upon normalization of the volume of the Azo-SURMOF EC to the volume of the UiO-67 EC, four ECs of the SURMOF fit into that of UiO-67. This means, for the Azo-SURMOF membrane, a maximal switchable amount of 20 AZB moieties is available. Comparing these data, we can actually address around half the amount of AZB moieties inside the UiO-67 crystal structure, which is quite good, when it is acknowledged that the comparison is made between a tailored MOF and a host−guest system. Upon examination of the permeance while switching (cf. Figure 3b), both the H_2 and CO_2 permeances decrease in the *trans* state. Here, the CO_2 permeance is more affected, thus substantiating the assumption of permeation changes through gating mechanisms.

In the Azo-SURMOF membrane, the switching could be assigned to be almost only an electrostatic effect, and a decreasing CO_2 permeance was observed in *cis* due to strong electrostatic adsorption.[16] Hence, this was the opposite effect compared to that of the AZB@UiO-67 membrane.

Why does AZB influence the gate here? Through interpretation of the IR spectra of the UiO-67 membrane and AZB@UiO-67 membrane (Figure 4a), a mechanistic explanation can be formulated.[34] Here, an alteration of C−C skeletal vibrations is observed when AZB has been loaded into the framework of UiO-67. Other vibrations decrease, for example, the O−C−O vibration at 1409 cm^{-1}, while the collective BPDC linker vibration at 1190 cm^{-1} is also lowered for AZB@UiO-67. The azo function itself is IR-inactive, but C−N vibrations can be found in the AZB@UiO-67 spectrum. This indicates the presence of AZB.

These data can be explained with AZB forming a π-stacking adsorption complex inside UiO-67 with the benzene rings of the BPDC linker molecules. Such sandwich adsorption alters vibrational modes as shown for different π-stacking on graphene.[35]

Thus, an electrostatic change will happen here, but its influence is rather weak compared to the main reason for the

Article

permeation switching, gating effects. A schematic illustration of how the *trans* state of AZB is believed to reduce the aperture of the gate is shown in Figure 4d. From these data, AZB is apparently π-stacking at the benzene rings of the UiO-67 and thereby affects the effective gate size. The AZB *trans* isomer has a length of 9 Å, and the dipolar moment is 0 D; the AZB in the *cis* form results in a length of 5.5 Å and a dipole moment of 3 D.[11] It is clear that the pore window would close and open with a great effect (window size of 8 Å[29]).

The switching of AZB itself in the activated AZB@UiO-67 powder and of the pure AZB molecules in ethanol is shown by UV−vis measurements in panels b and c of Figure 4, respectively.

4. CONCLUSION

On the basis of the experimental findings, it was possible for the first time to synthesize a supported ultrathin high-flux UiO-67 membrane by solvothermal crystallization. The densely intergrown submicrometer sized membrane layer had a thickness of only 200 nm as determined by EDXM and the corresponding SEM image.

It could be shown that AZB can be adsorbed into the MOF up to a maximal loading of 35.6 wt %. However, at complete pore filling with AZB, the pores are blocked by the guest molecules for any gas adsorption or gas permeation, and consequently, no *trans*−*cis* switching of AZB could occur. After activation through controlled *in situ* desorption of AZB at 353 K under constant irradiation at $\lambda = 365$ nm, AZB can be addressed optically and switching of both gas permeation and separation could be achieved. The optimal switchable amount of AZB could be determined by thermogravimetric analysis of a similarly processed UiO-67 powder and was 19 wt %. Calculations showed that per unit cell of UiO-67 the large number of nine AZB guest molecules is switchable.

AZB switching to the *cis* isomer at 365 nm and back to the *trans* isomer at 455 nm was possible and reversible in cycles as shown by *in situ* gas permeation and UV−vis spectroscopy. From UV−vis spectroscopy, it follows that 12% of the AZB in the pore is switchable. A mechanism could be proposed relying on data from IR spectroscopy, showing that the pore entrances of UiO-67 are affected by AZB due to formation of π-stacking complexes. AZB molecules suppress and alter especially C−C vibrations of the BPDC linker through π-stacking, when adsorbed inside the pores. This permits completely reversible gate opening and closing through light. In summary, a novel supported, ultrathin UiO-67 membrane was successfully synthesized and modified with AZB, yielding a smart host−guest membrane, which is a stimulus-responsive, remote controllable, and reversible switching membrane material for gas separation. In addition, it may find use in the field of sensors or as a molecular light switch in microelectronics.

■ ASSOCIATED CONTENT

Ⓢ Supporting Information

The Supporting Information is available free of charge on the ACS Publications website at DOI: 10.1021/acs.chemmater.7b00147.

Experimental setup and permeation data, powder XRD, TG, DSC, and DTG (PDF)

■ AUTHOR INFORMATION

Corresponding Authors
*E-mail: alexander.knebel@pci.uni-hannover.de.
*E-mail: juergen.caro@pci.uni-hannover.de.
ORCID ⊙
Alexander Knebel: 0000-0002-5866-1106

■ ACKNOWLEDGMENTS

■ REFERENCES

(1) Wang, Z.; Heinke, L.; Jelic, J.; Cakici, M.; Dommaschk, M.; Maurer, R. J.; Oberhofer, H.; Grosjean, S.; Herges, R.; Bräse, S.; et al. Photoswitching in nanoporous, crystalline solids: an experimental and theoretical study for azobenzene linkers incorporated in MOFs. *Phys. Chem. Chem. Phys.* **2015**, *17*, 14582−14587.

(2) Brown, J. W.; Henderson, B. L.; Kiesz, M. D.; Whalley, A. C.; Morris, W.; Grunder, S.; Deng, H.; Furukawa, H.; Zink, J. I.; Stoddart, J. F.; et al. Photophysical pore control in an azobenzene-containing metal−organic framework. *Chem. Sci.* **2013**, *4*, 2858−2864.

(3) Krause, S.; Bon, V.; Senkovska, I.; Stoeck, U.; Wallacher, D.; Tobbens, D. M.; Zander, S.; Pillai, R. S.; Maurin, G.; Coudert, F.-X.; et al. A pressure-amplifying framework material with negative gas adsorption transitions. *Nature* **2016**, *532*, 348−352.

(4) Castellanos, S.; Kapteijn, F.; Gascon, J. Photoswitchable metal organic frameworks: Turn on the lights and close the windows. *CrystEngComm* **2016**, *18*, 4006−4012.

(5) Castellanos, S.; Goulet-Hanssens, A.; Zhao, F.; Dikhtiarenko, A.; Pustovarenko, A.; Hecht, S.; Gascon, J.; Kapteijn, F.; Bleger, D. Structural Effects in Visible-Light-Responsive Metal-Organic Frameworks Incorporating ortho-Fluoroazobenzenes. *Chem. - Eur. J.* **2016**, *22*, 746−752.

(6) Heinke, L.; Cakici, M.; Dommaschk, M.; Grosjean, S.; Herges, R.; Bräse, S.; Wöll, C. Photoswitching in Two-Component Surface-Mounted Metal-Organic Frameworks: Optically Triggered Release From a Molecular Container. *ACS Nano* **2014**, *8*, 1463−1467.

(7) Modrow, A.; Zargarani, D.; Herges, R.; Stock, N. The first porous MOF with photoswitchable linker molecules. *Dalton Trans.* **2011**, *40*, 4217−4222.

(8) Bétard, A.; Bux, H.; Henke, S.; Zacher, D.; Caro, J.; Fischer, R. A. Fabrication of a CO2-selective membrane by stepwise liquid-phase deposition of an alkylether functionalized pillared-layered metal-organic framework [Cu2L2P]n on a macroporous support. *Microporous Mesoporous Mater.* **2012**, *150*, 76−82.

(9) Valadez Sánchez, E. P.; Gliemann, H.; Haas-Santo, K.; Wöll, C.; Dittmeyer, R. ZIF-8 SURMOF Membranes Synthesized by Au-Assisted Liquid Phase Epitaxy for Application in Gas Separation. *Chem. Ing. Tech.* **2016**, *88*, 1798−1805.

(10) Hermann, D.; Emerich, H.; Lepski, R.; Schaniel, D.; Ruschewitz, U. Metal-organic frameworks as hosts for photochromic guest molecules. *Inorg. Chem.* **2013**, *52*, 2744−2749.

(11) Weh, K.; Noack, M.; Hoffmann, K.; Schröder, K.-P.; Caro, J. Change of Gas Permeation by Photoinduced Switching of Zeolite-

Azobenzene Membranes of Type MFI and FAU. *Microporous Mesoporous Mater.* **2002**, *54*, 15−26.

(12) Yanai, N.; Uemura, T.; Inoue, M.; Matsuda, R.; Fukushima, T.; Tsujimoto, M.; Isoda, S.; Kitagawa, S. Guest-to-host transmission of structural changes for stimuli-responsive adsorption property. *J. Am. Chem. Soc.* **2012**, *134*, 4501−4504.

(13) Liu, Z.; Luo, F.; Ju, X.-J.; Xie, R.; Luo, T.; Sun, Y.-M.; Chu, L.-Y. Positively K + -Responsive Membranes with Functional Gates Driven by Host-Guest Molecular Recognition. *Adv. Funct. Mater.* **2012**, *22*, 4742−4750.

(14) Baroncini, M.; d'Agostino, S.; Bergamini, G.; Ceroni, P.; Comotti, A.; Sozzani, P.; Bassanetti, I.; Grepioni, F.; Hernandez, T. M.; Silvi, S.; et al. Photoinduced reversible switching of porosity in molecular crystals based on star-shaped azobenzene tetramers. *Nat. Chem.* **2015**, *7*, 634−640.

(15) Modrow, A.; Zargarani, D.; Herges, R.; Stock, N. Introducing a Photo-Switchable Azo-Functionality Inside Cr-MIL-101-NH2 by Covalent Post-Synthetic Modification. *Dalton Trans.* **2012**, *41*, 8690−8696.

(16) Wang, Z.; Knebel, A.; Grosjean, S.; Wagner, D.; Bräse, S.; Wöll, C.; Caro, J.; Heinke, L. Tunable Molecular Separation by Nanoporous Membranes. *Nat. Commun.* **2016**, *7*, 13872.

(17) Miyamoto, M.; Hori, K.; Goshima, T.; Takaya, N.; Oumi, Y.; Uemiya, S. An Organoselective Zr-Based Metal Organic Framework UiO-66 Membrane for Pervaporation. *Eur. J. Inorg. Chem.* **2017**, DOI: 10.1002/ejic.201700010.

(18) Liu, X.; Wang, C.; Wang, B.; Li, K. Novel Organic-Dehydration Membranes Prepared from Zirconium Metal-Organic Frameworks. *Adv. Funct. Mater.* **2017**, *27*, 1604311.

(19) Liu, X.; Demir, N. K.; Wu, Z.; Li, K. Highly Water-Stable Zirconium Metal-Organic Framework UiO-66 Membranes Supported on Alumina Hollow Fibers for Desalination. *J. Am. Chem. Soc.* **2015**, *137*, 6999−7002.

(20) Liu, J.; Canfield, N.; Liu, W. Preparation and Characterization of a Hydrophobic Metal−Organic Framework Membrane Supported on a Thin Porous Metal Sheet. *Ind. Eng. Chem. Res.* **2016**, *55*, 3823−3832.

(21) Kwon, H. T.; Jeong, H.-K. In situ synthesis of thin zeolitic-imidazolate framework ZIF-8 membranes exhibiting exceptionally high propylene/propane separation. *J. Am. Chem. Soc.* **2013**, *135*, 10763−10768.

(22) Yang, Q.; Guillerm, V.; Ragon, F.; Wiersum, A. D.; Llewellyn, P. L.; Zhong, C.; Devic, T.; Serre, C.; Maurin, G. CH4 storage and CO2 capture in highly porous zirconium oxide based metal-organic frameworks. *Chem. Commun.* **2012**, *48*, 9831−9833.

(23) Siampiringue, N.; Guyot, G.; Monti, S.; Bortolus, P. The cis -> trans Photoisomerization of Azobenzene: An Experimental Re-Examination. *J. Photochem.* **1987**, *37*, 185−188.

(24) Schulze, F. W.; Petrick, H. J.; Cammenga, H. K.; Klinge, H. Thermodynamic Properties of the Structural Analogues Benzo[c]-cinnoline, Trans-azobenzene, and Cis-azobenzene. *Z. Phys. Chem.* **1977**, *107*, 1−19.

(25) Hoffmann, K.; Marlow, F.; Caro, J. Photoinduced switching in nanocomposites of azobenzene and molecular sieves. *Adv. Mater.* **1997**, *9*, 567−570.

(26) Birnbaum, P. P.; Linford, J. H.; Style, D. W. The Absorption Spectra of Azobenzene and Some Derivatives. *Trans. Faraday Soc.* **1953**, *49*, 735−744.

(27) Katz, M. J.; Brown, Z. J.; Colon, Y. J.; Siu, P. W.; Scheidt, K. A.; Snurr, R. Q.; Hupp, J. T.; Farha, O. K. A facile synthesis of UiO-66, UiO-67, and their derivatives. *Chem. Commun.* **2013**, *49*, 9449−9451.

(28) Goesten, M. G.; de Lange, M. F.; Olivos-Suarez, A. I.; Bavykina, A. V.; Serra-Crespo, P.; Krywka, C.; Bickelhaupt, F. M.; Kapteijn, F.; Gascon, J. Evidence for a chemical clock in oscillatory formation of UiO-66. *Nat. Commun.* **2016**, *7*, 11832.

(29) Cavka, J. H.; Jakobsen, S.; Olsbye, U.; Guillou, N.; Lamberti, C.; Bordiga, S.; Lillerud, K. P. A new zirconium inorganic building brick forming metal organic frameworks with exceptional stability. *J. Am. Chem. Soc.* **2008**, *130*, 13850−13851.

(30) Li, J.-R.; Kuppler, R. J.; Zhou, H.-C. Selective gas adsorption and separation in metal-organic frameworks. *Chem. Soc. Rev.* **2009**, *38*, 1477−1504.

(31) Schaate, A.; Dühnen, S.; Platz, G.; Lilienthal, S.; Schneider, A. M.; Behrens, P. A Novel Zr-Based Porous Coordination Polymer Containing Azobenzenedicarboxylate as a Linker. *Eur. J. Inorg. Chem.* **2012**, *2012*, 790−796.

(32) Park, J.; Yuan, D.; Pham, K. T.; Li, J.-R.; Yakovenko, A.; Zhou, H.-C. Reversible Alteration of CO2 Adsorption Upon Photochemical or Thermal Treatment in a Metal-Organic Framework. *J. Am. Chem. Soc.* **2012**, *134*, 99−102.

(33) Robertson, J. M. Crystal Structure and Configuration of the Isomeric Azobenzenes. *J. Chem. Soc.* **1939**, *0*, 232−236.

(34) Oien-Odegaard, S.; Bouchevreau, B.; Hylland, K.; Wu, L.; Blom, R.; Grande, C.; Olsbye, U.; Tilset, M.; Lillerud, K. P. UiO-67-type Metal-Organic Frameworks with Enhanced Water Stability and Methane Adsorption Capacity. *Inorg. Chem.* **2016**, *55*, 1986−1991.

(35) Deka, M. J.; Chowdhury, D. Tuning Electrical Properties of Graphene with Different π-Stacking Organic Molecules. *J. Phys. Chem. C* **2016**, *120*, 4121−4129.

5. Electric Field Switching of Metal-Organic Framework Membranes

5.1. Summary

After controlling gas transport with electromagnetic fields such as light the idea of using electrical fields in connection with a MOF membrane was highly interesting to us. As MOFs often exhibit highly flexible frameworks that limit gas selectivity and molecular sieving properties, an electric field was meant to improve these. Since this was never done before, it could not be determined what will happen. Possible scenarios could have been alignment of linker molecules or distortion of the crystals.

In chapter 5.2. a study on the electric field influence on the MOF structure of ZIF-8 is shown. A reactor design with the possibility of building a MOF membrane-capacitor was invented. The electric field applied with the field strength of 500 V/mm showed an influence on the lattice of ZIF-8, influencing gas permeation properties. The gas diffusivities of all species were decreased, given in the lowered permeances through the membrane. However, molecular separation by size-exclusion was decreased for smaller molecules such as H_2, CH_4 and CO_2, but an increase of 33 % in selectivity was found for propylene/propane mixtures. In XRD analysis we found that the ZIF-8 reflex intensities vary and the positions are collectively shifted towards higher angles 2θ. This proves an increase in the pore diameter and a phase shift into polymorphs through the polarization. With DFT calculations the phase transformation into polarized polymorphs was found to be exactly the reason for the crystallographic changes from our experimental data. The average pore-limiting diameter had changed from 3.4 to 3.6 Å decreasing selectivity for smaller molecules but increasing the selectivity for bigger molecules. This was achieved due to strain inside the lattice, limiting the rotation of the linker molecules inside the ZIF-8 strut, also limiting diffusivities. Polarization curves were measured to determine the reaction on the lattice of a single crystal, which was not found to be a piezoelectric, nor a ferroelectric response.

However, we could estimate that our electric field is not strong enough to align linker molecules. Nevertheless, the distortion of the Zn-ions in ZIF-8 through the electric field is responsible for a blockade of the linker and lattice motions. This sharpens molecular sieving properties of the material only for gases that can be separated by molecular sieving at 3.6 Å, such as propylene and propane.

5.2. Defibrillation of Soft Porous Metal-Organic Frameworks with Electric Fields

A. Knebel, B. Geppert, K. Volgmann, D. I. Kolokolov, A. G. Stepanov, J. Twiefel, P. Heitjans, D. Volkmer, J. Caro

6. Conclusion and Outlook

6.1. Summary

The thesis gives an insight into the development of modern membrane synthesis technologies for high-end MOF-based ceramic supported membranes and also for mixed matrix membranes with respect to the key parameters, such as high flux and good separation values. This is highly interesting to give industrial relevant state-of-the-art properties to the membranes for applications such as carbon sequestration and chemical purification. Furthermore, this thesis highlights the equipment designs and preparation of smart, switchable MOFs membrane systems, which rely on contactless tuning of the gas transport properties via external stimuli.

In the first part of the thesis a review paper is given, serving as an overview for several types of applications of switchable membranes. We show switchable MOFs and switchable MOF membranes, which also supports the introduction part of the thesis with a lot more in-depth details. We give examples for different types of polymeric membranes that react to thermal or chemical triggers and open/close their gates dependent on the circumstances. Diving deeper into the field of MOFs, we introduce research based on switching mechanisms, for example the response of selected guest molecules to light or electric fields, but also the reaction of the MOF lattices itself to these stimuli. In the end we show research that reports the control over the porous structures of MOFs. With control over the pores of MOFs, gas transport control – by combining the approach of switchable MOF systems with membrane systems – is possible.

The second part of this thesis shows the facilitated synthesis procedures of MOFs and MOF membranes through a self-assembly approach towards highly controllable layers and particles. Here, we give an insight into the possibilities of these techniques, controlled layer-by-layer growths and nanoparticles synthesis of ZIF-67-on-ZIF-8 structures and their characterization with XRD, SEM, TEM and EDXM. Also we show that, through the easy approach of hierarchically build nanostructures, the single material properties can add up, making new materials with improved properties. The herein presented MOF-on-MOF (ZIF-67-on-ZIF-8) system is especially interesting for pre-combustion carbon capture and/or hydrogen separation. We also show that nanostructures are inevitable for the application in industrial systems and this approach could be highly interesting for industry.

With the techniques described in the second part we go over to the third part, where three papers are given. With the presented layer-by-layer technique we can easily produce smart-MOFs as membrane layers on ceramic supports by the same self-assembly synthesis protocol and obtain UV/vis and only-vis light-switchable copper-based SURMOFs. We show that these pillared-layer structures are able to continuously tune the gas transport through these layers. Through a specialised reactor design we were able to switch the membranes in situ and sense gas transport changes as soon as they appear. The first examples are tailor-made MOFs with switchable AZB or fluoro-AZB side-chains, mounted in those pillared-layer fashion structures. They offer enough free space to enable cis-trans isomerism, just by shining light on these layers. We could show that the separation of H_2/CO_2, CO_2/N_2, $H_2/$ethylene and $H_2/$propylene mixtures can be switched. Further, we could implement AZB guest-molecules by physisorption into novel UiO-67 thin layer membranes and also switch guest molecules inside the pores. In all cases we give an insight into the possibly underlying mechanisms of gas transport and selectivity switching, which is relying on either steric, or adsorptive processes. Whereas the dipolar moment of the cis-trans conformers is responsible for switching selectivity in the SURMOF membranes by adsorption, the AZB guest molecules in the UiO-67 membrane switch selectivity relying on gating mechanisms.

In the last part of this thesis a single publication is shown that describes gas transport switching through a MOF membrane by a simultaneously applied external electric field. This is a pioneering work on influencing the porous structure of a MOF with an electric field. We could show by ex-situ XRD that the lattice of ZIF-8 is getting distorted under the stimulus of an electric field of the field strength of 500 V/mm, switching it into metastable polymorphs. In experiments we found evidence that molecular sieving for a binary mixture of propylene and propane is enhanced, while it is decreased for smaller gases. However, it is suggested that the overall flexibility of the framework is decreased, because the diffusivities of the gaseous species were overall lower. From theoretical DFT simulations we determined the final polymorphic structure of ZIF-8 and the changes to the lattice: The average pore opening diameter is slightly increased, so that the size-selectivity of smaller molecules decreases, but is just correctly adjusted to improve separation for propylene/propane mixtures. Additionally, the bulk modulus of the material is strongly increased. This is because the flexibility and rotational freedom of the Hmim linkers is suppressed, leading to a more sharp molecular sieving.

Thus, we could show that MOF preparation as layers as well as particles is possible with growth control on the nanometre scale, which definitely improves their possible applicability in industrial systems. These improved synthetic strategies are highly controllable and easy at the same time and especially we utilized it for preparation of membrane systems. The urgent need for membranes for a more economical resource separation and purification will play a crucial role in the future. We can tune the material parameters for these processes by different approaches: We can use two types of materials at the same time, adding intrinsic materials properties. We can tailor linker molecules and enable MOFs to switch their properties by light irradiation. But we can also exploit the flexibility of the framework. Within an industrial process, the control over the parameters and compositions is crucial and switchable materials make easy and contact free regulation possible. Utilizing electric field to improve the intrinsic parameters by extrinsic stimuli means next-level process controllability and may help to make the MOF materials applicable for high-end industrial separation and purification processes. Moreover, switchable properties, such as dipole moments, adsorption sides and polymorphs can be applied in multifunctional systems. This could lead to a single membrane that is applicable in all kind of separation processes just by using the correct external stimulus. For each process it could be individually configured by the right irradiation wavelength or the right electric field strength to fit the requirements for the process.

Nevertheless, our studies also led to deeper understanding of the materials parameters, how to tune them and how to evaluate the mechanisms. Future works could aim for pressure-swing adsorptive processes under external stimuli or microelectronic switches, memristors or drug-delivery systems. Especially in microelectronics, for computer systems or similar applications, a molecular switch in a highly ordered system could lower the size of modules and devices. Drug delivery systems are highly desired for medical applications and light or electric stimuli are easy to deliver to the patient's body regions. Releasing medication to the right spots at the right time could yield highly controllable treatments, for example to fight cancer.

In adsorptive processes, such as pressure swing adsorbers, the switchable dipolar moments could also be used to remove ions or organic waste selectively from water or gas mixtures. In an electric field, the speed of adsorption or desorption could be tuned. This also leads to possible applications in the field of specific and highly selective sensing of polar/non-polar or big/small species in a multifunctional sensor device. However, systems that react to external

stimuli, for example the light-responsive systems may have a more simple way to be used. Chemicals like odours, pesticides could be released at any time, when the sun is rising or when an electric field is applied. This could also be utilized for protecting animals and plants.

We can think about many useful features for smart systems and through tailor-made MOFs we have smart and porous materials that show changes in their porous properties upon an influence of external stimuli. We expect a lot of research to start on the topics of switchable MOFs in the future.

APPENDIX

Publications Included in this Thesis

Order of appearance:

[1]   **A. Knebel**, C. Zhou, A. Huang, J. Zhang, L. Kustov, J. Caro, *Smart Metal-Organic Frameworks (MOFs): Switching Gas Permeation through MOF Membranes by External Stimuli*, Chemical Engineering Technology 41 (2018) 224–234.

[2]   **A. Knebel**, P. Wulfert-Holzmann, S. Friebe, J. Pavel, I. Strauß, A. Mundstock, F. Steinbach, J. Caro, *Hierarchical Nanostructures of Metal-Organic Frameworks Applied in Gas Separating ZIF-8-on-ZIF-67 Membranes*, Chemistry – A European Journal 24 (2018) 5728–5733.

[3]   **A. Knebel**, P. Wulfert-Holzmann, S. Friebe, J. Pavel, I. Strauß, A. Mundstock, F. Steinbach, J. Caro, *Cover Feature: Hierarchical Nanostructures of Metal-Organic Frameworks Applied in Gas Separating ZIF-8-on-ZIF-67 Membranes* (Chem. Eur. J. 22/2018), Chemistry – A European Journal 24 (2018) 5678.

[4]   K. Müller, **A. Knebel**, F. Zhao, D. Bléger, J. Caro, L. Heinke: *Switching Thin Films of Azobenzene-Containing Metal-Organic Frameworks with Visible Light*. Chemistry - A European Journal 23 (2017) .

[5]   **A. Knebel**, L. Sundermann, A. Mohmeyer, I. Strauß, S. Friebe, P. Behrens, J. Caro: *Azobenzene Guest Molecules as Light-Switchable CO2 Valves in an Ultrathin UiO-67 Membrane*. Chemistry of Materials 29, 7 (2017) 3111-3117.

[6]   Z. Wang, **A. Knebel**, S. Grosjean, D. Wagner, S. Bräse, C. Wöll, J. Caro, L. Heinke: *Tunable molecular separation by nanoporous membranes*. Nature Communications 12/2016; 7:13872.

[7]   **A. Knebel**, B. Geppert, K. Volgmann, D. I. Kolokolov, A. G. Stepanov, J. Twiefel, P. Heitjans, D. Volkmer, J. Caro: *Defibrillation of soft porous metal-organic frameworks with electric fields* Science 358 (2017) 347–351.

Publications not Included in this Thesis

[1]   I. Strauss, A. Mundstock, D. Hinrichs, R. Himstedt, **A. Knebel**, C. Reinhardt, D. Dorfs, J. Caro: *On the interaction of guest molecules with Co-MOF-74: A Vis/NIR and Raman approach*. Angewandte Chemie International Edition, in press, DOI:10.1002/anie.201801966

[2]   H. Fan, J. Gu, H. Meng, **A. Knebel**, J. Caro, *Back Cover: High-Flux Membranes Based on the Covalent Organic Framework COF-LZU1 for Selective Dye Separation by Nanofiltration* (Angew. Chem. Int. Ed. 15/2018), Angewandte Chemie International Edition 57 (2018) 4104.

[3] H. Fan, J. Gu, H. Meng, **A. Knebel**, J. Caro, *High-Flux Membranes Based on the Covalent Organic Framework COF-LZU1 for Selective Dye Separation by Nanofiltration*, Angewandte Chemie International Edition 57 (2018) 4083–4087.

[4] H. Fan, J. Gu, H. Meng, **A. Knebel**, J. Caro, *Wasser-Hochflussmembranen auf Basis der kovalenten organischen Gerüststruktur COF-LZU1 für die Farbstoffabtrennung durch Nanofiltration*, Angewandte Chemie 130 (2018) 4147–4151.

[5] S. Friebe, L. Diestel, **A. Knebel**, A. Wollbrink, J. Caro: *MOF-Based Mixed-Matrix Membranes in Gas Separation - Mystery and Reality*. Chemie Ingenieur Technik 88 (2016) 1788–1797.

[6] **A. Knebel**, S. Friebe, N. C. Bigall, M. Benzaqui, C. Serre, J. Caro: *Comparative Study of MIL-96(Al) as Continuous MOF-Layer and Mixed-Matrix-Membrane*. ACS Applied Materials & Interfaces 8 (2016) 7536–7544.

Patents

[1] **A. Knebel**, J. Caro: *WO2018010951 (A1) Device and Process for Controlled Gas Transport on Metal-Organic Framework Membranes* Year: 01/2018, Status: Application.

[2] **A. Knebel**, J. Caro: *EP 3269441 A1 Device and process for controlled gas transport on metal-organic framework membranes*. Year: 01/2018, Status: Application.

[3] **A. Knebel**, J. Caro, L. Heinke, S. Grosjean, C. Wöll, Z. Wang, S. Bräse: *EP3305392 (A1)Photo-switching and tuning of gas transport through metal-organic framework membranes.* Year: 04/2018, Status: Application.

Contributions to Conferences and Talks

EuroMOF 2017

> 29.10.-01.11.2017 in Delft, Netherlands
> TU Delft Aula Conference Center
> Poster presentation
> Title: *Defibrillation of Soft-Porous Metal-Organic Frameworks*

7th International FEZA Conference

> 03.-07.07.2017 in Sofia, Bulgaria
> Natural Palace of Culture
> Poster presentation
> Title: *Metal-organic framework membranes with light-switchable gas transport*

29. Deutsche Zeolith Tagung

> 01-03.03.2017 in Frankfurt am Main, Germany
> DECHEMA-Haus Frankfurt am Main
> Invited oral presentation and conference paper
> Title: *Controlling the Molecular Separation of Metal-Organic Framework Membranes Remotely via External Stimuli*

Final Report Presentation Evonik-Cooperation

> Industry cooperation
> September 2016, Marl, Evonik-Creavis
> Oral Presentation

7th International Zeolite Membrane Meeting

> 20-23.08.2016 in Dalian, China
> Dalian Institute of Technology
> Invited oral presentation and conference paper
> Title: *Controlled Optical Switching of the Gas Transport through SURMOF Membrane Layers*

Invited Oral Presentation within the Karlsruhe Institute of Technology Seminar

> 08.08.2016 in Karlsruhe, Germany
> Karlsruhe Institute of Technology
> Invited Oral Presentation
> Title: *Towards Intelligent Materials – Push the Right Buttons: How to Stimulate the Gas Transport through MOFs*

28. Deutsche Zeolith-Tagung

> 02.-04.03.2016 in Gießen, Germany
> Justus-Liebig-University of Gießen
> Poster presentation and conference paper
> Title: *Comparative Study of MIL-96(Al) as Continuous MOF-Layer and Mixed-Matrix-Membrane*

CURRICULUM VITAE

Alexander Knebel

Born on 27.03.1991
in Burgwedel, Germany.

Nationality: German

Education and Research Experience

October 2015 – present (2018)	**Leibniz University Hanover, Germany** Doctoral Studies Research group of Prof. Dr. Jürgen Caro
January 2018 – Mai 2018	**KAUST Catalysis Center, King Abdullah University of Science and Technology (KAUST), Saudi Arabia** Internship Catalysis and Porous Liquids Research group of Prof. Dr. Jorge Gascon
April 2017	**Instituto de Magnetismo Aplicado (IMA), Universidad Complutense de Madrid (UCM), Spain** Internship superconducting quantum interference Research group of Prof. Dr. Patricia de la Presa Muñoz de Toro
October 2013 – September 2015	**Leibniz University Hanover, Germany** Master of Science, Chemistry Title of thesis: *"Pre-Combustion Hydrogen Separation with Continuous MIL-96 Metal-Organic Framework Membranes and Mixed-Matrix Membranes"* Prepared in the research group of Prof. Dr. Jürgen Caro
October 2010 – September 2013	**Leibniz University Hanover, Germany** Bachelor of Science, Chemistry Title of thesis: *"Synthesis and Characterization of Porous Superstructures of Plasmonic Colloidal Nanocrystals"* Prepared in the research group of Prof. Dr. Nadja Bigall
2010	**Gymnasium Mellendorf, Wedemark, Germany** Abitur Exam modules: Chemistry, Biology, German, Religion, Latin

Awards & Grants

Starting from January 2018   Scholarship: Graduierten Akademie Hannover Auslandsstipendium.

July 2017   Award: poster award Federation of European Zeolite Association (FEZA) 2017.

July 2017   Scholarship: DECHEMA travel grant to the FEZA 2017 conference in Sofia, Bulgaria.

October 2017   Scholarship: DECHEMA travel grant to the EuroMOF 2017 conference at TU Delft, Netherlands.

Starting from October 2016   Graduate member of the Hannover School of Nanotechnology (HSN) Scholarship Program